Final Report

Higher-Order Decoupled Direct Method (HDDM) for Ozone Modeling Sensitivity Analyses and Code Refinements

Work Order
582-07-84005-FY08-07

Prepared for

Mark Estes
Texas Commission on Environmental Quality
12118 Park 35 Circle
Austin, Texas 78753

Prepared by

Bonyoung Koo
Greg Yarwood

ENVIRON International Corporation
773 San Marin Drive, Suite 2115
Novato, California 94998

And

Daniel S. Cohan

Rice University
6100 Main Street, MS 317
Houston, Texas 77005

31 August 2008

TABLE OF CONTENTS

Page

EXECUTIVE SUMMARY ES-1

1. INTRODUCTION..... 1-1

1.1. Background..... 1-1
1.2. Report Organization..... 1-1

2. IMPROVING HDDM IMPLEMENTATION IN CAMX..... 2-1

2.1. New Fast Chemistry Solver 2-1
2.2. Sensitivity to Rate Constants 2-7
2.3. Flexi-DDM..... 2-11

3. SENSITIVITY ANALYSIS OF HOUSTON OZONE MODELING..... 3-1

3.1. Sensitivity to Emissions..... 3-1
3.2. Sensitivity to Rate Constants 3-34
3.3. Uncertainty Analysis..... 3-45

REFERENCES..... R-1

APPENDICES

Appendix A: Updated DDM Section of CAMx User's Guide

TABLES

Table 2-1. CPU times required for full grid run and Flexi-DDM run (CPU times for HDDM runs are based on simulations with 1 sensitivity parameter) 2-11
Table 3-1. First-order sensitivity parameters for the preliminary modeling 3-3
Table 3-2. Second-order sensitivity parameters for the preliminary modeling..... 3-4
Table 3-3. Peak 8-hour ozone concentrations in Houston region during episode..... 3-21
Table 3-4. Proposed list of reactions for reaction rate sensitivity analysis for TCEQ 3-36

FIGURES

Figure ES-1. Ozone isopleths for HRVOC and NOx emissions from the west and east ship channels and Mont Belvieu for the 4-km grid cell containing episode maximum ozone sensitivity to the HRVOC emissions; yellow arrows represent the amount of added HRVOC emissions by reconciliation ES-2
Figure 2-1. Daily average differences in 8-hr average ozone concentrations in the surface layer between LSODE and other chemistry solvers (IEH, CMC, and EBI). 2-1
Figure 2-2. Average CPU time per simulation day for different chemistry solvers; Plotted for HDDM runs are the CPU time required to calculate sensitivities per sensitivity parameters (from the runs with 4 sensitivity parameters); based on OMP runs with four 2.8 GHz processors. 2-2
Figure 2-3. Comparison between first-order sensitivities of 8-hour average ozone to the domain-wide NOx emissions by the HDDM and BFM 2-3
Figure 2-4. Comparison between first-order sensitivities of 8-hour average ozone to the domain-wide VOC emissions by the HDDM and BFM 2-4
Figure 2-5. Comparison between second-order sensitivities of 8-hour average ozone to the domain-wide NOx emissions by the HDDM and BFM 2-5
Figure 2-6. Comparison between second-order sensitivities of 8-hour average ozone to the domain-wide VOC emissions by the HDDM and BFM 2-6
Figure 2-7. Comparison between the first-order sensitivities of 8-hour average ozone to the selected rate constants by the HDDM and BFM 2-8
Figure 2-8. Comparison between the second-order sensitivities of 8-hour average ozone to the selected rate constants by the HDDM and BFM 2-9
Figure 2-9. Comparison between the changes in 8-hour ozone estimated by the HDDM and BFM due to 50% increase in rate constants of both NO2 photolysis and HRVOC + OH reactions 2-10
Figure 2-10. Ozone sensitivities to all Houston emissions by the full grid run and Flexi-DDM run at 8 am, June 22 when maximum difference in the sensitivities between the two runs occurs; the 4-km (top) and 2-km (bottom) grids 2-12
Figure 3-1. Modeling domain for the HGB 8-hour ozone SIP modeling 3-2
Figure 3-2. Six point source clusters shown on ethene emissions spatial map: West Ship Channel; East Ship Channel; Bayport; Mont Belvieu; Texas City; and Chocolate Bayou 3-5
Figure 3-3. Differences in ozone concentrations and sensitivities to all Houston emissions between 1-way and 2-way nesting runs at 3 pm on June 22, 2005 (the hour of episode maximum 1-hour ozone concentration) 3-6
Figure 3-4. Episode average daily total NOx and VOC emissions of the Houston region (the 2-km grid) for area, mobile, and nonroad sub-categories 3-7
Figure 3-5. Episode average daily total point source NOx and VOC emissions of the Houston region (the 2-km grid): PSCF v2 (point source correction factor version 2) represents increased VOC emissions due to the reconciliation; the regular8 elevated emissions exclude emissions from fires and ships 3-8
Figure 3-6. Episode average daily total NOx and VOC emissions from anthropogenic and biogenic sources: Anthropogenic emissions are shown for the

Houston region (the 2-km grid); biogenic VOC emissions are grouped into the Houston region and the rest of the 4-km grid 3-8
Figure 3-7. Episode average daily total NOx and HRVOC point source emissions from each of the point source clusters: West Ship Channel (WSC), East Ship Channel (ESC), Bayport (BP), Mont Belvieu (MB), Texas City (TC), and Chocolate Bayou (CB) 3-9
Figure 3-8. Episode average ozone concentrations with regular3 and regular8 (with and without reconciliation) emissions 3-10
Figure 3-9. Episode average first-order ozone sensitivities to the Houston NOx emissions for area, mobile, and nonroad sub-categories 3-11
Figure 3-10. Episode average first-order ozone sensitivities to the Houston VOC emissions for area, mobile, and nonroad sub-categories 3-12
Figure 3-11. Episode average first-order ozone sensitivities to NOx and VOC emissions from point sources in the Houston region 3-13
Figure 3-12. Episode average first-order ozone sensitivities to (collective and individual) HRVOC emissions from point sources in the Houston region 3-13
Figure 3-13. First- and second-order sensitivities of episode average ozone to anthropogenic NOx, VOC, and FORM emissions in the Houston region by the revised modeling (regular8; reconciled) 3-15
Figure 3-14. First- and second-order sensitivities of episode average ozone to biogenic VOC emissions in the 4-km domain; cross sensitivity to the Houston region anthropogenic VOC and the 4-km domain biogenic VOC; by the revised modeling (regular8; reconciled)..... 3-16
Figure 3-15. Cross sensitivities of episode average ozone to the Houston region anthropogenic NOx and VOC emissions; to the Houston region anthropogenic NOx and the 4-km domain biogenic VOC emissions; by the revised modeling (regular8; reconciled) 3-17
Figure 3-16. Episode average first-order ozone sensitivities to HRVOC emissions from each point source cluster by the revised modeling (regular8; reconciled)..... 3-18
Figure 3-17. Episode average first-order ozone sensitivities to NOx emissions from each point source cluster by the revised modeling (regular8; reconciled)..... 3-19
Figure 3-18. Episode maximum first-order 1-hour ozone sensitivities to HRVOC emissions from West and East Ship Channels and Mont Belvieu by the revised modeling (regular8; reconciled) 3-20
Figure 3-19. Ozone concentrations (top), their sensitivities to Houston-region anthropogenic NO_x (middle L) and VOC (middle R), and the zero-out contribution of Houston NO_x and VOC, on June 21, 2005 3-23
Figure 3-20. As in Figure 1, for June 22, 2005..... 3-24
Figure 3-21. As in Figure 1, for June 23, 2005..... 3-25
Figure 3-22. Second-order HDDM approximation of the response surface of peak 8-hour ozone concentrations to changes in Houston region anthropogenic NO_x and VOC emissions, for June 19 (top) and June 20 (bottom), 2005. The circle marks base case conditions (i.e., 0% change in NO_x and VOC)..... 3-27
Figure 3-23. As in Figure 3-22, for June 21 (top) and June 22 (bottom) 3-28
Figure 3-24. **As** in Figure 3-22, for June 23 (top) and June 24 (bottom) 3-29
Figure 3-25. As in Figure 3-22, for June 25 (top) and June 26 (bottom) 3-30

Figure 3-26. As in Figure 3-22, for June 27 (top) and June 28 (bottom) 3-31
Figure 3-27. As in Figure 3-22, except for a downtown location on June 21 (top) and June 22 (bottom) 3-32
Figure 3-28. As in Figure 3-27, for June 23 3-33
Figure 3-29. As in Figure 3-22, for a Ship Channel location on June 23 3-33
Figure 3-30. First-order sensitivity coefficients of 8-hour ozone on June 21 to rate constants for: all photolysis rates (top left), NO_2+OH (top right), HRVOC oxidation (bottom left), and N_2O_5 hydrolysis (bottom right). Ozone sensitivity to N_2O_5 equilibrium was extremely small (not shown). Note the different scales for each plot 3-38
Figure 3-31. As in Figure 3-30, for June 22 3-39
Figure 3-32. As in Figure 3-30, for June 23 3-40
Figure 3-33. Cross-sensitivity coefficients of 8-hour ozone to NO_x emissions (left) and VOC emissions (right) crossed with photolysis rates (top), $OH+NO_2 \rightarrow HNO_3$ (middle), and HRVOC oxidation (bottom), for June 21, 2005. Note the different scales for each plot 3-42
Figure 3-34. As in Figure 3-33, for June 22 3-43
Figure 3-35. As in Figure 3-33, for June 23 3-44
Figure 3-36. First-order sensitivity coefficient of ozone to Houston NO_x emissions if actual NO_x emissions are 30% less than modeled (left) or 30% more than modeled (right), for June 21-23, 2005 3-47
Figure 3-37. First-order sensitivity coefficient of ozone to Houston VOC emissions if actual Houston NO_x emissions are 30% less than modeled (left) or 30% more than modeled (right), for June 21-23, 2005 3-48
Figure 3-38. First-order sensitivity coefficient of ozone to Houston NO_x emissions if actual Houston VOC emissions are 30% less than modeled (left) or 30% more than modeled (right), for June 21-23, 2005 3-49
Figure 3-39. First-order sensitivity coefficient of ozone to Houston VOC emissions if actual Houston VOC emissions are 30% less than modeled (left) or 30% more than modeled (right), for June 21-23, 2005 3-50
Figure 3-40. First-order sensitivity coefficient of ozone to Houston NO_x emissions if all photolysis rates are 30% smaller (left) or 30% larger (right) than modeled, for June 21-23, 2005 3-52
Figure 3-41. First-order sensitivity coefficient of ozone to Houston VOC emissions if all photolysis rates are 30% smaller (left) or 30% larger (right) than modeled, for June 23, 2005 3-53
Figure 3-42. First-order sensitivity coefficient of ozone to Houston NO_x emissions if the rate constant for $OH+NO_2 \rightarrow HNO_3$ is 30% smaller (left) or 30% larger (right) than modeled, for June 21-23, 2005 3-54
Figure 3-43. First-order sensitivity coefficient of ozone to Houston VOC emissions if the rate of $OH+NO_2 \rightarrow HNO_3$ is 30% smaller (left) or 30% larger (right) than modeled, for June 23, 2005 3-55
Figure 3-44. First-order sensitivity coefficient of ozone to Houston VOC emissions if the rate of HRVOC oxidation is 30% smaller (left) or 30% larger (right) than modeled, for June 23, 2005 3-55

EXECUTIVE SUMMARY

The Decoupled Direct Method (DDM) is an efficient and accurate way of performing sensitivity analysis to model inputs. Originally the DDM was implemented in CAMx to calculate first-order sensitivities only. However, the higher-order sensitivities can be important if model response becomes non-linear to model input changes. Under the previous TCEQ Work Order, the Higher-order DDM (HDDM) has been implemented in CAMx. In this project, we extended the HDDM implementation in CAMx to sensitivity to reaction rate constants, and performed analysis on ozone sensitivities to emissions and chemistry reaction rates for the June 2005 Houston ozone modeling episode.

A couple of issues in the CAMx HDDM that were previously identified have also been addressed: (1) The issue on accuracy of the HDDM sensitivities with the CAMx CMC chemistry solver was resolved by replacing the CMC solver with a new solver based on the Euler Backward Iterative (EBI) scheme; (2) An alternative way of running the HDDM with multiple nested grids was developed in which the user is allowed to turn off sensitivity calculations for selected grids to improve computational efficiency.

The HDDM emissions sensitivity analysis shows transition from NOx-limited condition to VOC-limited at peak ozone location as the episode progresses. A disbenefit to NOx control is observed at the peak later in the episode. Downwind areas exhibit primarily NOx-limited condition. Contrary to the conceptual model of ozone formation in the Houston region, point source HRVOC emissions turned out to have little impact on ozone concentration, even with increased (reconciled) HRVOC emissions. HDDM sensitivities can be used to estimate how much additional ozone is formed due to the reconciliation. Ozone isopleths plots were constructed using the first- and second-order HDDM sensitivities to HRVOC and NOx emissions from the west and east ship channels and Mont Belvieu area (Figure ES-1). It can be seen that the reconciliation only increases ozone concentration by a few to several ppb for the grid cells of the highest sensitivity to HRVOC emissions from the point source clusters. All the isopleths plots indicate VOC-limited condition. Therefore, assuming the conceptual model is correct, the high ozone level observed by airplane measurement can only be reproduced by adding significantly more HRVOC emissions.

Ozone isopleths constructed by the HDDM sensitivities, although confidence in the estimates fades as emissions perturbations become too large, can also be used to answer questions like, "How much changes in the NOx (or VOC) emissions will switch a region from NOx-limited to VOC-limited (or vice versa)?" This type of applications of the HDDM sensitivities can give valuable insights to establish effective control strategies.

The HDDM reaction rate sensitivity analysis shows that ozone sensitivity to photolysis rates is very strong and tends to be greatest where ozone concentrations are highest. It is also shown that uncertainty in the photolysis rates has significant impact on sensitivities to NOx and VOC emissions. Poor performance of meteorological models in predicting cloud covers could lead to significant discrepancies in actinic flux and hence in photolysis rates. Such discrepancies might not only impact predicted ozone concentrations, but also significantly impact predictions of their sensitivities to control measures.

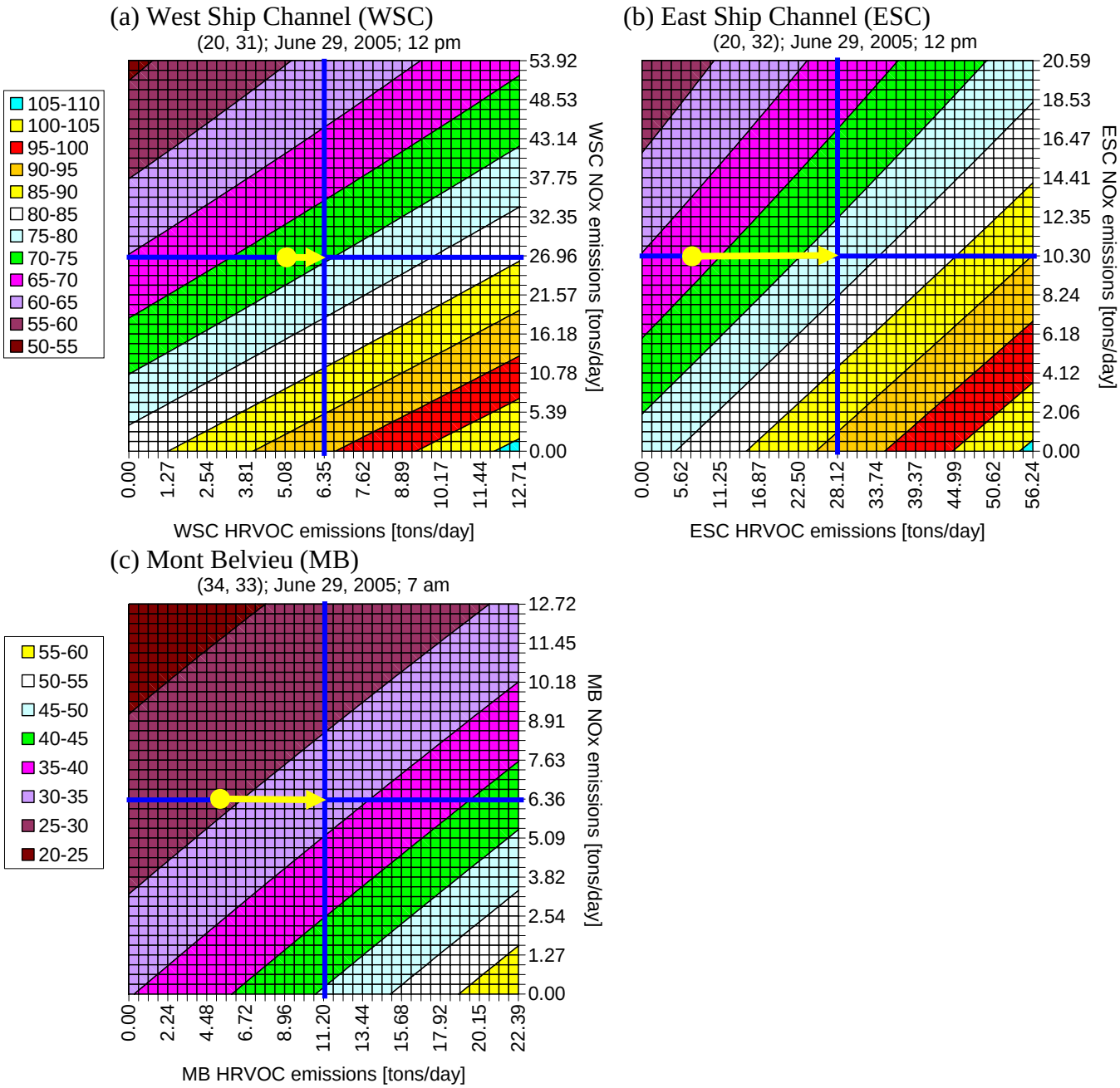

Figure ES-1. Ozone isopleths for HRVOC and NOx emissions from the west and east ship channels and Mont Belvieu for the 4-km grid cell containing episode maximum ozone sensitivity to the HRVOC emissions; yellow arrows represent the amount of added HRVOC emissions by reconciliation.

1. INTRODUCTION

1.1. Background

Air quality models are widely used to perform sensitivity analysis for evaluating model performance and developing effective emission control strategies. Traditional approach to conduct such sensitivity analysis has been using the brute force method (BFM) where model simulations are repeated with different model inputs. While the BFM is easy to apply and interpretation of the result is straightforward, the method is computationally demanding and susceptible to numerical uncertainty. The Decoupled Direct Method (DDM) offers an alternative to the traditional BFM by directly solving sensitivity equations derived from the governing equations of the model. Although the DDM is theoretically applicable to higher order sensitivities, most of the DDM implementation in 3-D air quality models including CAMx focused on the first-order sensitivity coefficient. Higher-order sensitivity may be useful where model response is non-linear to changes in model inputs. The Community Multi-scale Air Quality Model (CMAQ) implemented a variation of the DDM, called DDM-3D, and has recently been extended to calculate second-order sensitivities by Dr. Daniel Cohan and colleagues.

The TCEQ has been using CAMx for their ozone State Implementation Plan (SIP) modeling and had ENVIRON implement the high-order DDM capability in CAMx under Work Order 582-07-84005-03. Under the current Work Order (582-07-84005-FY08-07), ENVIRON, in collaboration with Dr. Cohan, expanded on the previous work and conducted a model sensitivity analysis for the Houston area using June 2005 ozone modeling database developed by the TCEQ. The goals are improve understanding of ozone formation in the Houston region and to inform SIP development efforts. Also, the HDDM implementation in CAMx has been updated and extended to reaction rate sensitivity.

1.2. Report Organization

Section 2 describes code refinements of the CAMx HDDM tool. The following tasks are discussed:

- Updating the HDDM implementation in CAMx for new EBI chemistry solver
- Extending the HDDM code to calculate sensitivities to reaction rate constants
- Developing an alternative approach to running HDDM to improve computational efficiency

Section 3 presents sensitivity analysis performed for the June 2005 Houston ozone episode using the updated CAMx HDDM tool. Ozone sensitivities to the Houston region emissions and important chemical reaction rates are examined and discussed. Analysis on the uncertainties in the emissions and rate constants is then presented.

2. IMPROVING HDDM IMPLEMENTATION IN CAMX

2.1. New Fast Chemistry Solver

The previous TCEQ work showed that the HDDM didn't work well with the CMC fast chemistry solver which is default chemistry solver in CAMx. Therefore, the previous TCEQ work and preliminary modeling in this work were performed using an alternative chemistry solver (IEH) that is slower than the CMC solver. Since then, a new chemistry solver based on Euler Backward Iterative (EBI) scheme (Hertel et al., 1993) was implemented in CAMx, which is going to replace the CMC solver. The EBI solver provides similar (during the day) or better (at night) accuracy with similar numerical efficiency to the CMC solver.

The HDDM implementation in CAMx was extended to the new EBI solver and the updated CAMx model was applied for the 36 km domain of the June 2005 Houston ozone modeling database (see Section 3.1.1). First, we compared accuracy of different chemistry solvers implemented in CAMx: LSODE, IEH, CMC, and EBI solvers. The LSODE, IEH, and CMC solvers are described in CAMx User's Guide (ENVIRON, 2008). LSODE is based on Gear's method, and regarded as the most accurate among the chemistry solvers in CAMx, thus serves as a reference for the comparison. Figure 2-1 shows that the EBI solver provides better agreement with LSODE than the CMC solver while IEH is slightly better than EBI. The numerical efficiency of the EBI solver is comparable to that of the CMC solver (Figure 2-2).

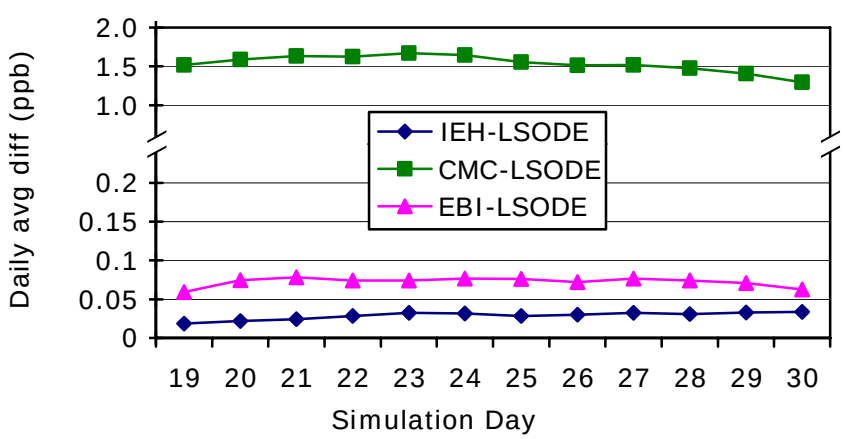

Figure 2-1. Daily average differences in 8-hr average ozone concentrations in the surface layer between LSODE and other chemistry solvers (IEH, CMC, and EBI)

To test the HDDM with the EBI solver, 8-hour average ozone sensitivities to the domain-wide emissions of NOx or VOC were calculated by the brute-force method (BFM) and the HDDM. Figures 2-3 to 2-6 show normalized mean bias (NMB) and error (NME) and coefficient of determination (r^2) from linear regression. The NMB and NME are defined as follows:

$$NMB = \frac{\sum\left(S(HDDM) - S(BFM)\right)}{\sum S(BFM)}$$

$$NME = \frac{\sum \left| S(HDDM) - S(BFM) \right|}{\sum S(BFM)}$$

where S(HDDM) and S(BFM) are first- or second-order sensitivities calculated by the HDDM and BFM, respectively. The first-order BFM sensitivities are calculated by running the standard model twice with small input changes:

$$\text{First-order } S(BFM) = \frac{C(+10\%) - C(-10\%)}{0.2}$$

where C(+10%) is the ozone concentration from the model run with 10% increase in NOx or VOC emissions and C(-10%) with 10% decrease in the emissions. The second-order BFM sensitivities are calculated as follows:

$$\text{Second-order } S(BFM) = \frac{C(+10\%) - 2\,C(base\ case) + C(-10\%)}{0.01}$$

On our testing, the HDDM with the EBI solver showed similar level of accuracy to the HDDM with the IEH solver, but runs much faster. Figure 2-2 compares computational efficiency of the HDDM with different chemistry solvers. The CPU times for the HDDM are shown as the time required for solving sensitivities only and defined as follows:

$$\frac{T_n - T_0}{n}$$

where T_n is the total CPU time to calculate the concentrations and sensitivities for n parameters together and T_0 is the time for the concentrations only (standard CAMx run). It is shown that efficiency of calculating HDDM sensitivities is little affected by the chemistry solver used as the HDDM does not follow the solution algorithm of individual chemistry solver.

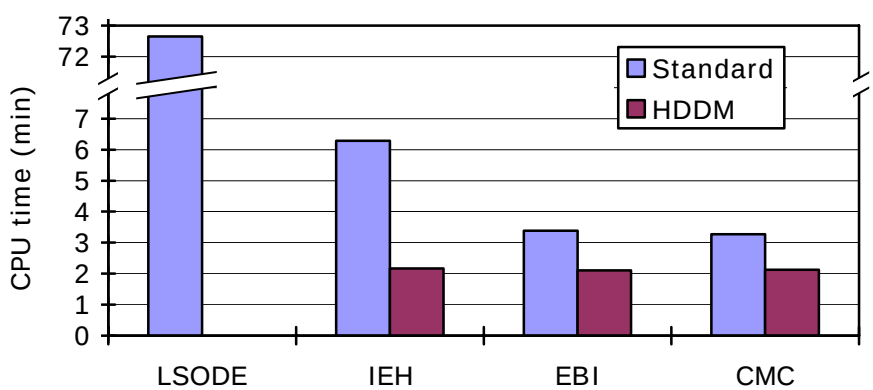

Figure 2-2. Average CPU time per simulation day for different chemistry solvers; Plotted for HDDM runs are the CPU time required to calculate sensitivities per sensitivity parameters (from the runs with 4 sensitivity parameters); based on OMP runs with four 2.8 GHz processors.

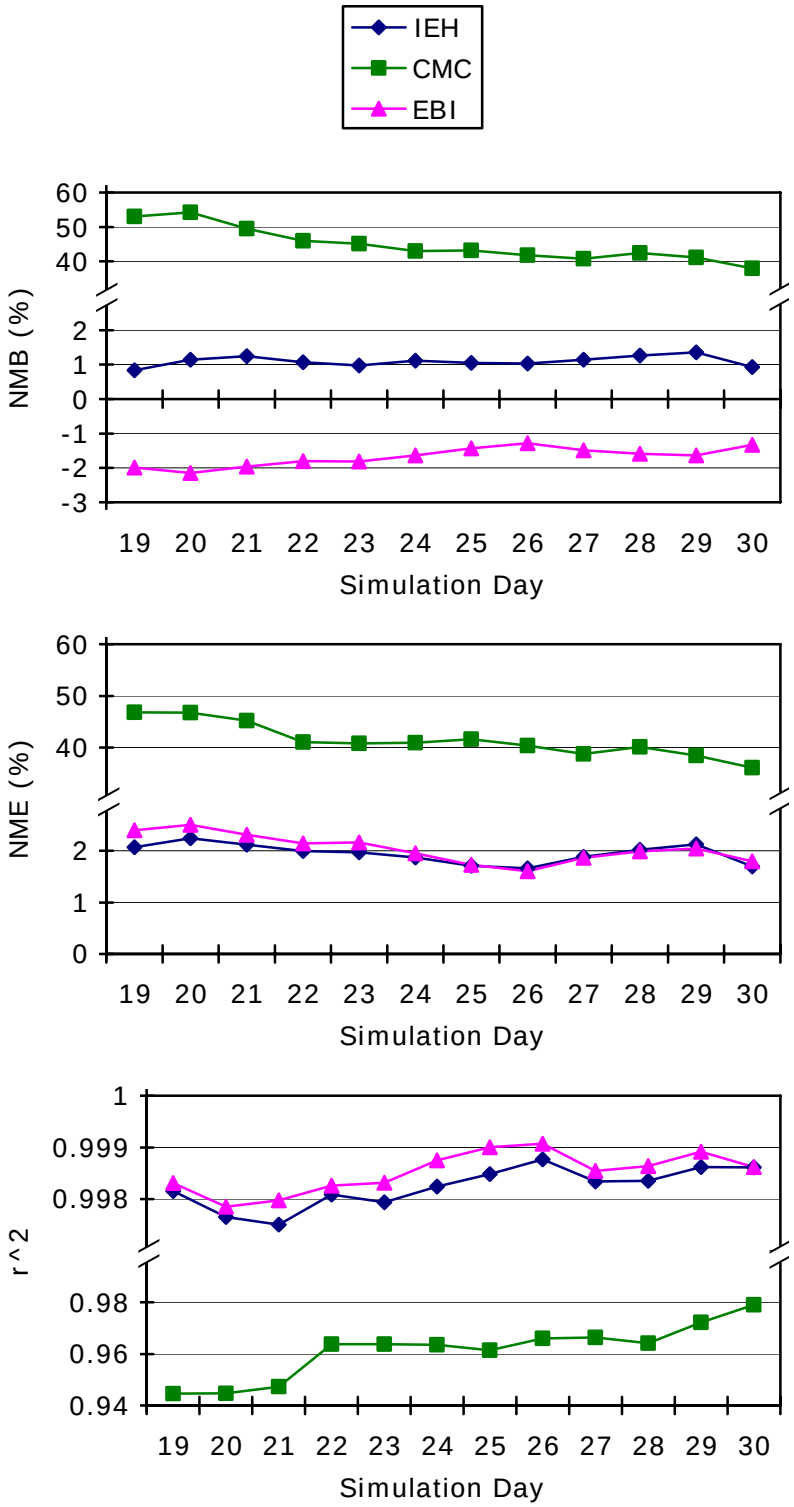

Figure 2-3. Comparison between first-order sensitivities of 8-hour average ozone to the domain-wide NOx emissions by the HDDM and BFM

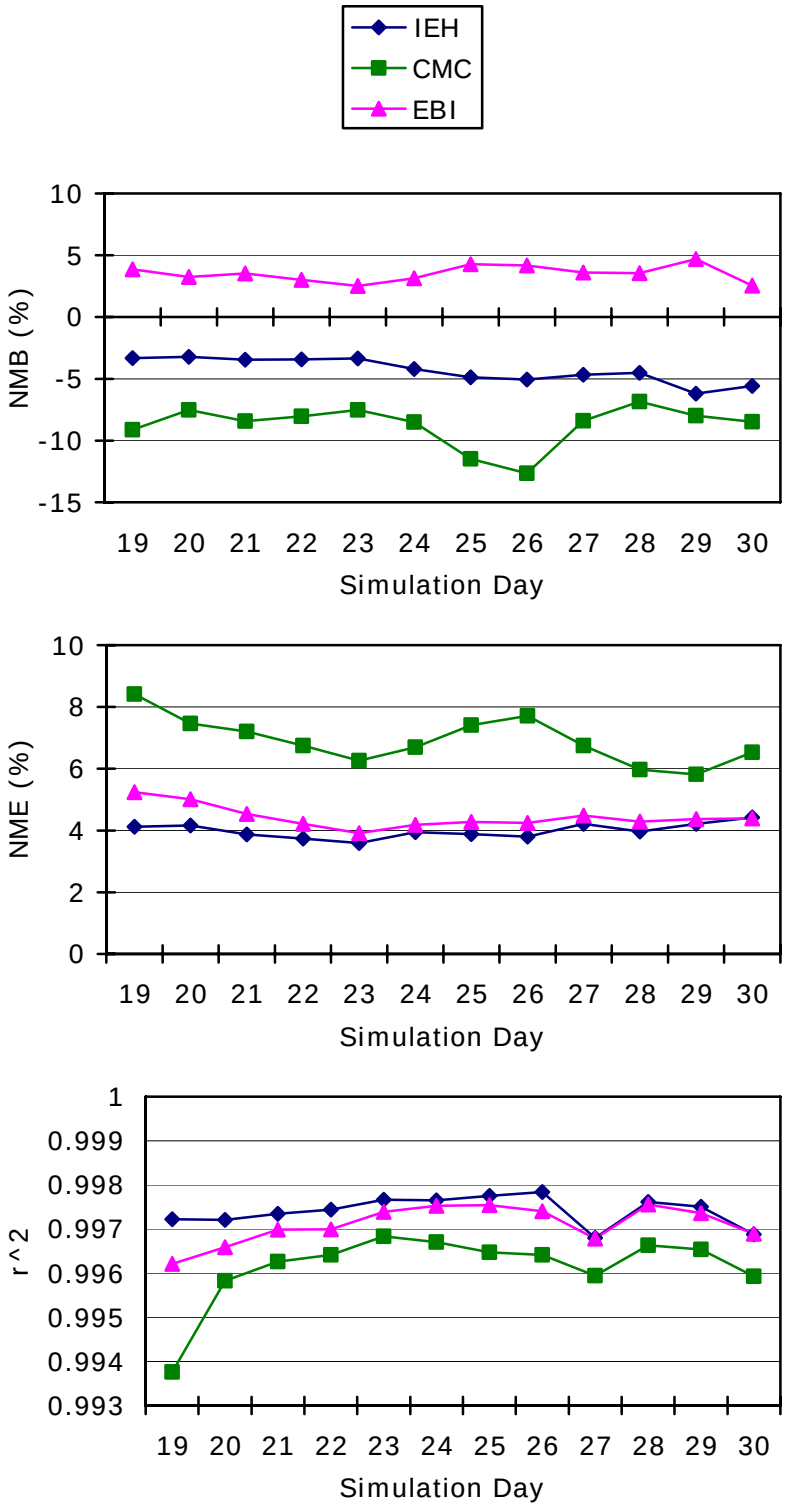

Figure 2-4. Comparison between first-order sensitivities of 8-hour average ozone to the domain-wide VOC emissions by the HDDM and BFM

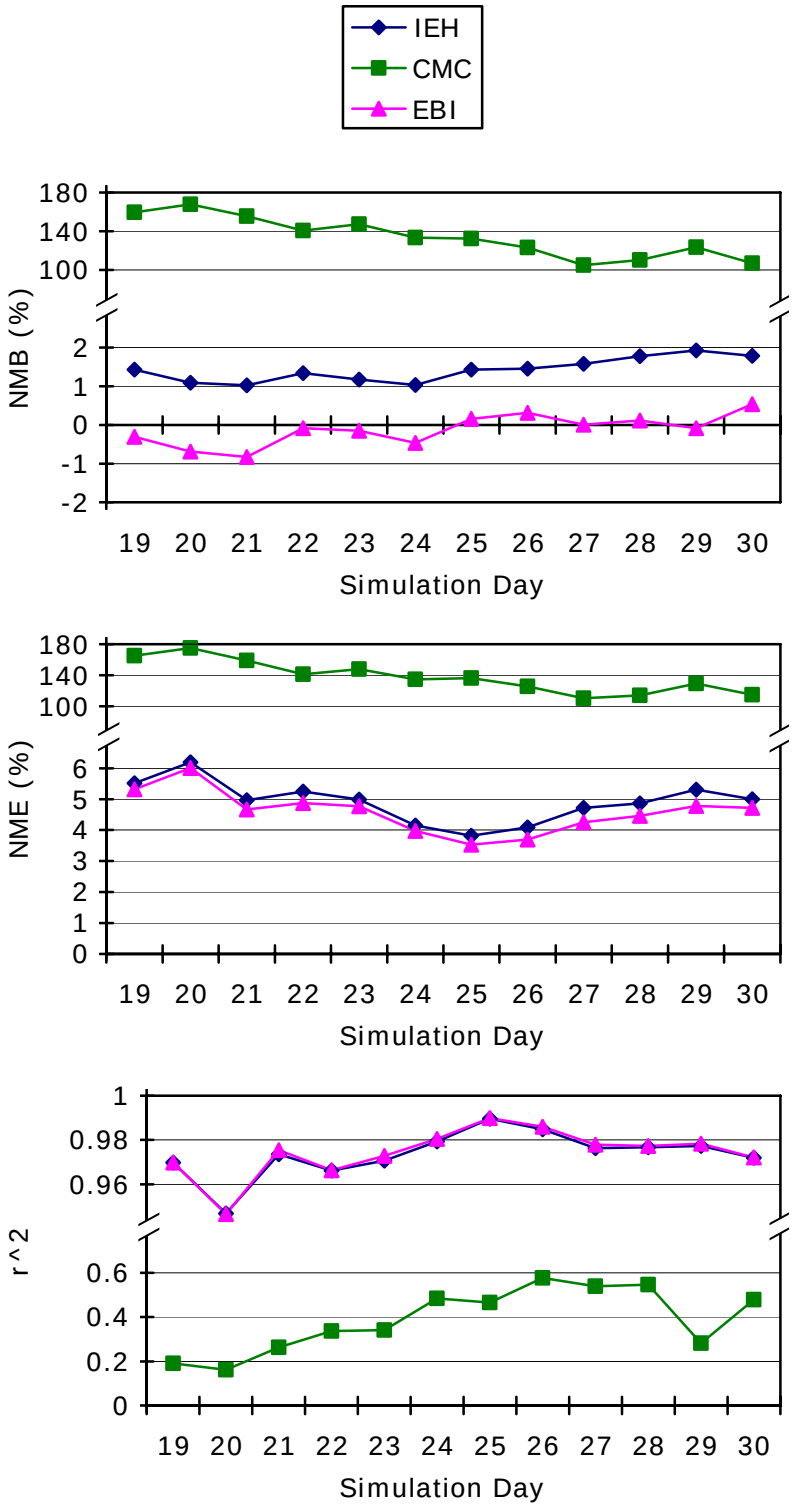

Figure 2-5. Comparison between second-order sensitivities of 8-hour average ozone to the domain-wide NOx emissions by the HDDM and BFM

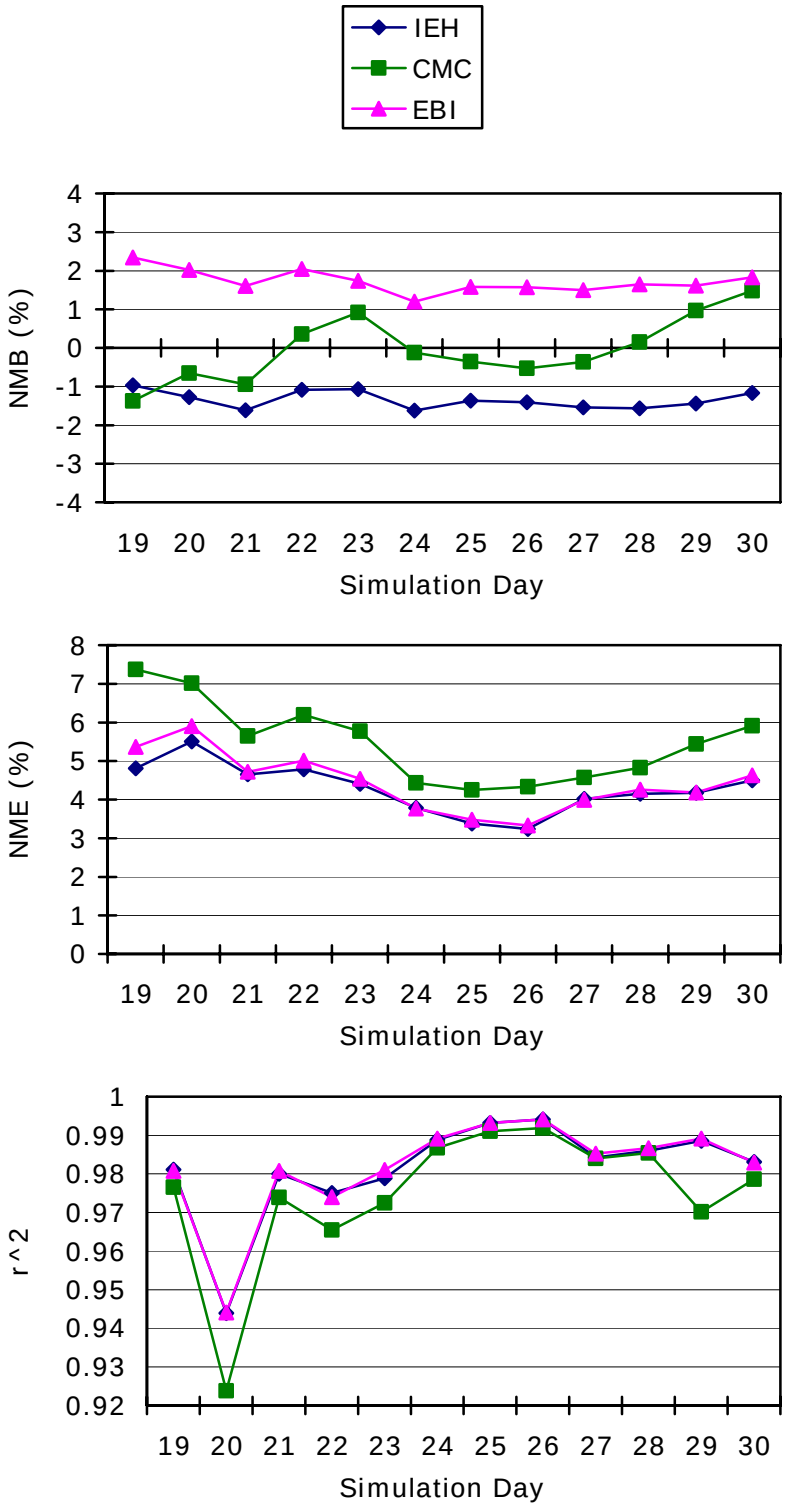

Figure 2-6. Comparison between second-order sensitivities of 8-hour average ozone to the domain-wide VOC emissions by the HDDM and BFM

2.2. Sensitivity to Rate Constants

The HDDM implementation in CAMx was extended to calculate sensitivities to chemistry reaction rate constants. Implementing reaction rate sensitivity involves accounting for how the changes in reaction rates affect the rates at which chemical reactants are lost and chemical products are formed. Outside of the chemistry solver, reaction rate sensitivities are advected, diffused, and so forth just as any other sensitivity parameter. The implementation of reaction rate sensitivity offers the flexibility to compute first- and second-order sensitivities to the rate constant(s) of any one or more reactions in the chemistry mechanism.

To test, 8-hour average ozone sensitivities to the following CB05 reactions were calculated by the HDDM and BFM:

- NO2 photolysis : NO2 → NO + O3P
- NO oxidation with O3 : NO + O3 → NO2
- ISOP oxidation with OH: ISOP + OH → …
- HRVOC oxidation with OH: ETH + OH → …
  (multiple reactions) OLE + OH → …
  IOLE + OH → …

Figures 2-7 and 2-8 compare the first- and second-order sensitivities by the HDDM and BFM, respectively. The agreement between the HDDM and BFM sensitivities is reasonably good. Cross sensitivity was tested using incremental Taylor series expansion. Changes in 8-hour ozone due to 50% increase in rate constants of both NO2 photolysis and HRVOC + OH reactions can be calculated by the BFM as follows:

BFM: $$C_{p_1=0.5;\, p_4=0.5} - C_{base}$$

The changes can be approximated by Taylor series expansion:

HDDM (1st): $$0.5\left(S^{(1)}_{p_1} + S^{(1)}_{p_4}\right)$$

HDDM (1st + 2nd): $$0.5\left(S^{(1)}_{p_1} + S^{(1)}_{p_4}\right) + \frac{0.25}{2}\left(S^{(2)}_{p_1} + S^{(2)}_{p_4}\right)$$

HDDM (1st + 2nd + cross): $$0.5\left(S^{(1)}_{p_1} + S^{(1)}_{p_4}\right) + \frac{0.25}{2}\left(S^{(2)}_{p_1} + S^{(2)}_{p_4} + 2\, S^{(2)}_{p_1;\, p_4}\right)$$

Figure 2-9 compares the above three HDDM approximation with the BFM. It can be seen that as the self second-order and cross terms are added, the agreement between the HDDM and BFM improves although the improvement due to cross sensitivity isn't significant because the cross sensitivity in this case is very small.

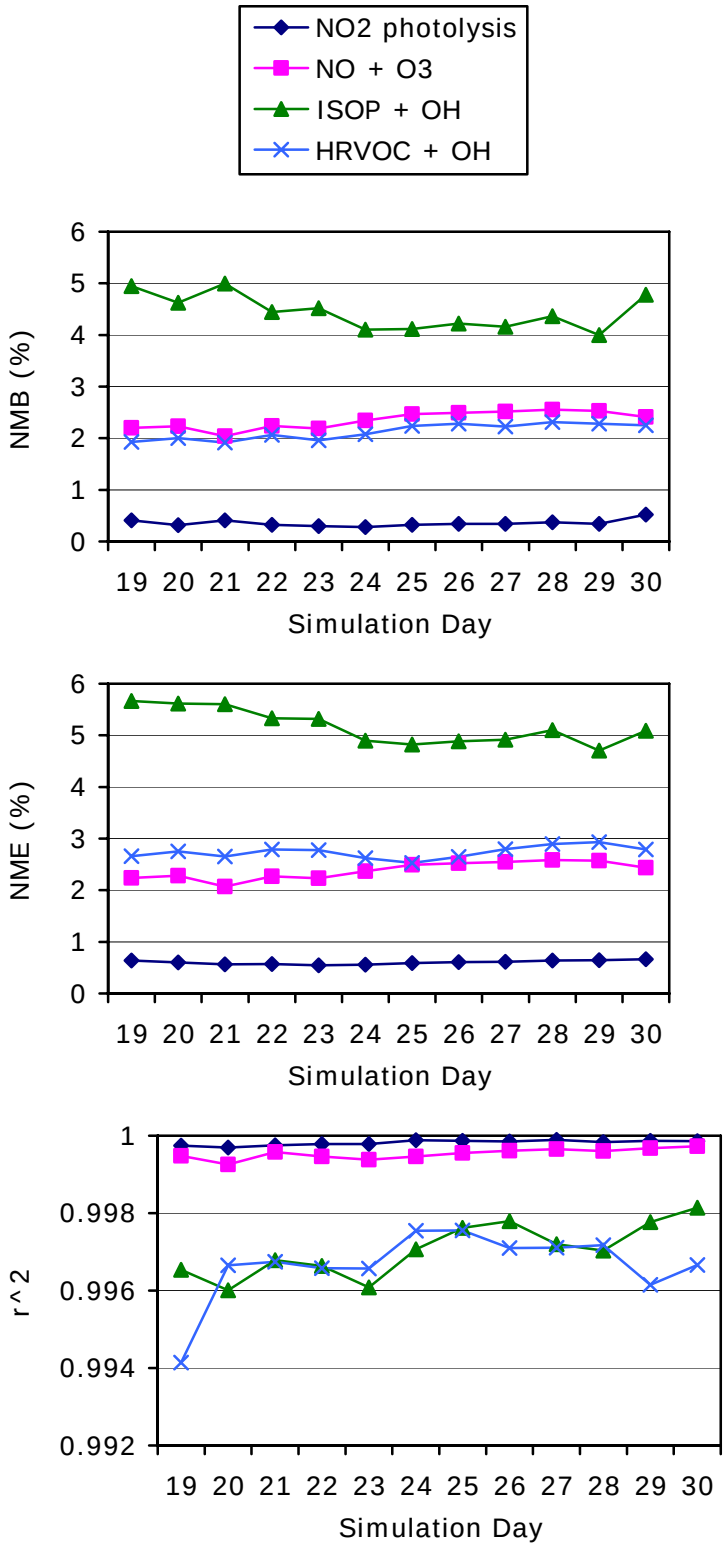

Figure 2-7. Comparison between the first-order sensitivities of 8-hour average ozone to the selected rate constants by the HDDM and BFM

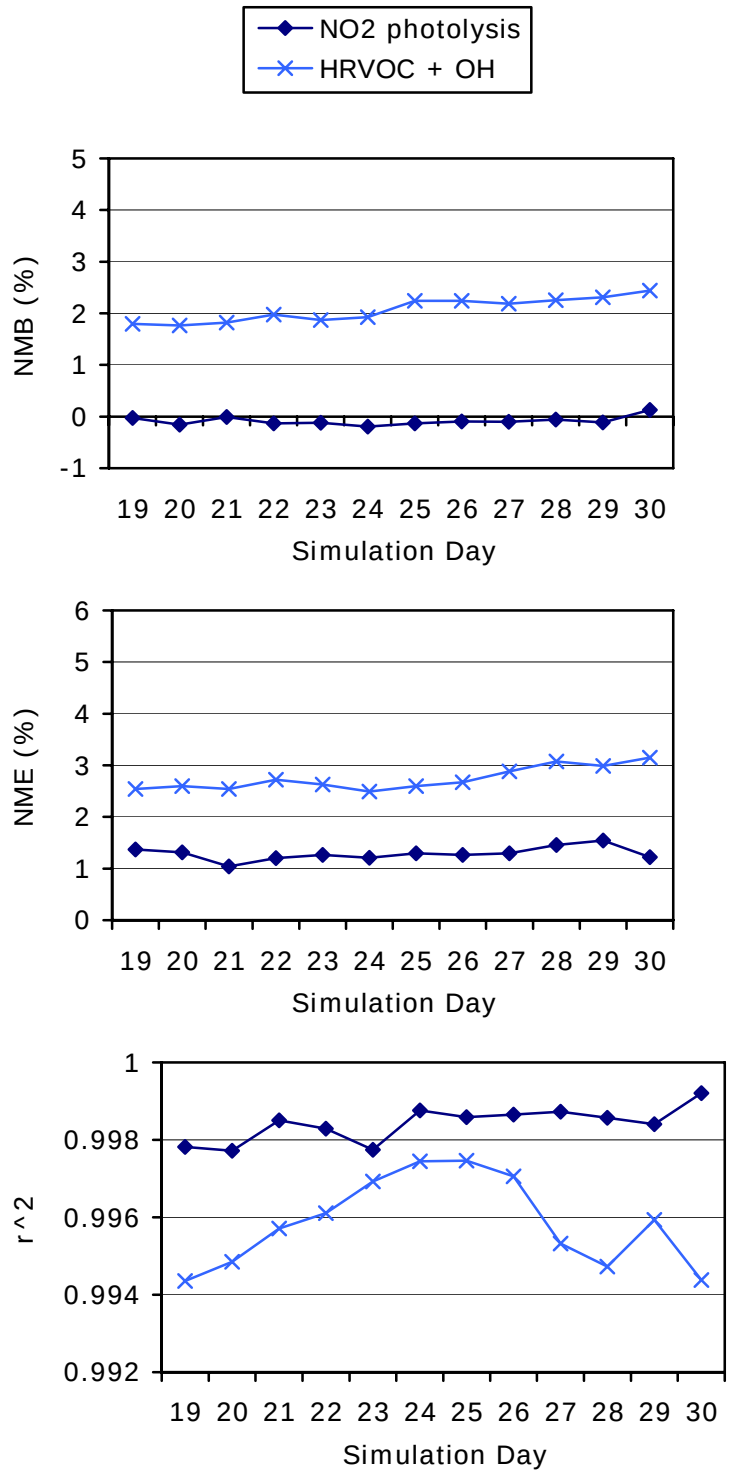

Figure 2-8. Comparison between the second-order sensitivities of 8-hour average ozone to the selected rate constants by the HDDM and BFM

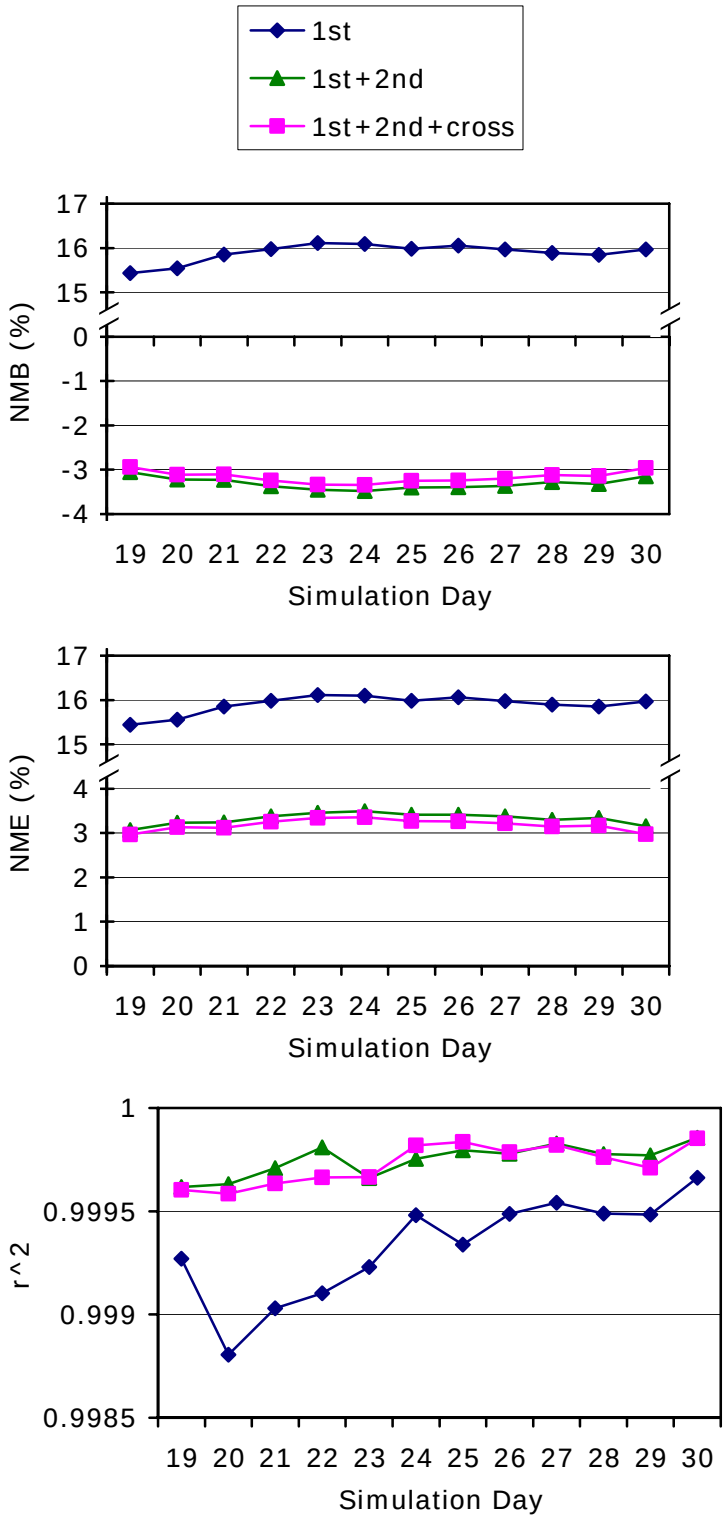

Figure 2-9. Comparison between the changes in 8-hour ozone estimated by the HDDM and BFM due to 50% increase in rate constants of both NO2 photolysis and HRVOC + OH reactions

2.3. Flexi-DDM

Although HDDM is computationally much more efficient than the BFM, it does require additional CPU time and memory space which can be significant especially when multiple grids are used in two-way nesting as in the Houston ozone modeling. The increased computational cost may not always be worthwhile if only part of the modeling domain is of interest. One way to enhance computational efficiency in such cases is to use one-way nesting where boundary conditions (BCs) for a nested grid are extracted from the full grid modeling. Subsequent runs with sensitivities are performed without outer grids. However, differences between the two nesting schemes (i.e. 1-way vs. 2-way) sometimes cause discrepancies in the model results (see Section 3.1.1). An alternative approach is running the full 2-way nested model while "turning off" sensitivity calculations outside nested grids of interest. This will reduce CPU-times but not reduce memory requirements. Also, note that turning off sensitivity calculations for outer grids is only appropriate for certain types of sensitivity calculations.

Flexi-DDM allows user to turn off sensitivity calculations for selected grids (normally grids far outside the area of interest) to improve computational efficiency of HDDM runs. To test, the June 2005 Houston ozone modeling was performed with the full grids (36-12-4-2-km) and with Flexi-DDM where the sensitivity calculation was turned off for the 36-12-km grids. Figure 2-10 shows differences in the ozone sensitivities to all Houston emissions calculated by the full grid run and Flexi-DDM run. Flexi-DDM sensitivities agree reasonably well with the sensitivities by the full grid run. Maximum sensitivity difference of ~5 ppb occurs near northwest corner of the 4-km grid. Maximum sensitivity difference over the 2-km grid is even smaller (~2 ppb).

Table 2-1 compares CPU times required for the full grid run and Flexi-DDM run. With Flexi-DDM, the number of grid cells for sensitivity calculation is reduced by 44%. The reason why the CPU time was only reduced by 18% is because grids with finer resolutions have shorter advection time steps thus perform more computations.

Flexi-DDM also saves storage space as sensitivities for outer grids are not stored.

Table 2-1. CPU times required for full grid run and Flexi-DDM run (CPU times for HDDM runs are based on simulations with 1 sensitivity parameter)

Model Setup	CPU time [hr] per simulation day	CPU time [hr] for sensitivity only	Reduction in CPU time for sensitivity only
Standard run with full grids	0.75		
HDDM run with full grids	2.62	1.87	
HDDM run with Flexi-DDM	2.29	1.54	18%

(a) ozone sensitivity by the full grid run over the 4-km domain

(b) sensitivity differences (Flexi-DDM – full grid) over the 4-km domain

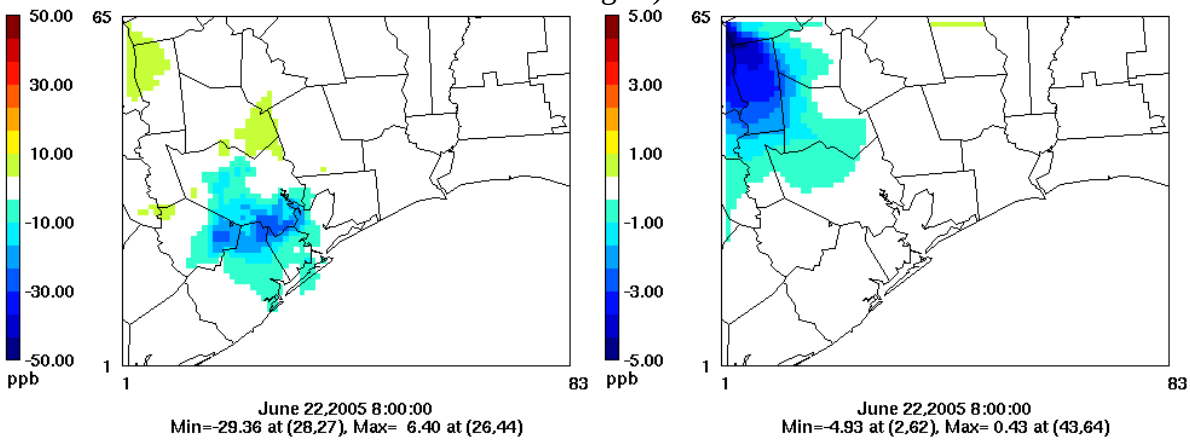

(c) ozone sensitivity by the full grid run over the 2-km domain

(d) sensitivity differences (Flexi-DDM – full grid) over the 2-km domain

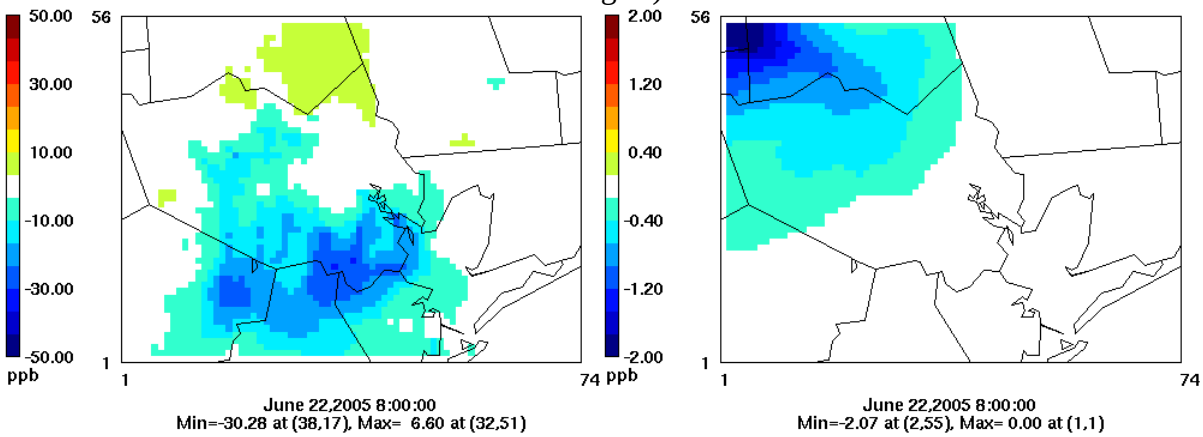

Figure 2-10. Ozone sensitivities to all Houston emissions by the full grid run and Flexi-DDM run at 8 am, June 22 when maximum difference in the sensitivities between the two runs occurs; the 4-km (top) and 2-km (bottom) grids.

3. SENSITIVITY ANALYSIS OF HOUSTON OZONE MODELING

The HDDM tool implemented in CAMx under the previous TCEQ project was applied to perform sensitivity analysis on ozone formation of the Houston region using the June 2005 Houston ozone modeling database. A preliminary HDDM run was performed and a few issues were identified. The second sensitivity modeling was then performed using the updated CAMx HDDM tool described earlier and revised emissions inventory. In this section, sensitivity of ozone concentrations to emissions of the Houston area is first discussed. Ozone sensitivity to reaction rate constants is presented later.

3.1. Sensitivity to Emissions

Sensitivity of ozone formation to the emissions of its precursors is directly related to evaluation of control strategies. Sensitivities to emissions may be calculated to all emissions, a sub-category of emissions (e.g., point sources) and/or emissions in a sub-region (e.g., Houston region). They can also be calculated for an individual chemical species (e.g., ethene) or a group of species (e.g., HRVOC). List of sensitivity parameters modeled is presented below.

3.1.1. Preliminary Run Setup

The preliminary modeling was performed using a 14-day episode (June 17 – 30, 2005; the first 2 days are spin-up days) taken from the Houston/Galveston/Brazoria (HGB) 8-hour ozone State Implementation Plan (SIP) modeling database developed by TCEQ. The modeling domain consists of four grids with 36, 12, 4 and 2 km resolutions covering Eastern US (Figure 3-1). Vertical layer structure of the 36 and 12 km grids includes 17 layers reaching up to 15 km above ground. That of the 4 and 2 km grids is expanded to 28 layers using vertical layer nesting. Meteorological inputs for the 36, 12 and 4 km grids were extracted from MM5 modeling for the episode and those for the 2 km grid were interpolated using flexi-nesting. The “regular3” emissions inventory was used for the preliminary runs.

For the preliminary run, CAMx sensitivity calculations were conducted on the 4-km resolution domain containing a 2-km sub-domain. The boundary concentrations (BCs) for the 4-km domain were extracted from a prior simulation of the entire (36-12-4-2-km) domain (1-way nesting). This approach was adopted to maximize the number of sensitivities that we can calculate for the area of interest, i.e., Houston. Originally, it was anticipated that Houston region ozone sensitivity to Houston region emissions could be adequately simulated on the 4-2-km domain alone (i.e., recirculation effect is negligible). To verify this assumption, we performed an additional sensitivity run with the full regional grids. The result will be discussed later.

The CB05 chemistry mechanism was used as the TCEQ SIP modeling inputs were based on the mechanism. Since it was discovered from the previous TCEQ project that the HDDM implementation based on DDM-3D did not work well with the CMC fast chemistry solver (see Section 2.1), the IEH solver was instead used for the preliminary sensitivity runs.

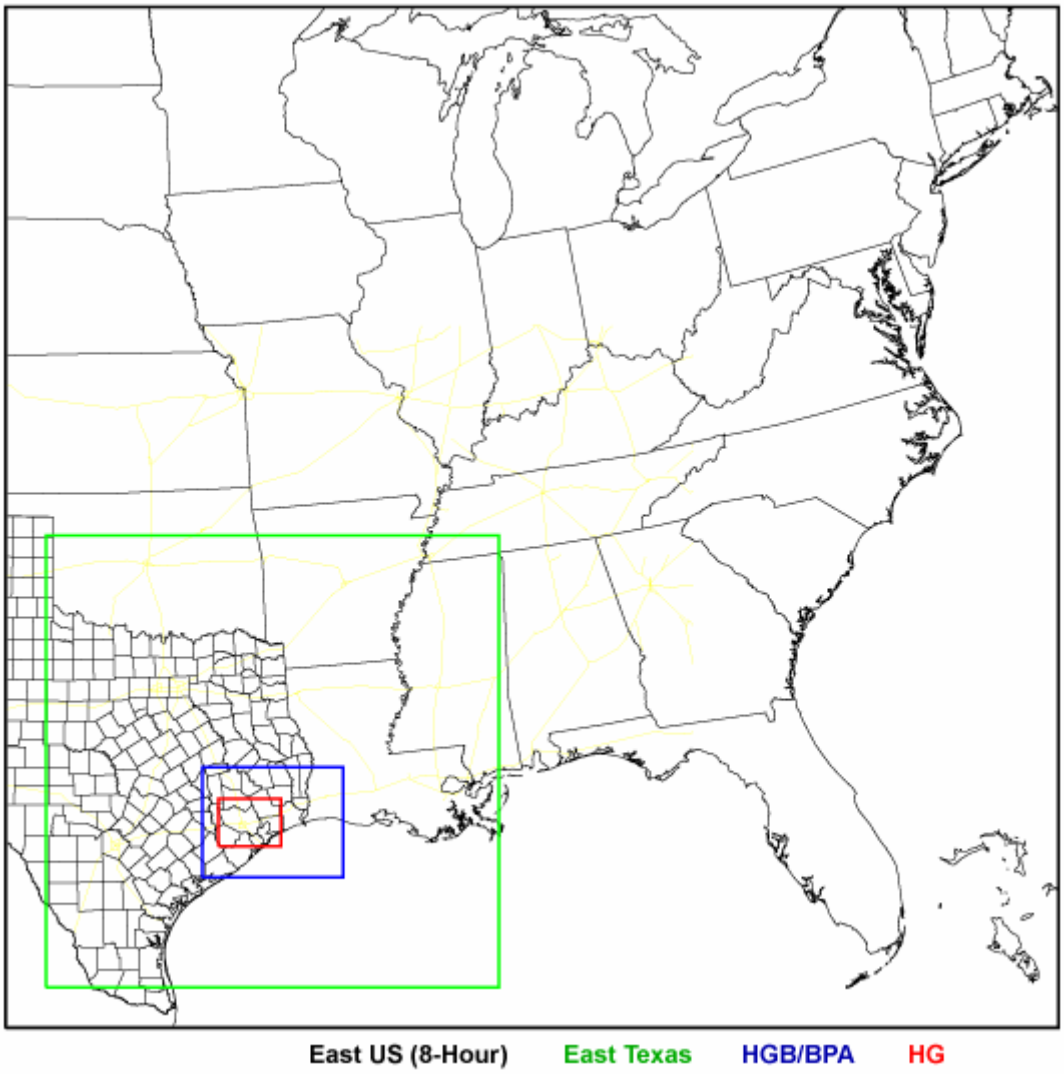

Figure 3-1. Modeling domain for the HGB 8-hour ozone SIP modeling (http://www.tceq.state.tx.us/implementation/air/airmod/data/hgb8h2/hgb8h2_camx_domain.html)

Table 3-1 shows the list of the first-order sensitivity parameters modeled for the preliminary sensitivity analysis. These sensitivity parameters were selected to be informative in their own right and also to help identify additional sensitivities for the second iteration of the sensitivity runs.

The "Houston region" referred to in Table 3-1 was defined as the 2-km sub-domain. Although it does not exactly match county boundaries, it does cover most sources in the region and is most convenient as the region is clearly defined model-wise.

Point source HRVOC emissions are of special interest because they are important in the conceptual model of Houston ozone formations and, accordingly, should be important in the photochemical modeling. Several sensitivities were calculated to Houston region HRVOCs collectively and individually. In addition, we intended to examine the relative importance of

HRVOCs released in different geographic locations and accordingly designed to calculate sensitivities to HRVOC emissions from six point source clusters (Figure 3-2):

- West Ship Channel
- East Ship Channel (including Channelview)
- Bayport
- Mont Belvieu
- Texas City
- Chocolate Bayou

Table 3-1. First-order sensitivity parameters for the preliminary modeling

Species	Category	Region	Parameter Name
NOx	Anthropogenic	Houston	E_anthNOx_HOU
	Area	Houston	E_areaNOx_HOU
	Mobile	Houston	E_mobileNOx_HOU
	Nonroad	Houston	E_nonroadNOx_HOU
	Point	Houston	E_pointNOx_HOU
		Each of 6 point source clusters	E_pointNOx_clusterX
VOC	Anthropogenic	Houston	E_anthVOC_HOU
	Area	Houston	E_areaVOC_HOU
	Mobile	Houston	E_mobileVOC_HOU
	Nonroad	Houston	E_nonroadVOC_HOU
	Point	Houston	E_pointVOC_HOU
	Biogenic	Entire 4-km grid	E_bioVOC_4kmGrid
FORM (formaldehyde)	Anthropogenic	Houston	E_anthFORM_HOU
HRVOC[1]	Point	Houston	E_pointHRVOC_HOU
		Each of 6 point source clusters	E_pointHRVOC_clusterX
ETH (ethene)	Point	Houston	E_pointETH_HOU
OLE (propene, but-1-ene, etc.)	Point	Houston	E_pointOLE_HOU
IOLE (but-2-enes, etc.)	Point	Houston	E_pointIOLE_HOU
All	All	Houston	E_All_HOU[2]

Notes:

1. HRVOC is defined as the combination of CB05 species ETH, OLE and IOLE.
2. This sensitivity was also run on the entire (36-12-4-2-km) domain to determine the importance of recirculation for sensitivities, discussed in the text.

The value of second-order sensitivities lies in understanding non-linear responses to emissions. Homogeneous second-order sensitivities, e.g. ($d^2O_3/dNOx^2$) may show that larger emission changes will produce growing, or diminishing, model response. Heterogeneous (cross) second-order sensitivities, e.g. ($d^2O_3/dNOx \cdot dVOC$) identify interactions between emissions of different types and/or from different sources.

Higher order sensitivities must be selected with care because the number of possible second-order sensitivities is geometrically larger than first-order. A practical constraint is that each second-order sensitivity relies upon one or two first-order sensitivities that must also be

computed (i.e., listed in Table 3-1). In the context of this study, second-order sensitivities were selected to address one or more of the following motivations, each relevant to understanding ozone formation and formulating control strategies:

- Nonlinearity of response: Homogeneous second-order sensitivities show how responsiveness to an emission perturbation changes with the size of the perturbation. This is crucial to predicting the impact of a large-scale control measure or a package of measures that affect the same emissions source, and can assist with model evaluation to identify potential causes of mismatches between model results and observations.
- Interactions of responses: Heterogeneous second-order sensitivities indicate the extent to which perturbations in one input parameter (e.g., an emission rate) impact model responsiveness to another parameter (e.g., emissions from another source). Due to these interactions, the net impact of an abatement plan may differ from the sum of the impacts of its component measures. Analysis of interactions can highlight which emissions sources most interact in their impacts on ozone and can help estimate the synergistic or counteracting effects of multiple control measures.
- Uncertainty analysis: For model evaluation, it is important to understand how uncertainty in emission rates might yield uncertainty in model predictions of concentrations and sensitivities. For Houston ozone, there has been particular interest in understanding how uncertainty in biogenic VOC, anthropogenic formaldehyde, and point source HRVOC emissions might impact model results and the predicted impact of control strategies. Homogeneous second-order sensitivities indicate uncertainty arising from uncertainty in the associated input parameter, whereas heterogeneous sensitivities indicate uncertainty due to another input parameter.

Table 3-2 presents the second-order sensitivities along with their motivations.

Table 3-2. Second-order sensitivity parameters for the preliminary modeling

Sensitivity to Emissions From		**Description / Motivation**
Source 1	**Source 2**	
E_anthNOx_HOU	E_anthNOx_HOU	Nonlinear response to changing Houston anthropogenic NOx (Nonlinearity)
E_anthVOC_HOU	E_anthVOC_HOU	Nonlinear response to changing Houston anthropogenic VOC (Nonlinearity)
E_anthNOx_HOU	E_anthVOC_HOU	Cross-sensitivity interaction of Houston NOx and VOC impacts (Interaction)
E_bioVOC_4kmGrid	E_bioVOC_4kmGrid	Nonlinear response to changing biogenic VOCs (Nonlinearity; Uncertainty)
E_bioVOC_4kmGrid	E_anthNOx_HOU	Cross-sensitivity interaction / uncertainty of Houston NOx impact due to uncertainty of biogenic VOCs (Interaction; Uncertainty)
E_bioVOCs_4kmGrid	E_anthVOC_HOU	Cross-sensitivity interaction / uncertainty of Houston anthropogenic VOC impact due to uncertainty of biogenic VOCs (Interaction; Uncertainty)
E_anthFORM_HOU	E_anthFORM_HOU	Nonlinear response to changing Houston anthropogenic formaldehyde (Nonlinearity; Uncertainty)

Sensitivity to Emissions From		Description / Motivation
Source 1	**Source 2**	
E_pointHRVOC_clusterX	E_pointHRVOC_clusterX	Nonlinear response to changing HRVOCs from each point source cluster (Nonlinearity; Uncertainty)
E_pointHRVOC_clusterX	E_pointNOx_clusterX	Interaction between each cluster of HRVOC emissions and Houston point NOx (Interaction; Uncertainty)

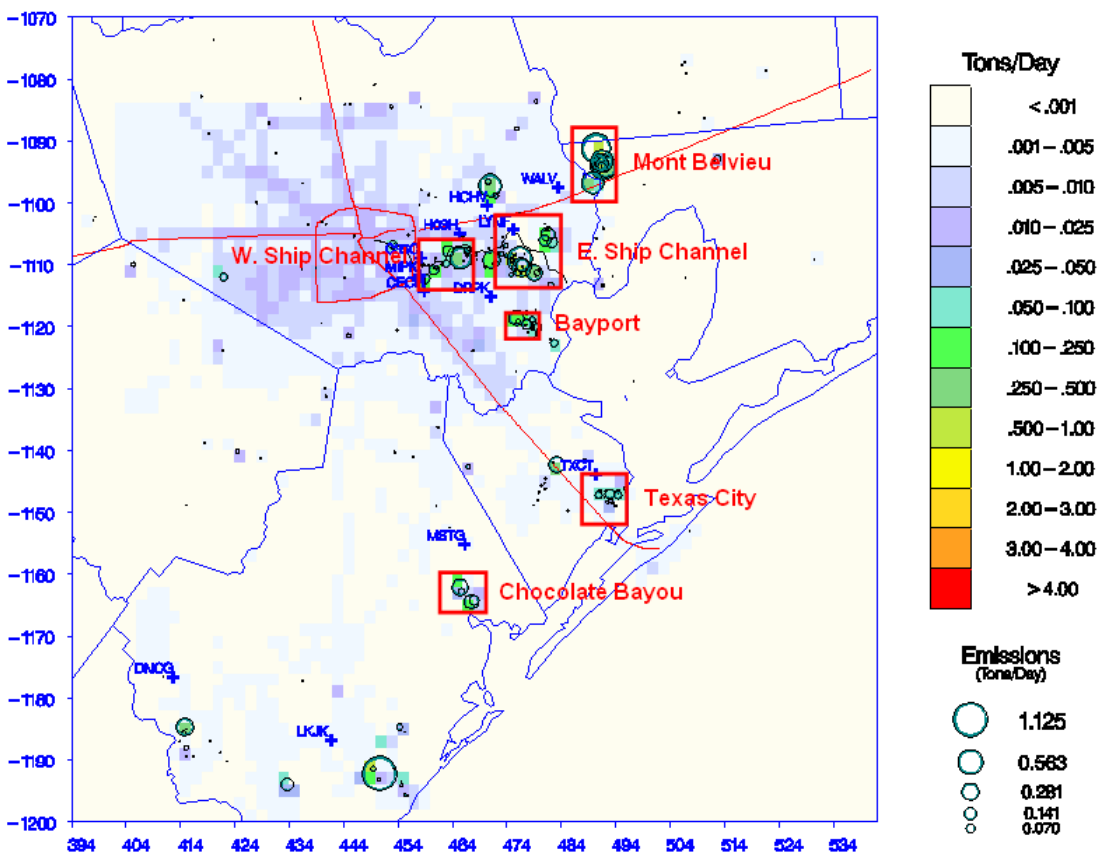

Figure 3-2. Six point source clusters shown on ethene emissions spatial map: West Ship Channel; East Ship Channel; Bayport; Mont Belvieu; Texas City; and Chocolate Bayou.

As mentioned earlier, the ozone sensitivity to all Houston emissions were calculated with both 1-way nesting (sensitivity run with 4-2-km grids and BCs for the 4-km grid extracted from a full grid run) and 2-way nesting (sensitivity run with the full grids). Contrary to the initial assumption, it was shown that the discrepancies in the ozone concentrations and sensitivities between the two runs can be significant (Figure 3-3). Therefore, a way to improve computational efficiency of sensitivity calculations while running the full grids (Flexi-DDM) was developed and implemented (see Section 2.3). The second round of sensitivity modeling was then performed using the full grids and Flexi-DDM.

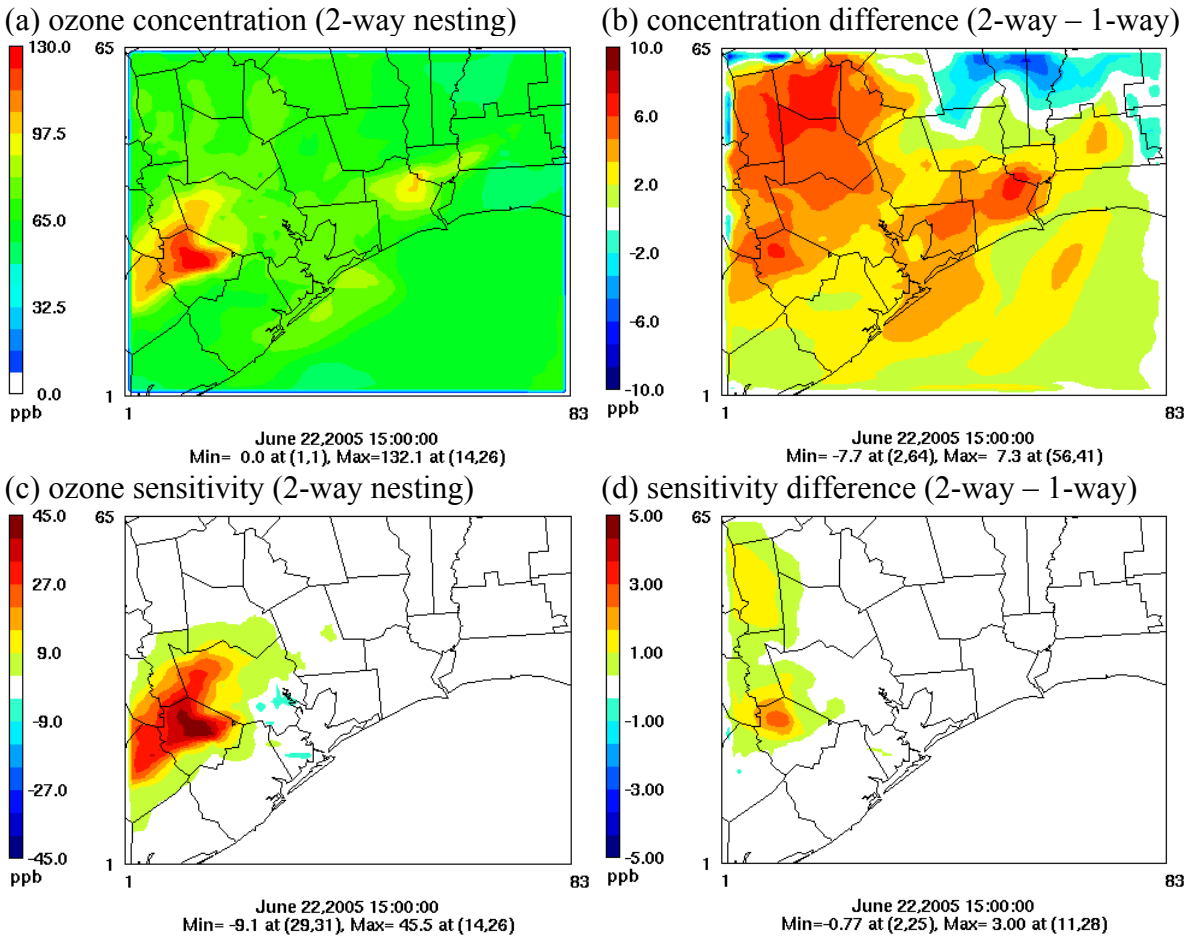

Figure 3-3. Differences in ozone concentrations and sensitivities to all Houston emissions between 1-way and 2-way nesting runs at 3 pm on June 22, 2005 (the hour of episode maximum 1-hour ozone concentration)

3.1.2. Revised Run Setup

One of the findings from the preliminary sensitivity modeling was that point source emissions of HRVOCs have little impact on ozone formation of the Houston region, which is inconsistent with the conceptual model and airplane measurement data. TCEQ has since updated the emissions inventory to "regular8" and also revised point source emissions with increased HRVOC emissions (reconciled emissions) in an attempt to improve model performance. This updated emissions inventory was used for the revised sensitivity runs along with updated meteorological data. The modeling domain and simulation period remain the same as the preliminary modeling.

The list of sensitivity parameters modeled for the revised sensitivity runs is also the same as that used for the preliminary runs (Tables 3-1 and 3-2). However, the point source emission category was redefined to exclude the emissions from fires and ships. The fire emissions were added to the biogenic emissions category. Initially, it was assumed that all the point source emissions were included in the elevated emissions files with the "regular8" emissions because no separate low-point emissions files were provided. However, it turned out that some point source emissions were still processed into low-level emissions. Affected sensitivity runs were later repeated with low-point emissions included. Note that results presented in this report are from the corrected runs.

In addition to the sensitivities to emissions, sensitivities to chemistry reaction rates were also calculated. Selected rate constants for the sensitivity modeling are listed and discussed in Section 3.2.

Since the HDDM was successfully implemented in the new EBI chemistry solver (Section 2.1), we used the EBI solver for the revised runs. Also, flexi-DDM was used instead of 1-way nesting: full grids were simulated for concentrations while sensitivity calculations were done only for the 4 and 2 km grids.

Main difference between the preliminary and revised run setups is in the emissions. Figures 3-4 to 3-7 compare "unreconciled" regular3 with "reconciled" regular8 for each sub-category of emissions.

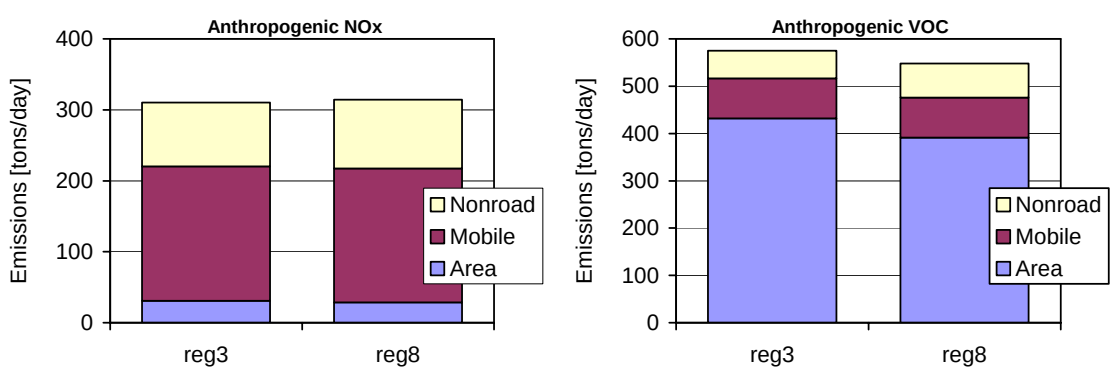

Figure 3-4. Episode average daily total NOx and VOC emissions of the Houston region (the 2-km grid) for area, mobile, and nonroad sub-categories

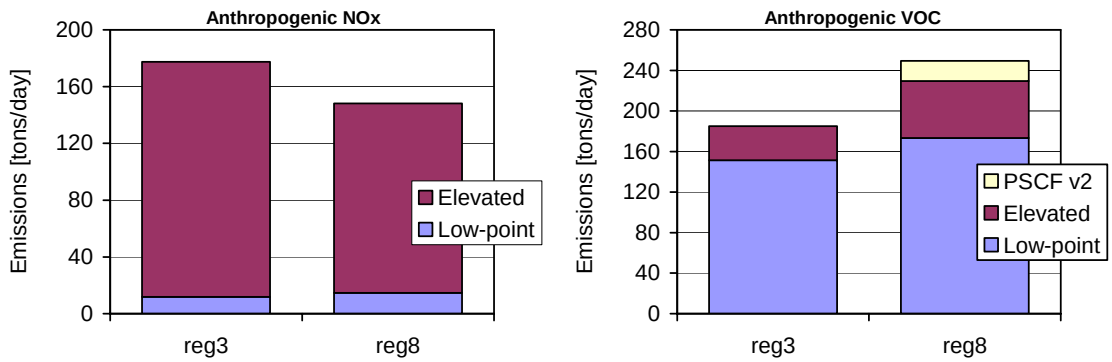

Figure 3-5. Episode average daily total point source NOx and VOC emissions of the Houston region (the 2-km grid): PSCF v2 (point source correction factor version 2) represents increased VOC emissions due to the reconciliation; the regular8 elevated emissions exclude emissions from fires and ships.

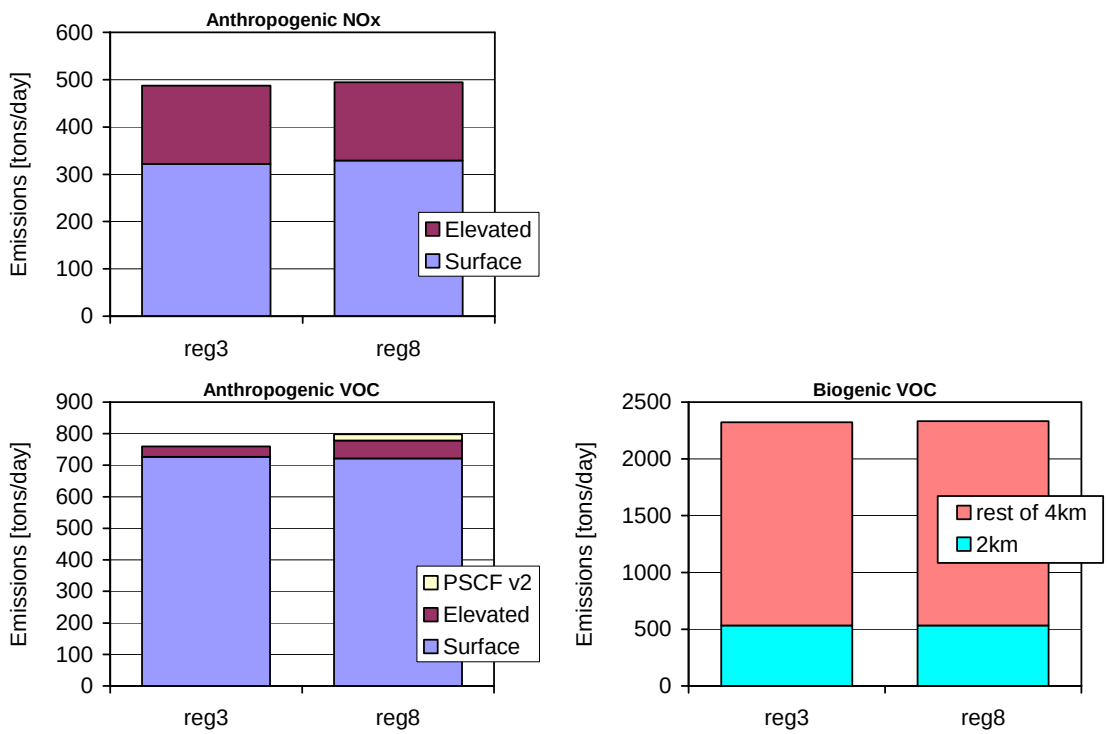

Figure 3-6. Episode average daily total NOx and VOC emissions from anthropogenic and biogenic sources: Anthropogenic emissions are shown for the Houston region (the 2-km grid); biogenic VOC emissions are grouped into the Houston region and the rest of the 4-km grid.

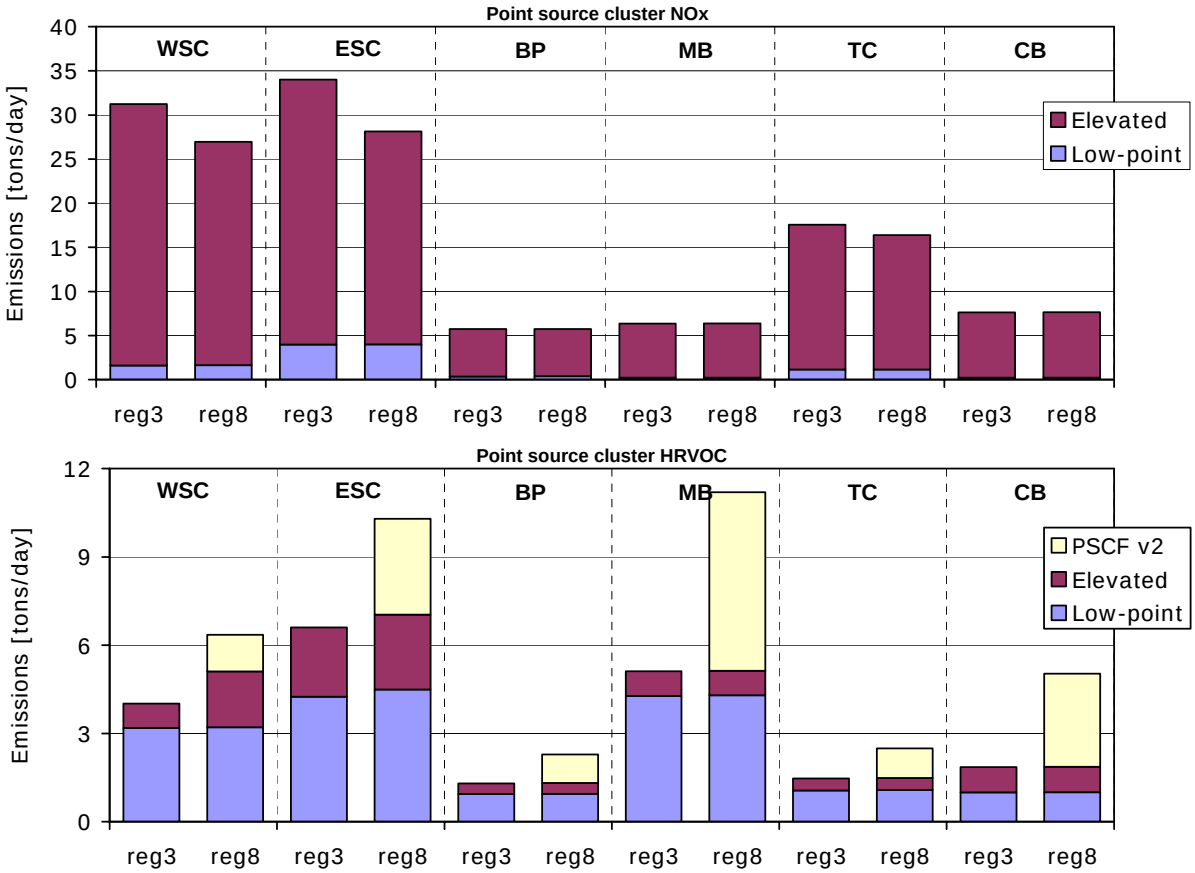

Figure 3-7. Episode average daily total NOx and HRVOC point source emissions from each of the point source clusters: West Ship Channel (WSC), East Ship Channel (ESC), Bayport (BP), Mont Belvieu (MB), Texas City (TC), and Chocolate Bayou (CB).

3.1.3. Episode Average Sensitivities

In this section, ozone sensitivities to the Houston emissions are presented on an episode average basis to show an overall picture for the whole episode. To emphasize the sensitivities at times of elevated ozone, the hours with less than 60 ppb of ozone were excluded from the averaging for each grid cell. The two spin-up days (17-18 June 2005) were also excluded. The following surface plots are based on the 4-km grid results (the nested 2-km grid results are aggregated into the parent 4-km grid results).

Figure 3-8 shows the episode average ozone concentrations from the preliminary runs (regular3) and the revised runs (regular8) with and without reconciliation. The episode average ozone concentration is slightly increased with the regular8 emissions primarily due to increased VOC emissions (Figure 3-6). While changing from 1-way nesting (preliminary) to 2-way nesting (revised) may also contribute the ozone difference, its effect on the episode average ozone is less pronounced. For the regular8 emissions, the reconciliation made little change in the average ozone concentration because the amount of added HRVOCs in the reconciled emissions is insignificant compared to the overall VOC emissions.

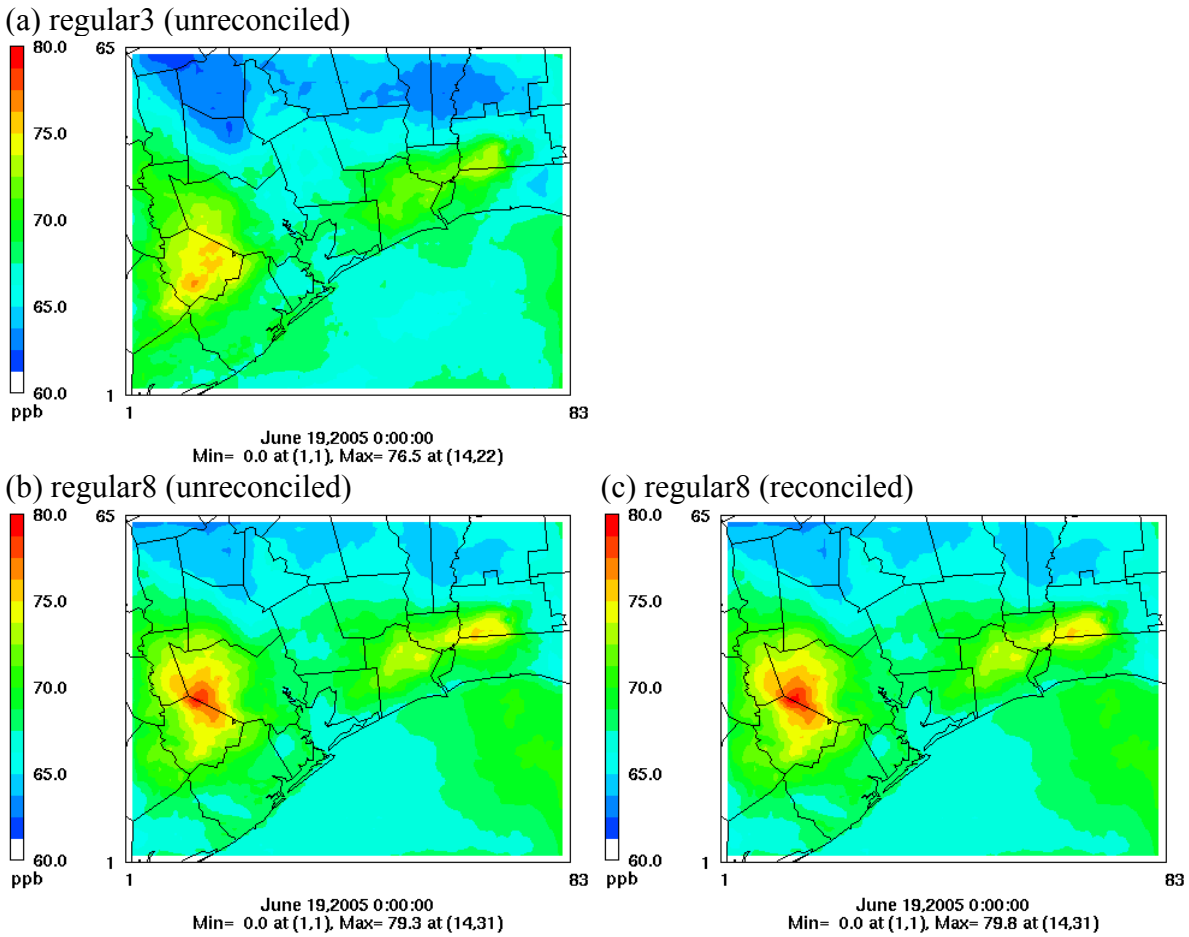

Figure 3-8. Episode average ozone concentrations with regular3 and regular8 (with and without reconciliation) emissions

Figure 3-9 compares episode average first-order ozone sensitivities to the Houston NOx emissions between the preliminary and revised runs for each of the area, mobile and nonroad emission categories. The ozone sensitivities to NOx emissions are mostly positive in the western region of the grid while negative sensitivity to NOx is observed in the south Harris County which indicates that ozone may increase with reduced NOx. The first-order sensitivities to the Houston VOC emissions show mostly positive response over Harris County (Figure 3-10). Both the preliminary and revised runs show similar results as the regular3 and regular8 emissions are mostly similar for these emission categories except for area emissions of VOC which are slightly lower with the regular8 emissions resulting less ozone sensitivity.

Differences between the regular3 and regular8 (reconciled) emissions are more pronounced in the point source emission category. NOx emissions are lower with regular8 because we excluded fires from the point source emissions. The regular8 (reconciled) VOC emissions are 35% higher than regular3. However, differences in the resulted ozone sensitivities are only a few ppb (Figure 3-11).

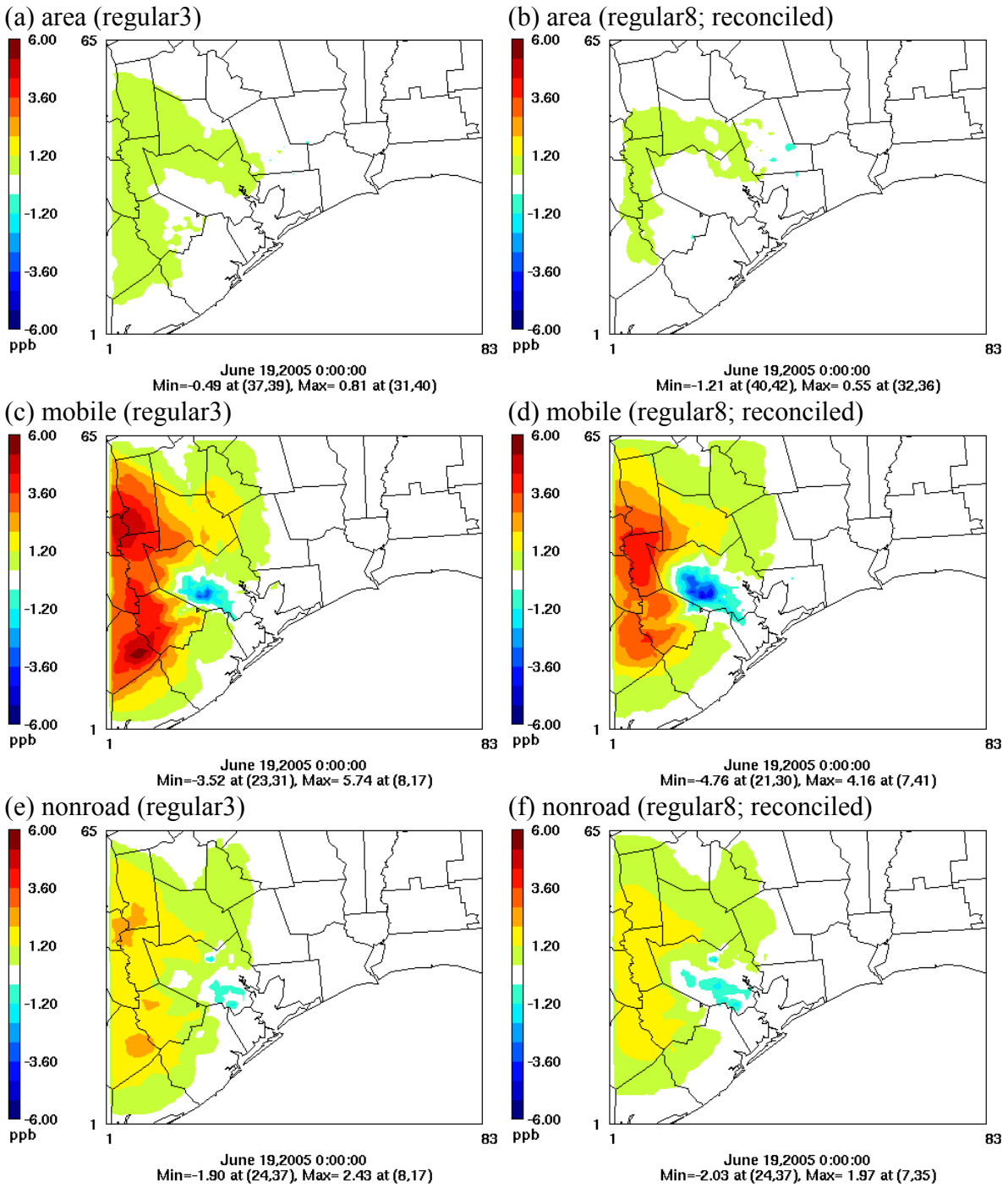

Figure 3-9. Episode average first-order ozone sensitivities to the Houston NOx emissions for area, mobile, and nonroad sub-categories

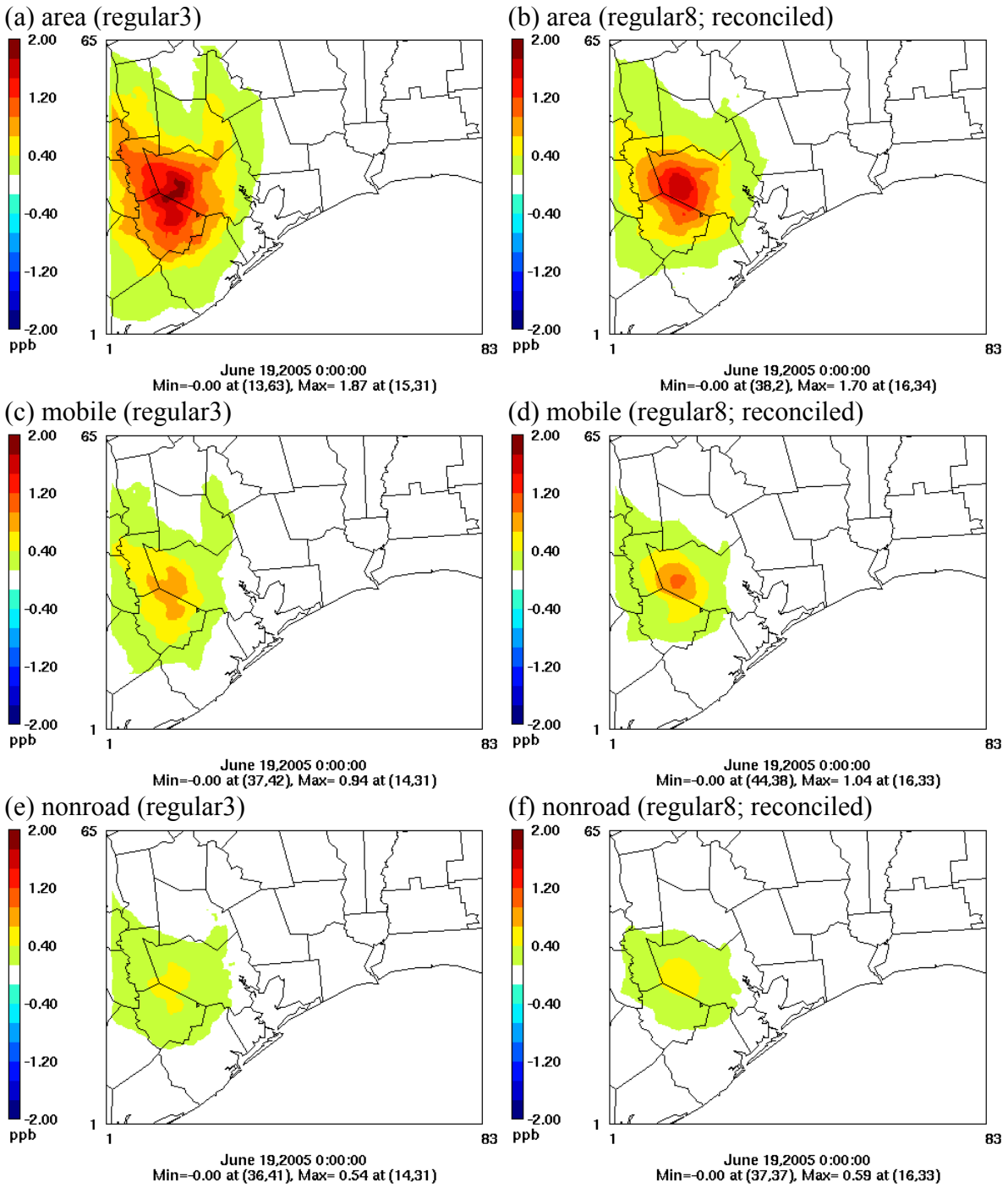

Figure 3-10. Episode average first-order ozone sensitivities to the Houston VOC emissions for area, mobile, and nonroad sub-categories

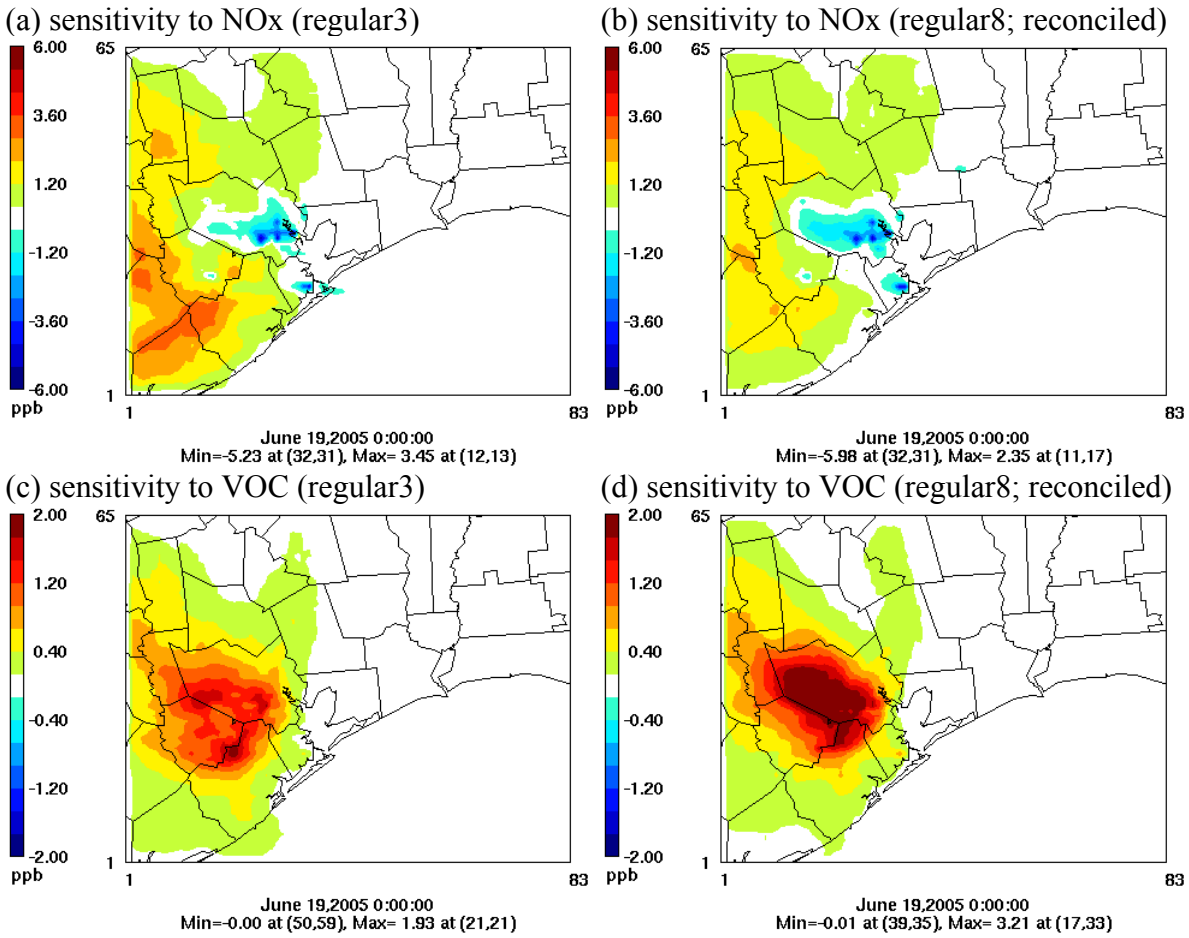

Figure 3-11. Episode average first-order ozone sensitivities to NOx and VOC emissions from point sources in the Houston region

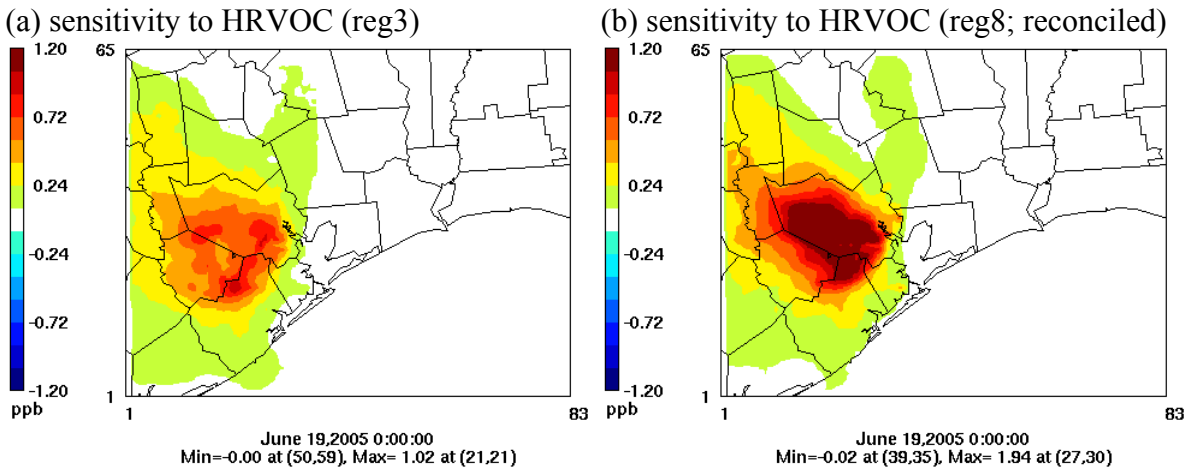

Figure 3-12. Episode average first-order ozone sensitivities to (collective and individual) HRVOC emissions from point sources in the Houston region

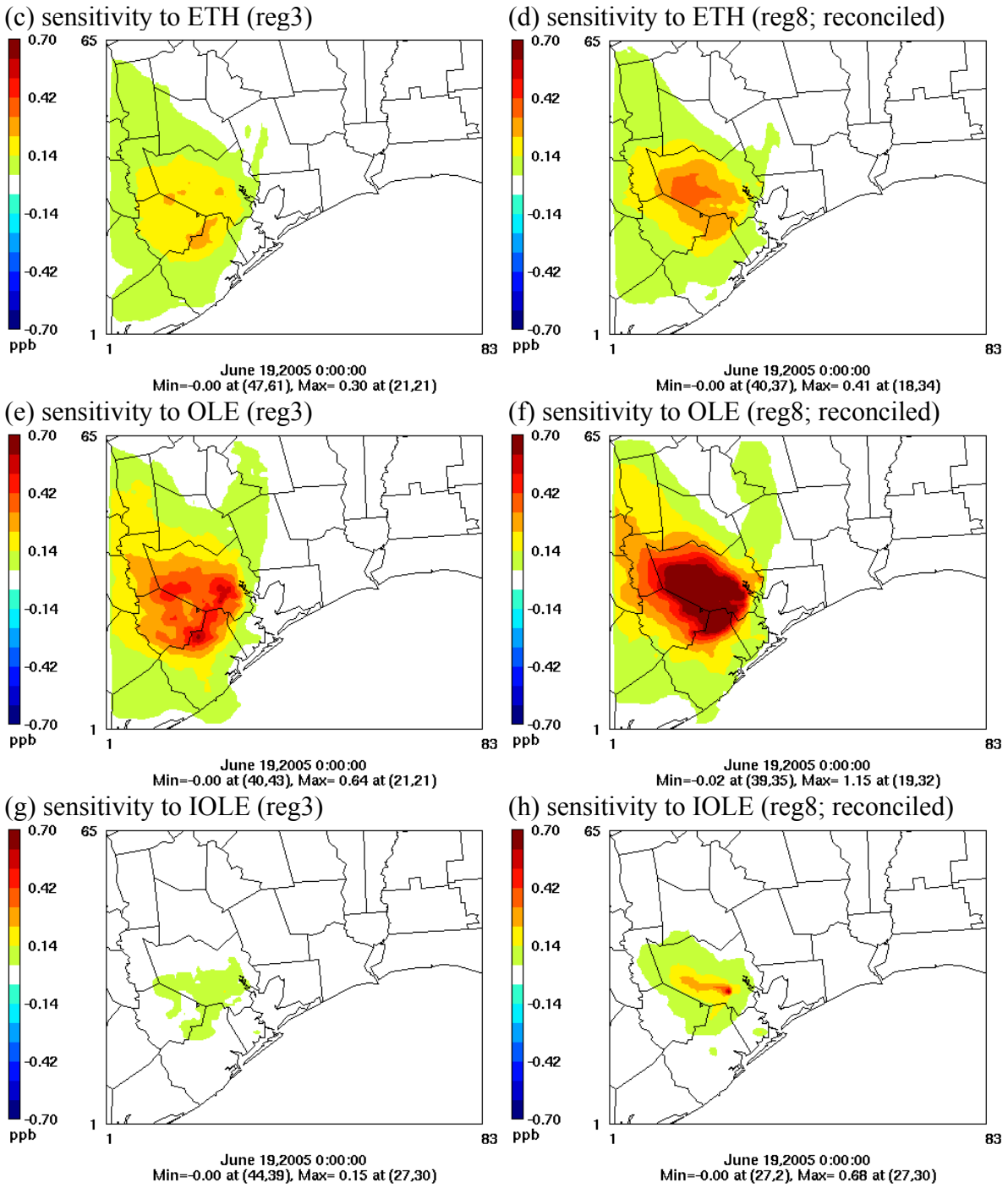

Figure 3-12. Episode average first-order ozone sensitivities to (collective and individual) HRVOC emissions from point sources in the Houston region (continued)

Figure 3-12 shows the impact of point source HRVOC emissions on ozone formation over the Houston region. OLE (terminal olefin carbon bond) is dominant among the CB05 HRVOC species. Again, overall sensitivity of ozone to HRVOC emissions is insignificant even with reconciliation.

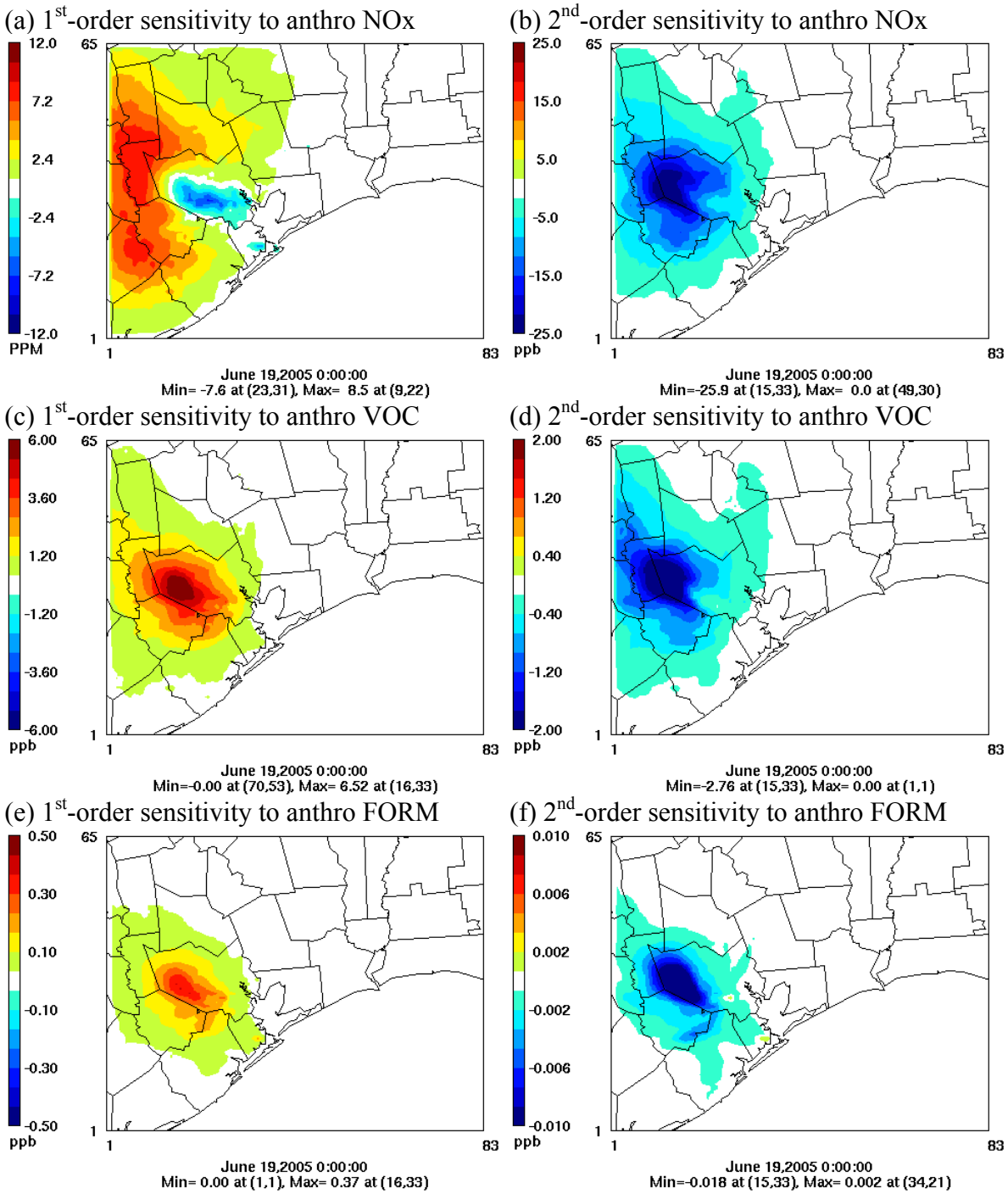

Figure 3-13. First- and second-order sensitivities of episode average ozone to anthropogenic NOx, VOC, and FORM emissions in the Houston region by the revised modeling (regular8; reconciled)

The first- and second-order sensitivities of episode average ozone to the Houston anthropogenic NOx, VOC, and formaldehyde (FORM) emissions (regular8; reconciled) are shown in Figure 3-13. The western part of the domain exhibits NOx-limited condition while Harris County shows VOC-limited condition (and NOx disbenefit). The self second-order ozone sensitivities to both NOx and VOC emissions are mostly negative indicating concave responses: ozone becomes less

responsive as the emissions increase. Spikes in formaldehyde concentrations observed during Texas Air Quality Study raised questions on the importance of primary formaldehyde emissions. However, sensitivities to formaldehyde emissions turned out to be insignificant for this episode.

The first- and self second-order sensitivities to the 4-km domain biogenic VOC emissions show similar characteristics to the sensitivities to anthropogenic VOC emissions, but with larger area of influence (Figure 3-14). Negative cross sensitivity to the emissions of biogenic and anthropogenic VOC emissions means that if biogenic VOC emissions increase, ozone will become less sensitive to anthropogenic VOC emissions, and vice versa.

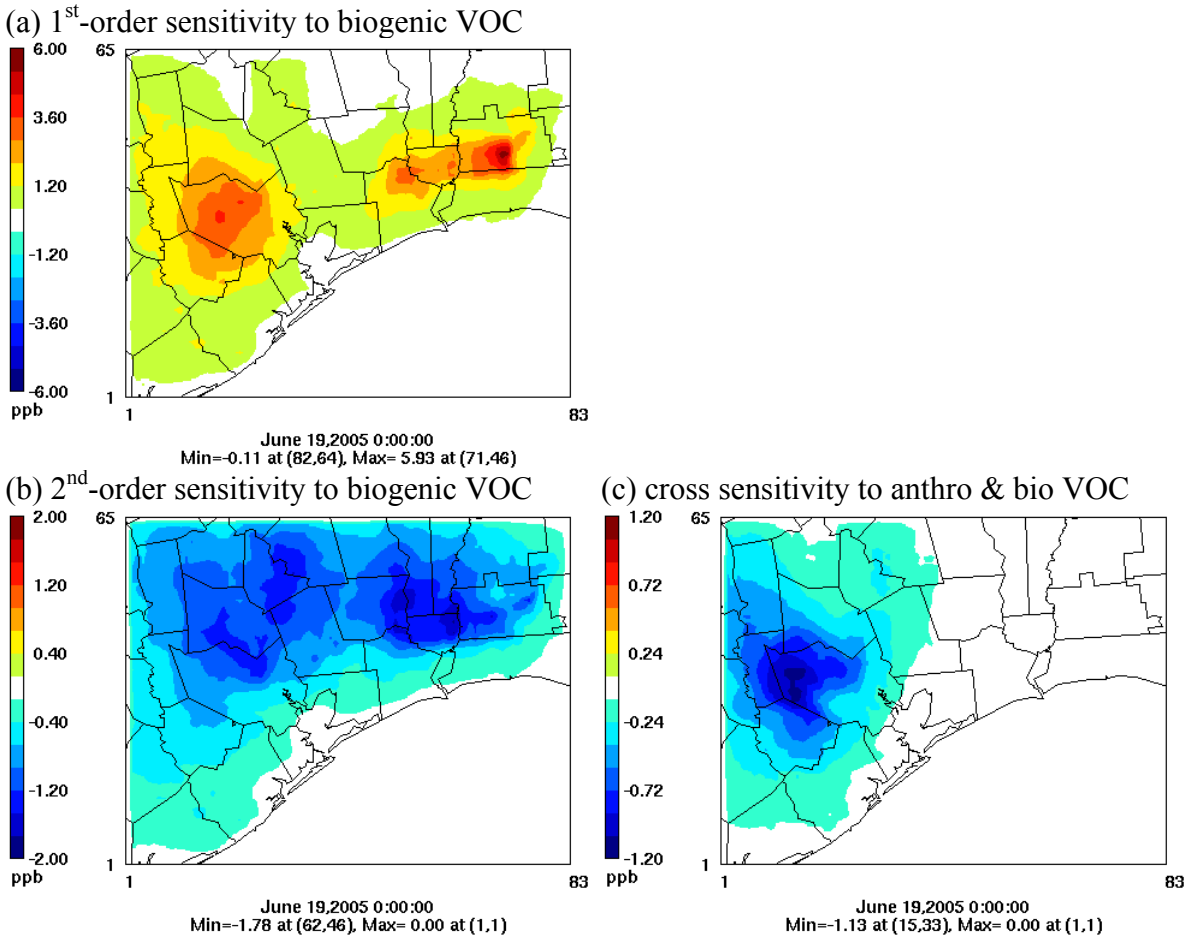

Figure 3-14. First- and second-order sensitivities of episode average ozone to biogenic VOC emissions in the 4-km domain; cross sensitivity to the Houston region anthropogenic VOC and the 4-km domain biogenic VOC; by the revised modeling (regular8; reconciled)

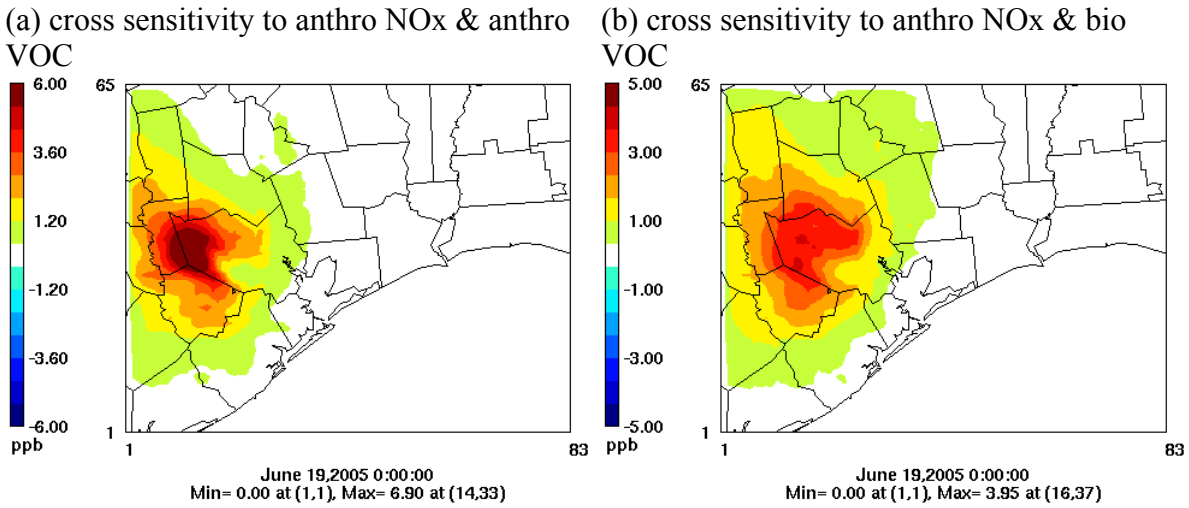

Figure 3-15. Cross sensitivities of episode average ozone to the Houston region anthropogenic NOx and VOC emissions; to the Houston region anthropogenic NOx and the 4-km domain biogenic VOC emissions; by the revised modeling (regular8; reconciled)

Cross sensitivities to NOx and VOC emissions are mostly positive in the downwind area indicating that ozone will become less responsive to NOx emission changes if VOC emissions are reduced, and vice versa (Figure 3-15). Cross sensitivities are useful in uncertainty analysis, which will be discussed in Section 3.3.

The preliminary sensitivity modeling resulted in similar sensitivity plots to Figures 3-13 to 3-15 (not shown).

Ozone sensitivities to HRVOC emissions from six point source clusters were also examined. Figures 3-16 and 3-17 show episode average first-order ozone sensitivities to HRVOC and NOx emissions from each point source clusters (with reconciled regular8 emissions). The sensitivities to HRVOC emissions are mostly positive, but very small even with reconciled emissions. The sensitivities to NOx emissions are negative near sources and positive downwind. HRVOC emissions from the two Ship Channels and Mont Belvieu have relatively higher impact on ozone concentrations. The second-order sensitivities to the point source cluster emissions are mostly negligible indicating almost linear response to emissions (not shown).

Since the episode average ozone sensitivities to the point source cluster HRVOC emissions are small, we looked at episode maximum 1-hour ozone sensitivities to HRVOC emissions from three clusters (West and East Ship Channels and Mont Belvieu) to see how much impact they can have on ozone formation in the region (Figure 3-18). HRVOC emissions from West and East Ship Channel clusters have the highest impact on ozone at noon on June 29 reaching maximum ozone sensitivities of 10 and 12 ppb, respectively. Mont Belvieu HRVOC emissions show maximum ozone sensitivity (8 ppb) in early morning (7 am) on the same day. However, peak ozone concentration on June 29 occurred at 2 pm and relatively low ozone concentrations are observed in the morning.

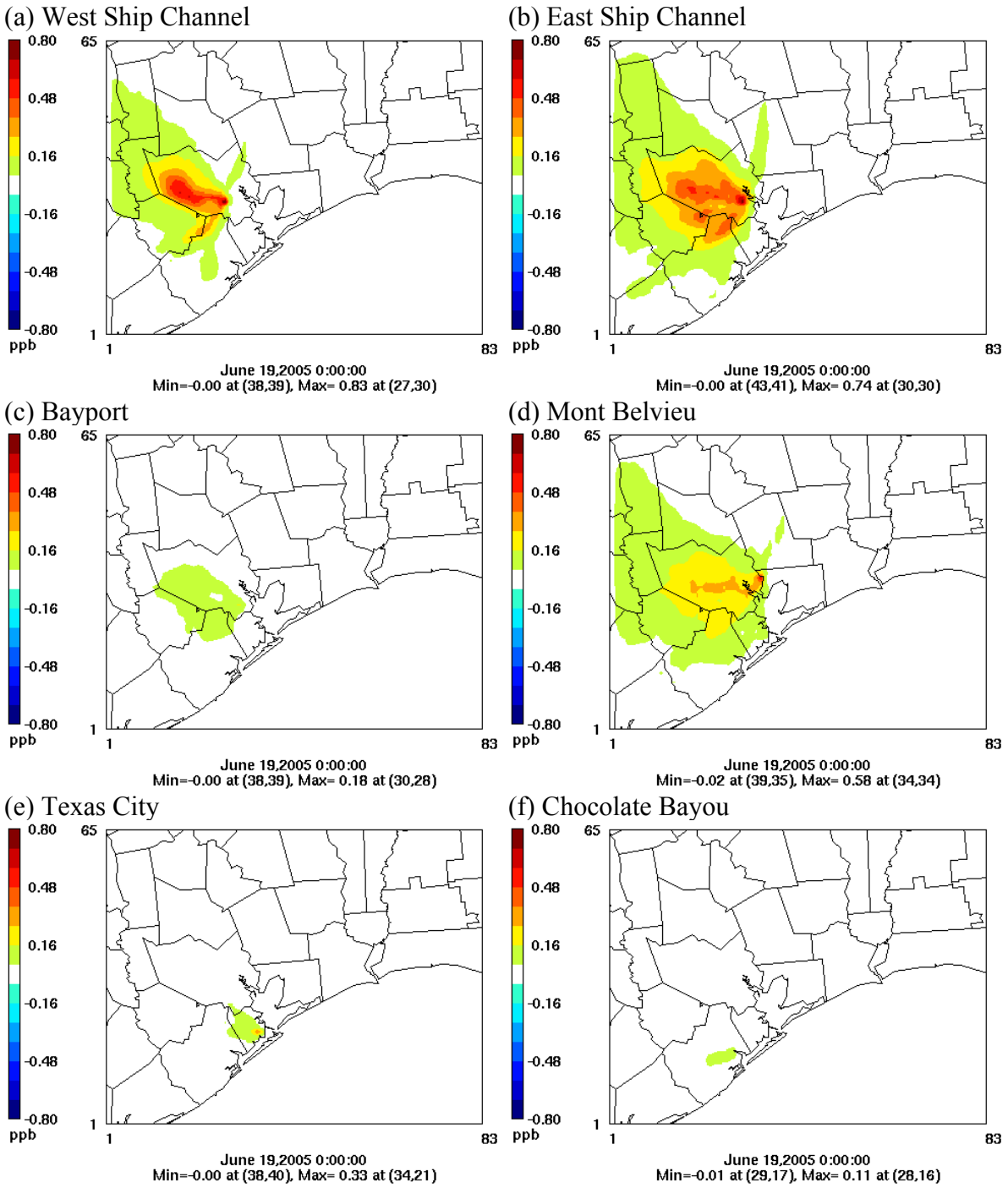

Figure 3-16. Episode average first-order ozone sensitivities to HRVOC emissions from each point source cluster by the revised modeling (regular8; reconciled)

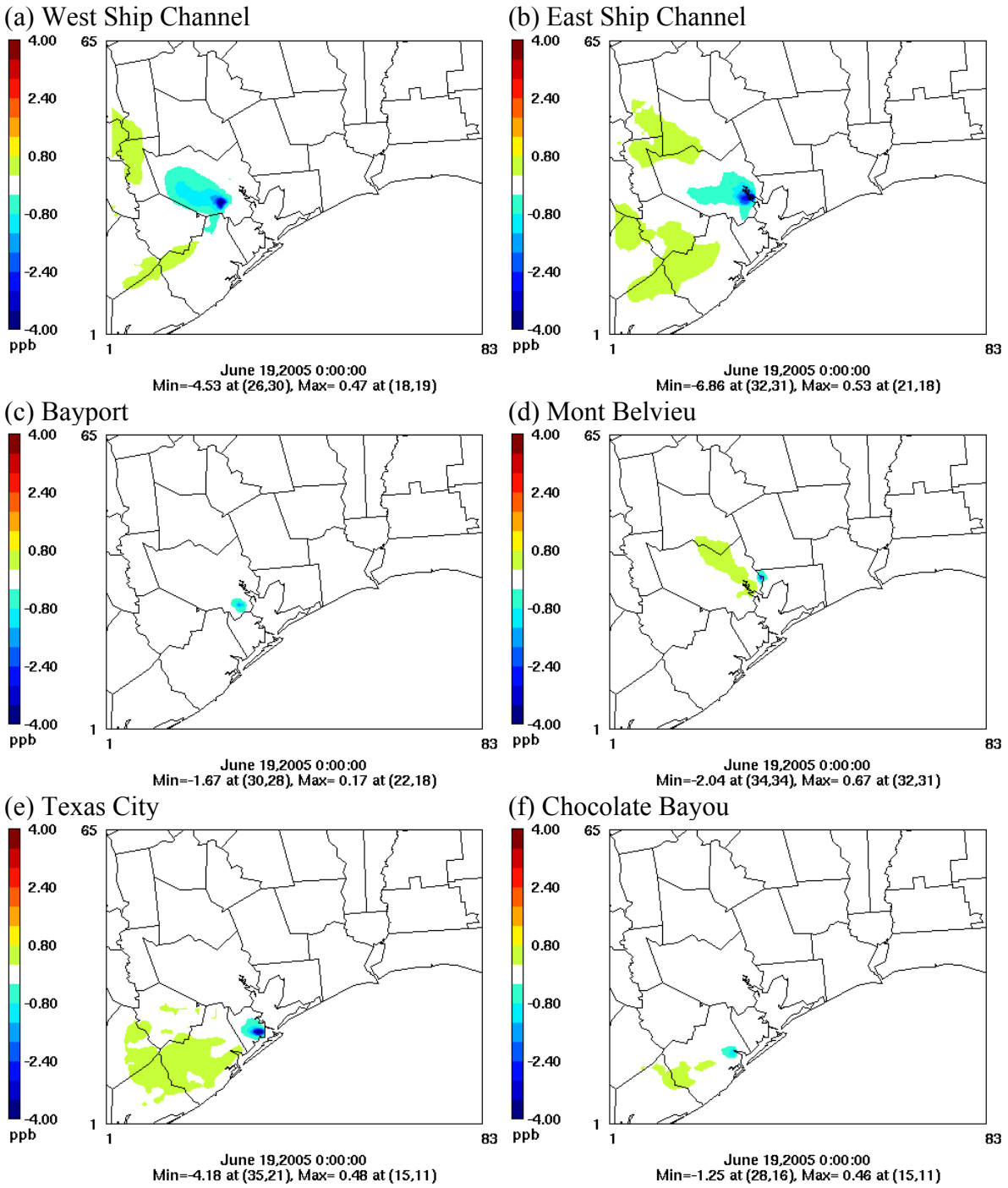

Figure 3-17. Episode average first-order ozone sensitivities to NOx emissions from each point source cluster by the revised modeling (regular8; reconciled)

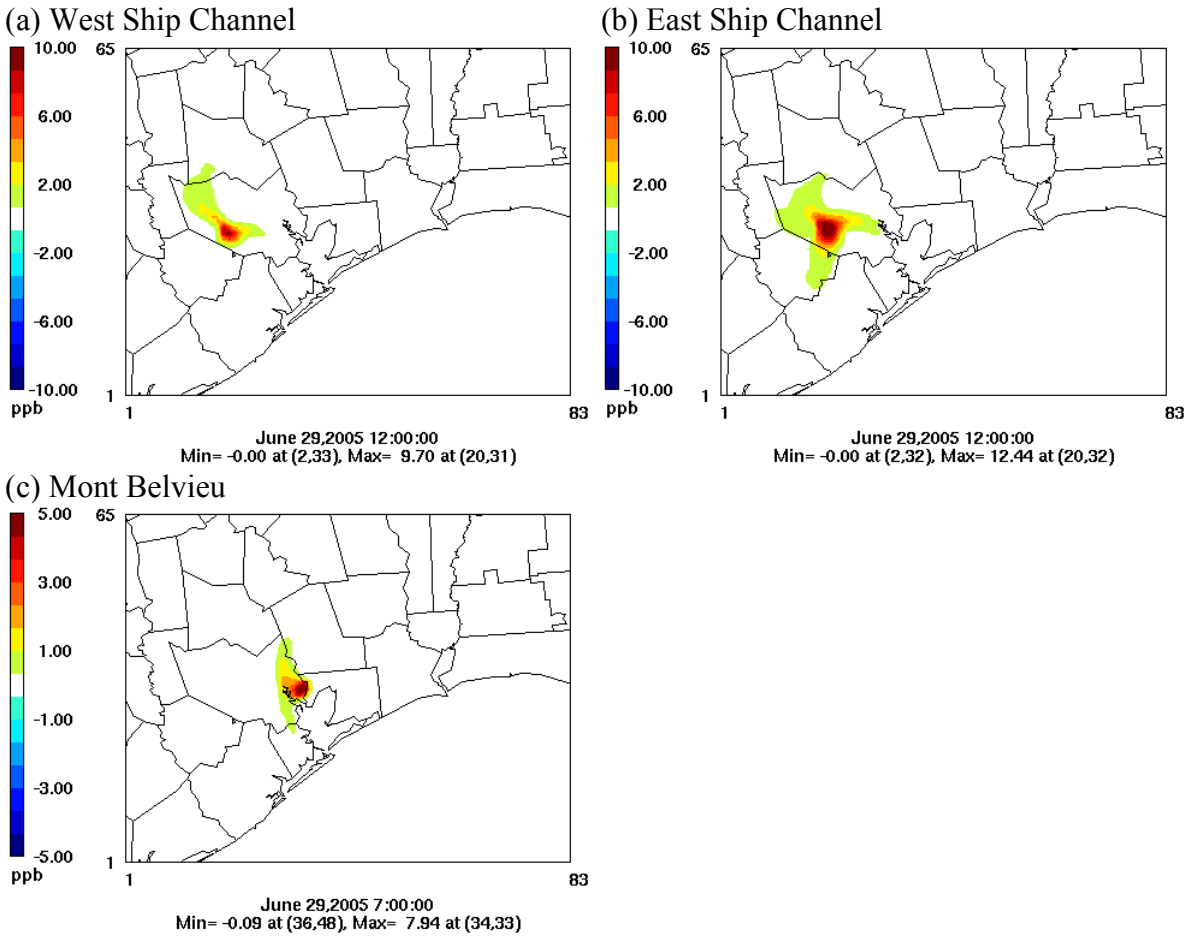

Figure 3-18. Episode maximum first-order 1-hour ozone sensitivities to HRVOC emissions from West and East Ship Channels and Mont Belvieu by the revised modeling (regular8; reconciled)

3.1.4. 8-hour Maximum Ozone Sensitivities

The previous section showed sensitivity results on an episode-average basis for times when ozone concentrations were above 60 ppb. For development of 8-hour ozone control strategies, it is often important to know how emissions influence ozone during the 8-hour window each day when ozone concentrations are modeled to be highest. To assess results on this basis, each day's model outputs for concentrations and sensitivities were processed to compute their average value in each grid cell over the 8-hour period when that gird cell had its maximal ozone concentration.

The peak 8-hour ozone concentrations in the Houston for each day of the episode are summarized in Table 3-3. These results are based on the 4-km resolution domain, in which each grid cell over the sub-domain averages results from four of the 2-km sub-domain grid cells. Because June 21, 22, and 23 had the highest 8-hour ozone concentrations of the episode, this report focuses on results from those days.

Table 3-3. Peak 8-hour ozone concentrations in Houston region during episode

Date	Peak 8-hr O3
June 19	91 ppb
June 20	91 ppb
June 21	101 ppb
June 22	102 ppb
June 23	93 ppb
June 24	78 ppb
June 25	88 ppb
June 26	90 ppb
June 27	90 ppb
June 28	86 ppb

Figures 3-19 to 3-21 show 8-hour ozone concentrations and their sensitivities to Houston region (defined as the 2-km sub-domain) emissions of anthropogenic NO_x and anthropogenic VOC, for June 21, 22, and 23, 2005. The middle plots for each day show the first-order sensitivity coefficients, reflecting the rate of change in ozone concentrations for emissions perturbations relative to the base case. These sensitivities can be scaled to predict the impacts of small changes in emissions. For example, on June 21, the largest 8-hour ozone sensitivity to Houston NO_x was 21 ppb. This indicates that a 10% reduction in Houston NO_x emissions would cause 8-hour ozone concentrations on that day in that grid cell to decline by about 2.1 ppb. The VOC sensitivities can be scaled and interpreted in a similar fashion. First-order sensitivities of ozone to emissions can typically scaled up to about +/- 30% before non-linearity causes significant loss of accuracy (Cohan et al., 2005).

The bottom images in Figures 3-19 to 3-21 show the zero-out contributions (ZOC) of Houston region anthropogenic NO_x and VOC emissions to 8-hour ozone concentrations. The ZOC of an emissions source is the amount by which concentrations would be reduced if that source was completely removed. The ZOCs are computed from the first- and second-order sensitivity coefficients as shown in Equation 1:

$$ZOC = S^{(1)} - \tfrac{1}{2} S^{(2)} \qquad (1)$$

Note that Equation 1 is equivalent to the second-order Taylor series expansion of sensitivity coefficients, with the amount of perturbation scaled to -100%.

The three days showed markedly different patterns of ozone responsiveness to NO_x and VOC (Figures 3-19 to 3-21). On June 21, ozone was primarily sensitive to NO_x, with some sensitivity to VOC. The magnitudes of the ZOCs were larger than the magnitudes of the first-order sensitivity coefficients, reflecting the negative values of the second-order sensitivity coefficients and the saturating responsiveness of ozone to each emission species. On June 22, the eastern part of the peak ozone plume was primarily sensitive to VOC and exhibited a disbenefit to NO_x controls. Meanwhile, the western or downwind portion of the plume was primarily NO_x sensitive and showed little sensitivity to VOCs.

June 23 showed an even more dramatic contrast between VOC-limited ozone conditions, with strong negative NO_x sensitivity over Harris County, but NO_x limited conditions downwind. Concentrations above 85 ppb on that day occurred within both regimes. The contrasts between the first-order sensitivity coefficients and the ZOCs for NO_x on that day were especially pronounced. Parts of northwest Harris County displayed negative first-order sensitivity to NO_x but large positive ZOC from NO_x. In DDM, this reflects strongly negative second-order sensitivity coefficients of ozone to NO_x in those locations. Physically, this implies that June 23 ozone concentrations might increase at those locations for small reductions in Houston NO_x, but decrease with larger reductions.

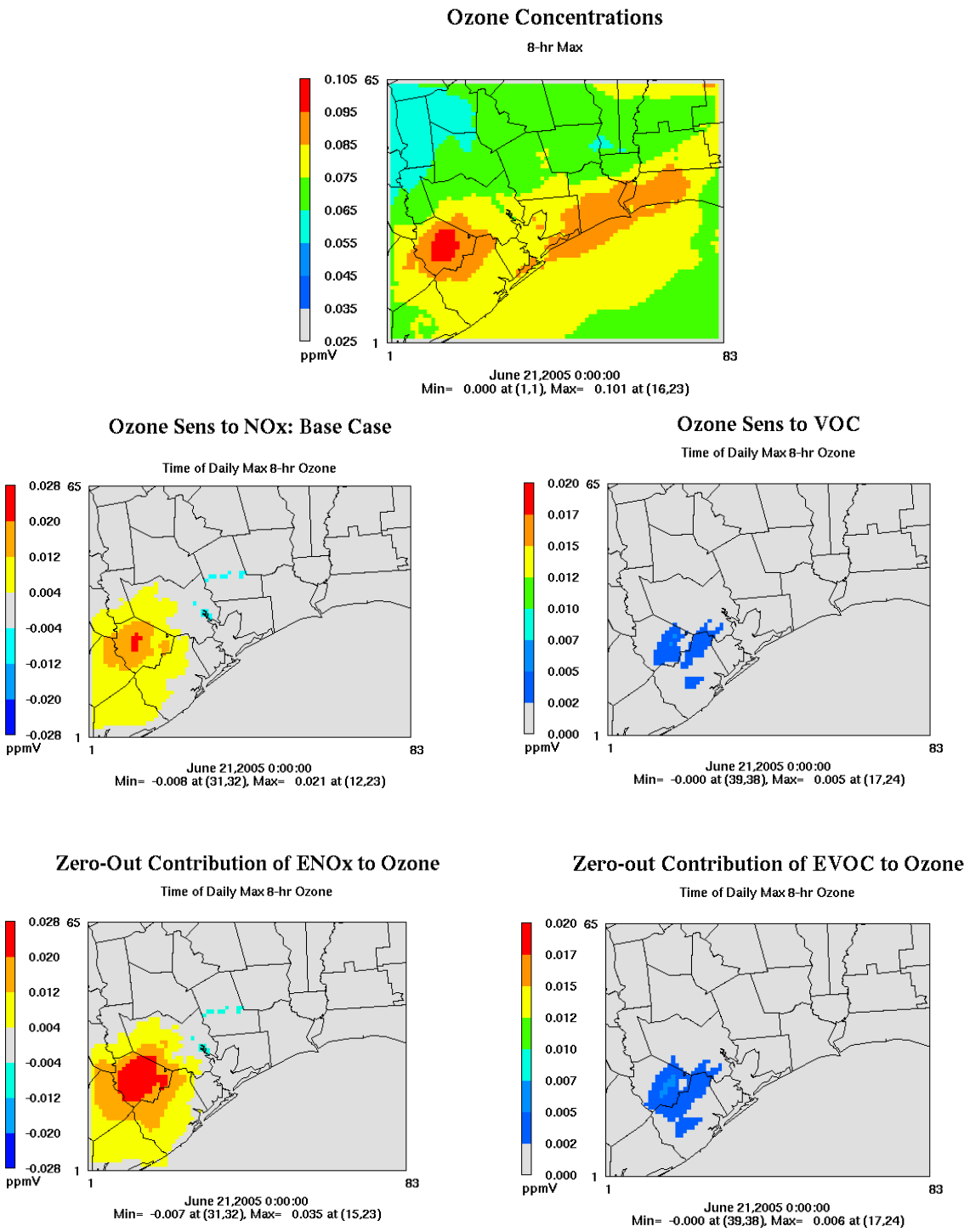

Figure 3-19. Ozone concentrations (top), their sensitivities to Houston-region anthropogenic NO_x (middle L) and VOC (middle R), and the zero-out contribution of Houston NO_x and VOC, on June 21, 2005.

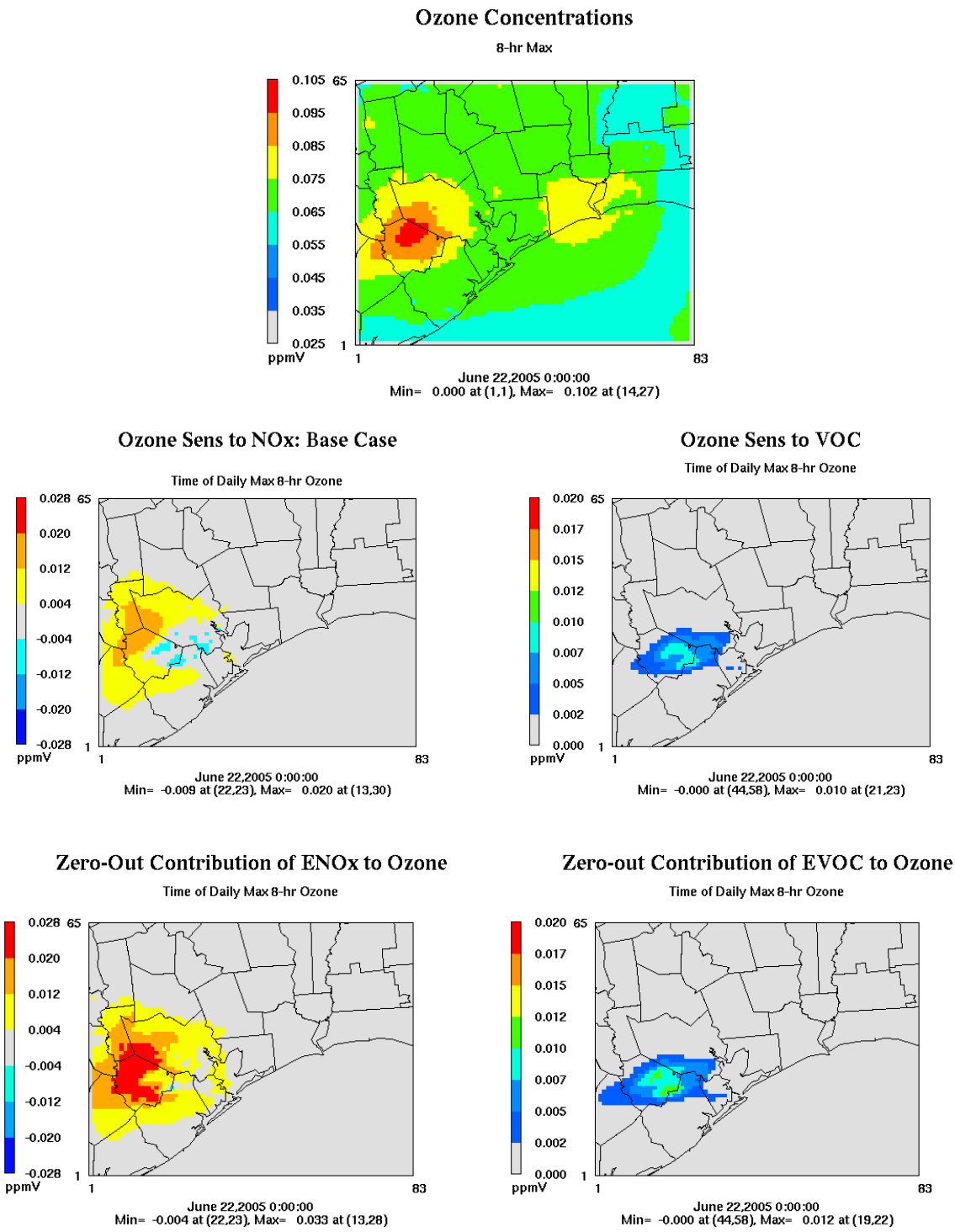

Figure 3-20. As in Figure 1, for June 22, 2005.

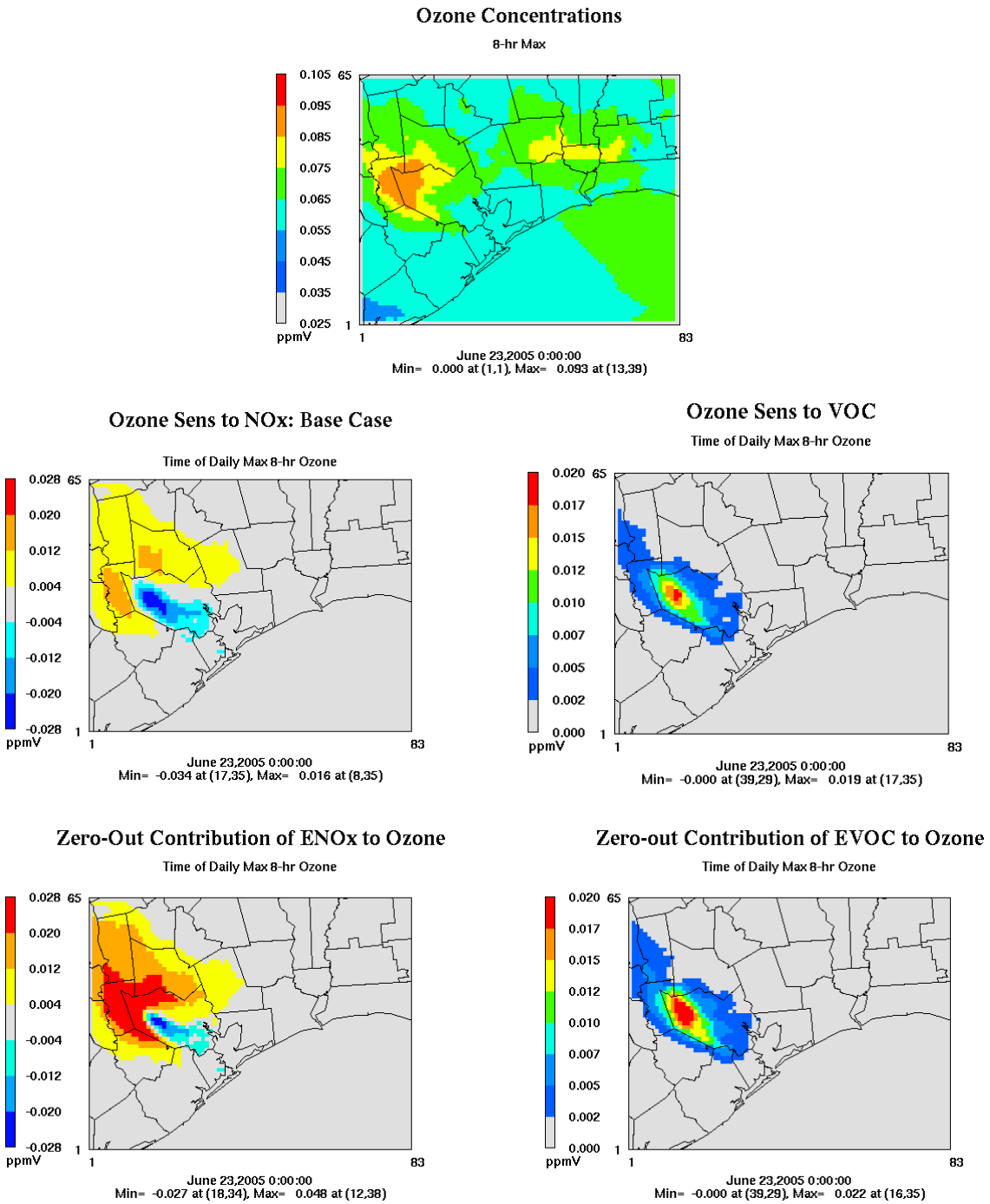

Figure 3-21. As in Figure 1, for June 23, 2005.

3.1.5. Ozone Isopleths

First- and second-order sensitivity coefficients can be used to estimate the concentrations that would result if two input parameters, p_j and p_k, are simultaneously perturbed by fractions ε_j and ε_k (Hakami et al., 2003). The estimation is computed by applying Equation 2, which also includes a cross-sensitivity term $S_{j,k}^{(2)}$ to account for interactions between the impacts of changing the two parameters.

$$C_{\varepsilon_j,\varepsilon_k} \approx C_{base} + \varepsilon_j S_j^{(1)} + \tfrac{1}{2}\varepsilon_j^2 S_j^{(2)} + \varepsilon_k S_k^{(1)} + \tfrac{1}{2}\varepsilon_k^2 S_k^{(2)} + \varepsilon_j \varepsilon_k S_{j,k}^{(2)} \qquad (2)$$

For predicting ozone changes when j and k represent joint controls of NO_x and VOCs, the second-order self sensitivities $S_j^{(2)}$ and $S_k^{(2)}$ will typically be negative, reflecting saturating (concave down) response. Meanwhile, the cross-sensitivity term $S_{j,k}^{(2)}$ will typically be positive, because reductions in emissions of one pollutant enhance ozone's sensitivity to the other pollutant.

We apply Equation 2 with CAMx-HDDM sensitivity coefficients to create isopleths (i.e., response surfaces) of ozone concentrations under various levels of Houston anthropogenic NO_x and VOC emissions, following the method of Hakami et al. (2004). Results were plotted each day for the 4-km grid cell containing the highest 8-hour ozone concentration (Figures 3-22 to 3-26). Although confidence in the estimates diminishes toward the corners of the plots where emissions perturbations are especially large, studies have shown that second-order Taylor expansions can remain accurate for perturbations beyond +/- 50% (Cohan et al., 2005; Napelenok et al., 2008).

The response surfaces show markedly different patterns of peak ozone responsiveness on different days. June 19-21 display mostly NO_x-limited conditions at the peak cell. On June 22-27, the peak cell base case falls close to the ridge line dividing NO_x-limited and VOC-limited conditions. On June 28, the base case is actually above the ridge line, and thus the cell would be expected to experience some disbenefit from NO_x controls before benefiting from larger controls.

Response surfaces were also plotted for a downtown location (Figures 3-27 and 3-28) and for a Ship Channel location between the East Ship Channel and West Ship Channel point source clusters described earlier (Figure 3-29). The plumes of greatest ozone concentrations occurred northwest of downtown on most days of the episode, so these locations exhibited moderate ozone concentrations and modest sensitivities to local emissions. The downtown location was slightly NO_x limited on June 21 and 22, but VOC limited on June 23. The Ship Channel location was also VOC limited on June 23.

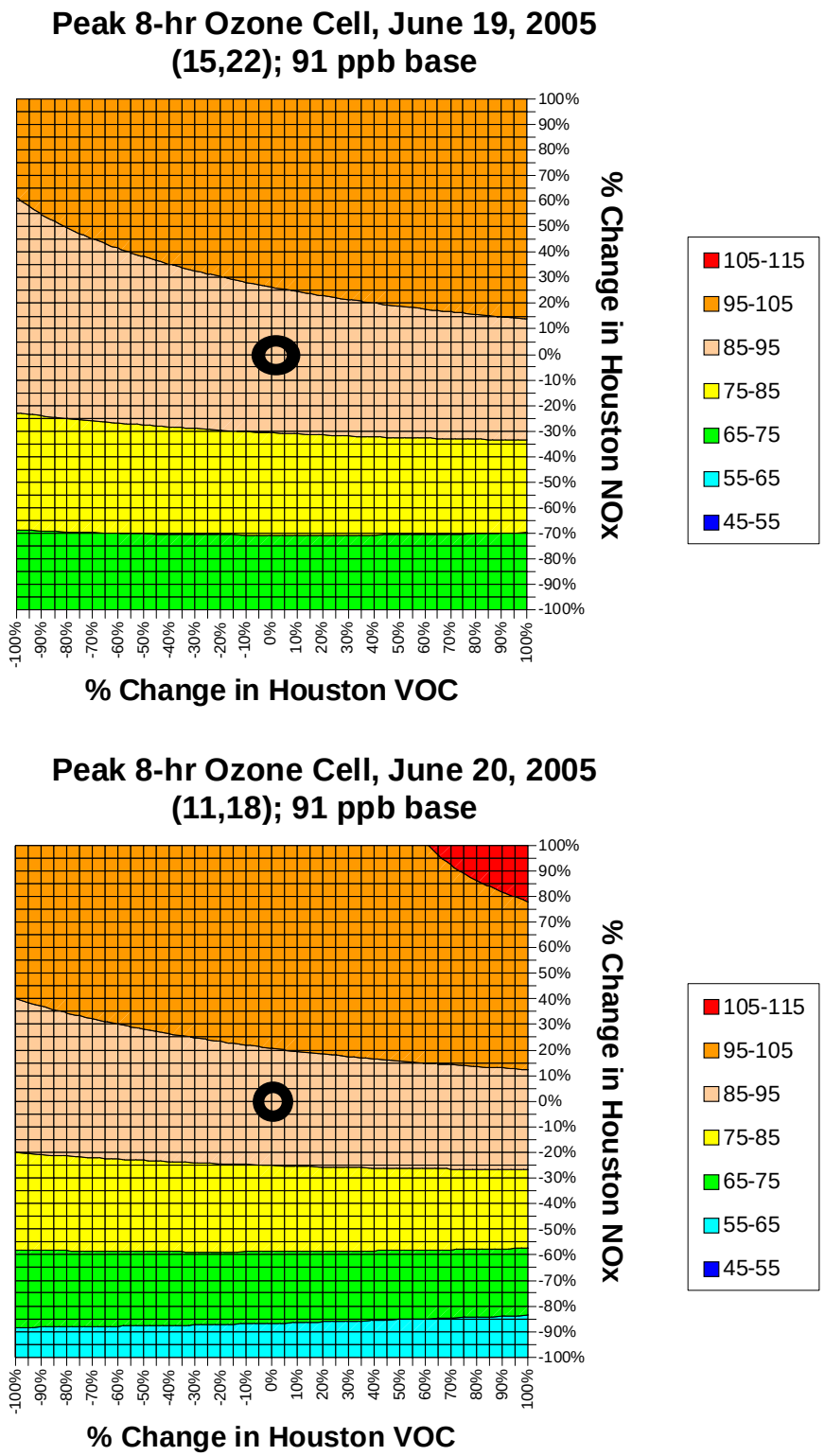

Figure 3-22. Second-order HDDM approximation of the response surface of peak 8-hour ozone concentrations to changes in Houston region anthropogenic NO_x and VOC emissions, for June 19 (top) and June 20 (bottom), 2005. The circle marks base case conditions (i.e., 0% change in NO_x and VOC).

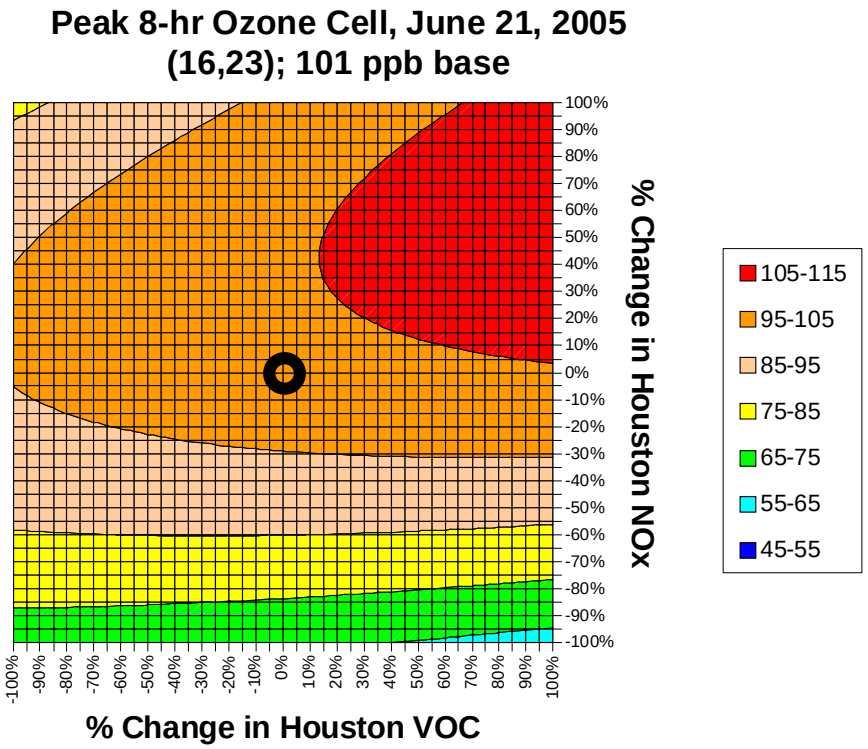

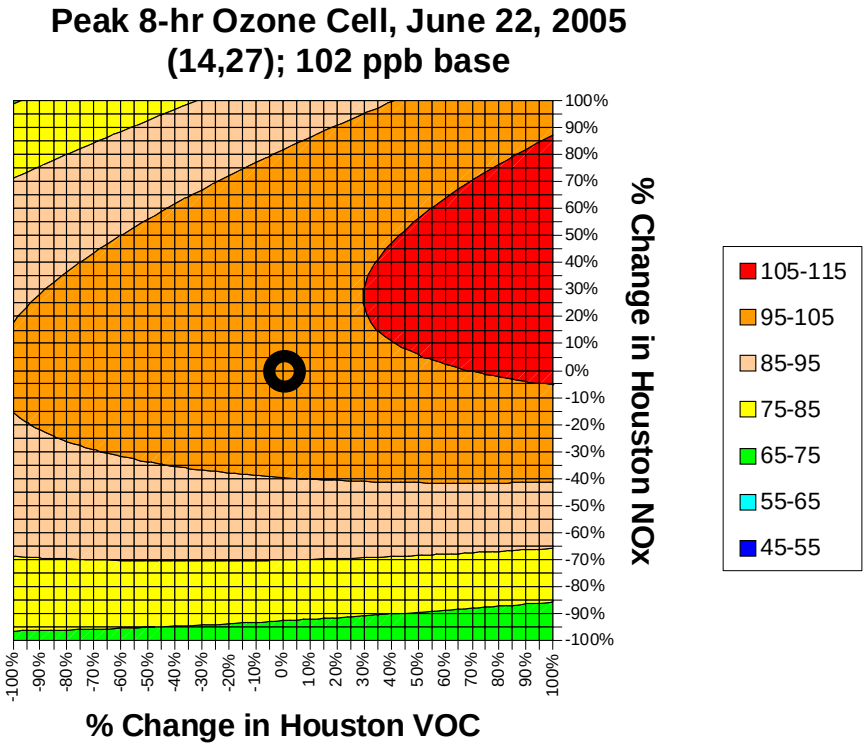

Figure 3-23. As in Figure 3-22, for June 21 (top) and June 22 (bottom).

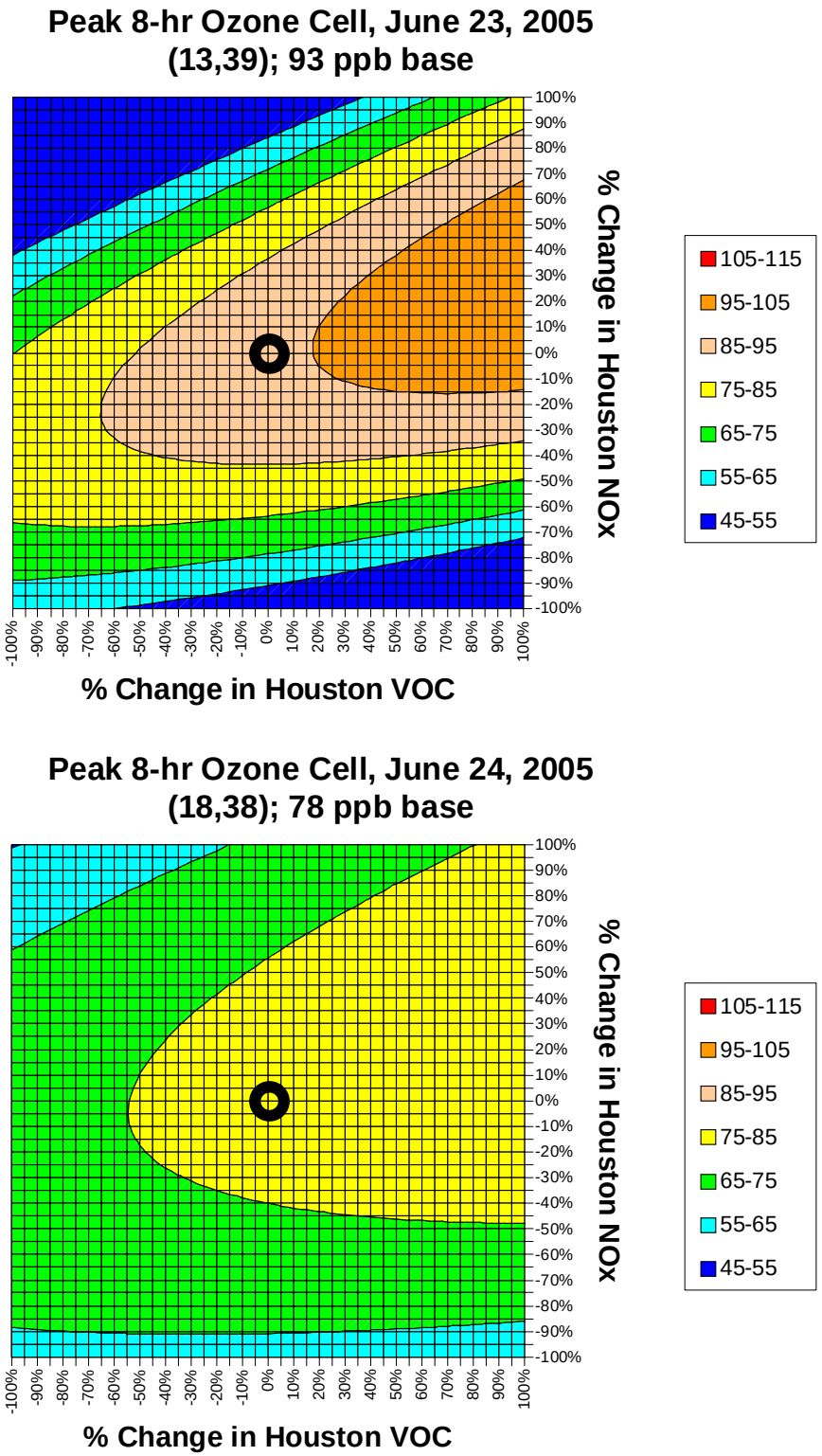

Figure 3-24. As in Figure 3-22, for June 23 (top) and June 24 (bottom).

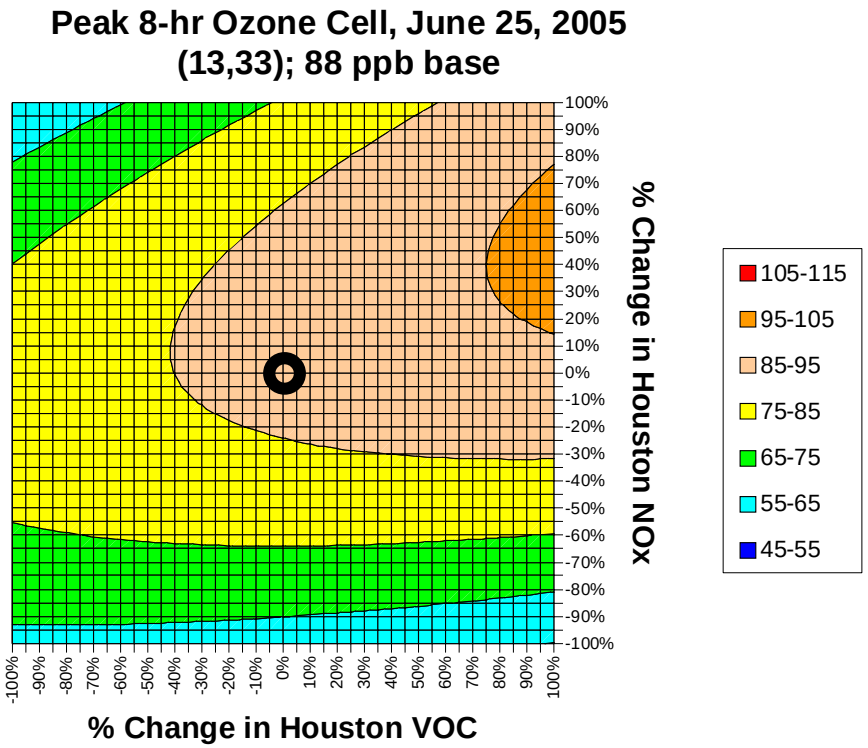

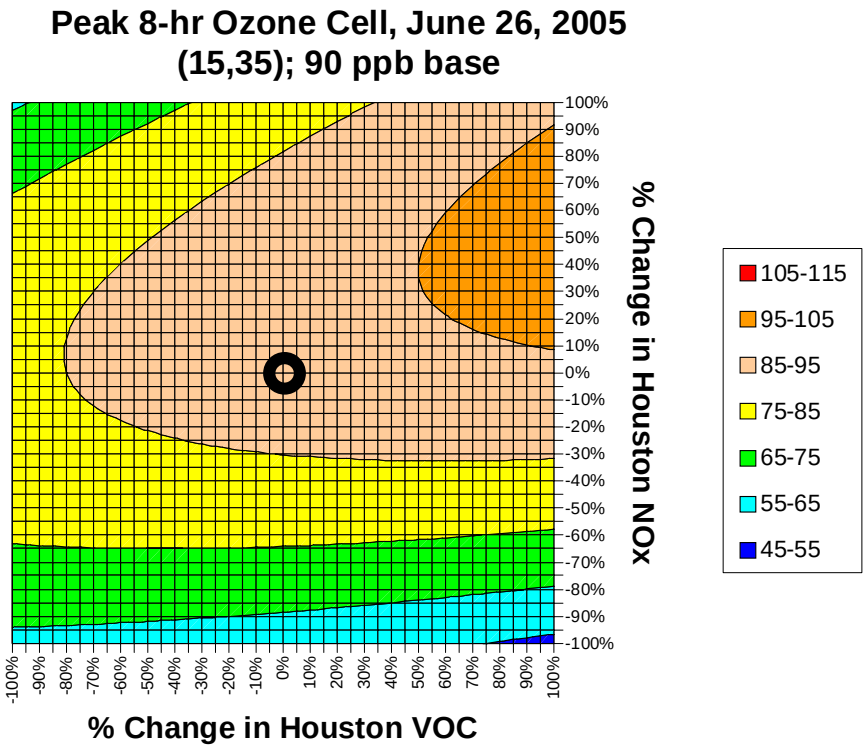

Figure 3-25. As in Figure 3-22, for June 25 (top) and June 26 (bottom).

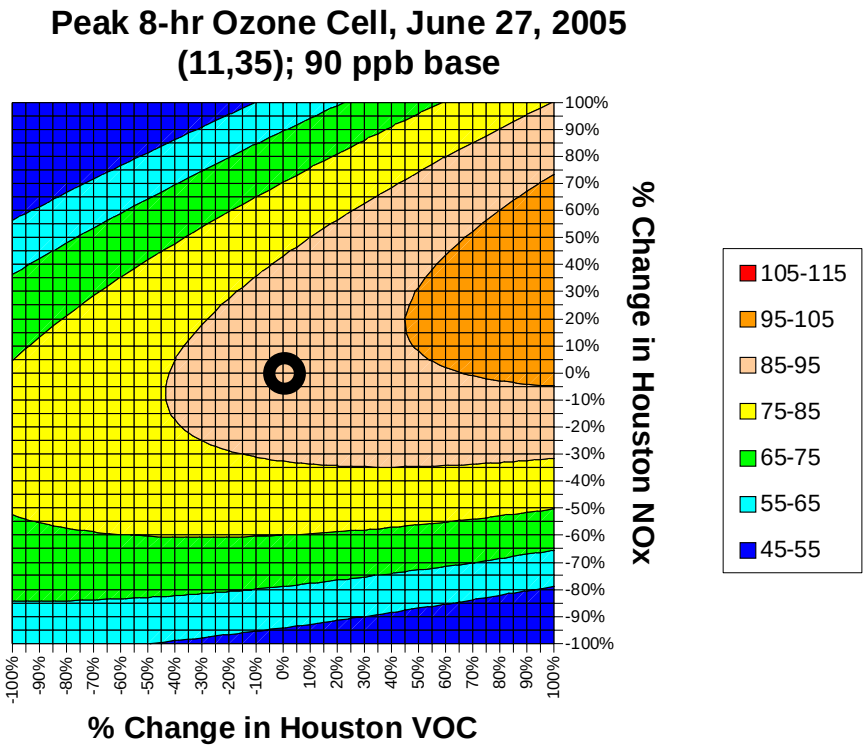

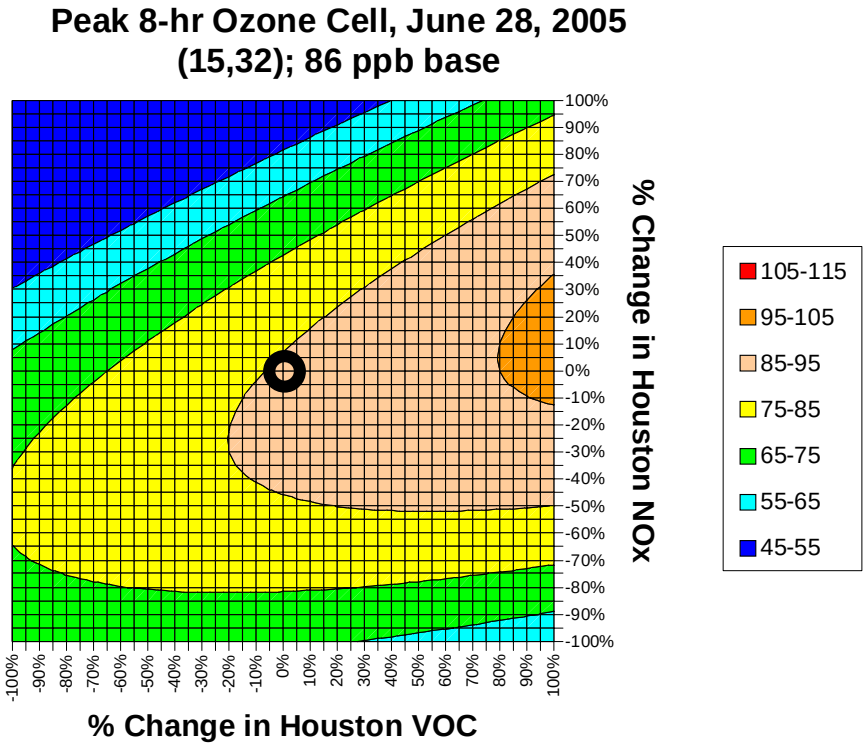

Figure 3-26. As in Figure 3-22, for June 27 (top) and June 28 (bottom).

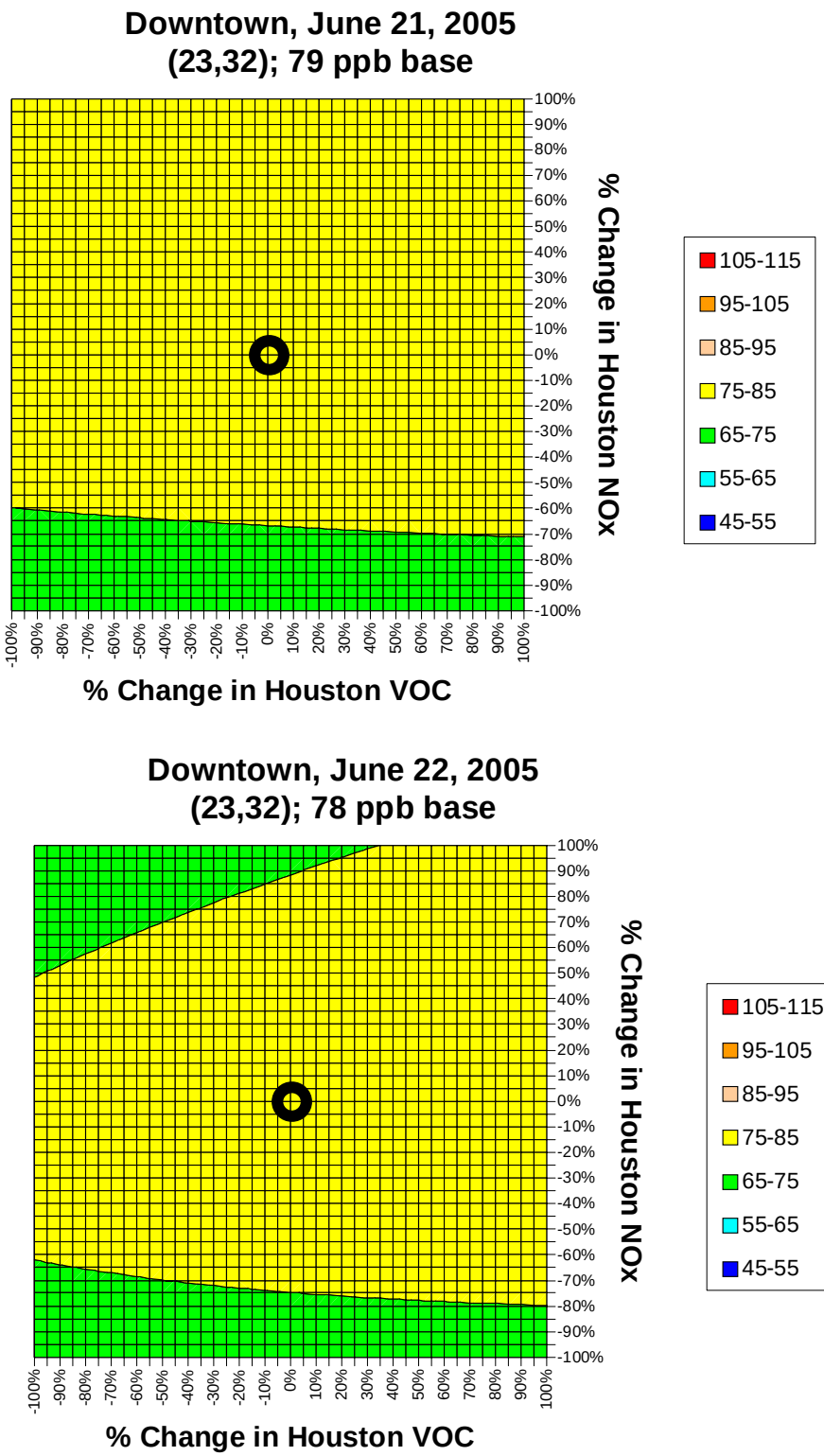

Figure 3-27. As in Figure 3-22, except for a downtown location on June 21 (top) and June 22 (bottom).

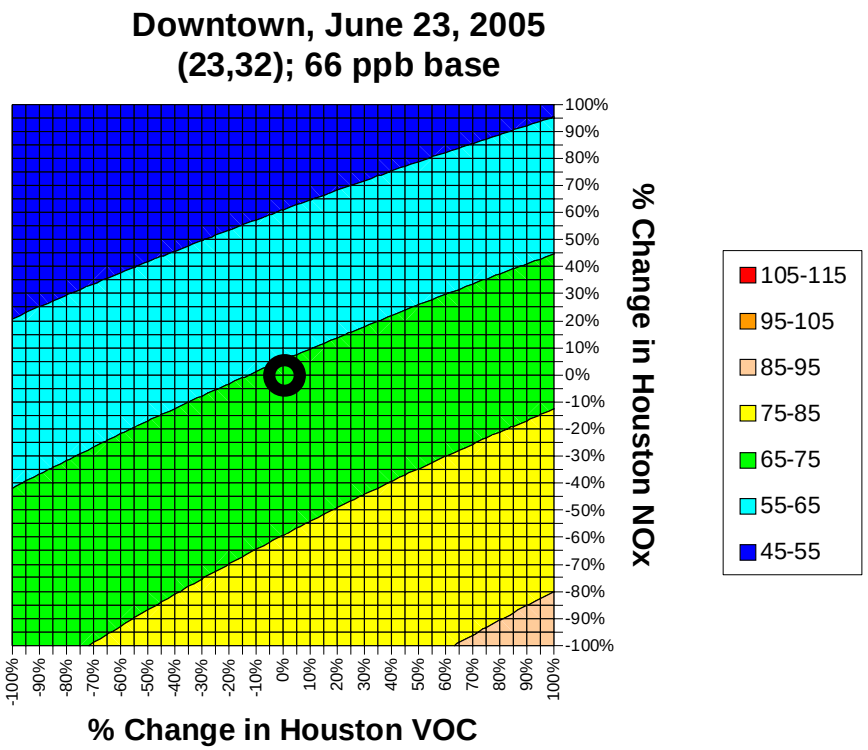

Figure 3-28. As in Figure 3-27, for June 23.

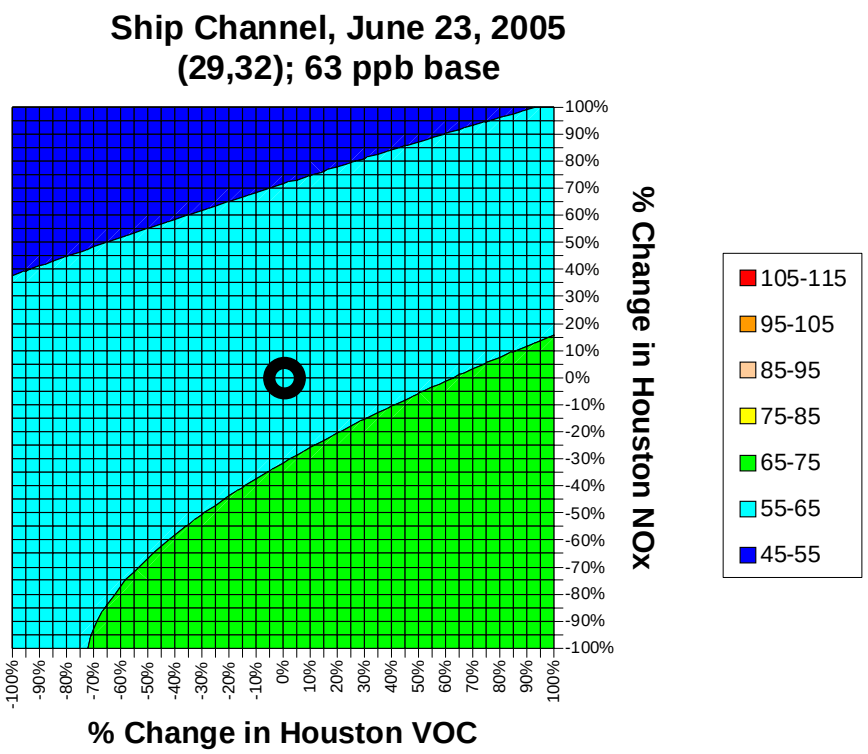

Figure 3-29. As in Figure 3-22, for a Ship Channel location on June 23.

3.2. Sensitivity to Rate Constants

Chemical mechanisms are developed with the best available estimates for chemical rate constants, but those constants are known to be uncertain. Compilations of atmospheric chemical reactions, such as those performed by NASA-JPL (2006), tabulate estimates of the uncertainty of the rate constants. Uncertainty in rate constants is known to be an important contributor to overall uncertainty in photochemical modeling (Fine et al., 2003; Russell and Dennis, 2000).

3.2.1. Selecting Rate Constants to Examine

The CB-05 chemical mechanism used in this study contains more than 150 chemical reactions. Thus, it would be impractical to model the sensitivity of results to each rate constant. A literature review was conducted to identify reactions or systems of reactions for which uncertainty of rates could be important to modeling of ozone concentrations and their sensitivities to emissions. The studies found to be best suited for identifying potential reaction rates of interest were as follows:

- Bergin et al. (1999) conducted formal uncertainty analysis using a Lagrangian trajectory model to consider ozone in southern California. Monte Carlo with Latin hypercube sampling (LHS) was applied for the uncertainty analysis. Their study ranked the leading contributors to uncertainty in ozone concentrations and their sensitivities to NO_x and VOC controls for several receptor locations. Contributors to uncertainty included reaction rates as well as emission rates, deposition rates, and meteorological parameters (e.g., mixing heights, atmospheric stability). The modeling was conducted using the SAPRC-93 chemical mechanism.
- Gao et al. (1995) applied Monte Carlo/LHS to a box model with the RADM-2 chemical mechanism to identify reaction rate constants that most contribute to uncertainty in concentrations of ozone and other species.
- Gao et al. (1996) applied Monte Carlo/LHS to a regional air quality model with the RADM-2 chemical mechanism. They identified reaction rate constants that most contribute to uncertainty in concentrations of ozone and other species, and to uncertainty in their sensitivities to reductions in NO_x and VOCs. They tabulated results for various urban and rural regimes with VOC/NO_x ratios ranging from 6:1 to 100:1.
- A series of studies in France (Beekman and Derognat, 2003; Deguillaume et al., 2008; Deguillaume et al., 2007) conducted Bayesian Monte Carlo analysis to examine uncertainty in ozone responsiveness to emissions. The studies quantified uncertainties in reaction rate constants and other parameters that they expected to be important, but did not characterize the relative contributions of each input uncertainty to overall uncertainty in results.
- Tonnesen (1999) investigated how uncertainty in a single reaction rate constant, $OH + NO_2 \rightarrow HNO_3$, influences ozone concentrations and their sensitivities to emissions. This reaction is potentially important because it removes both NO_x and HO_x radicals to form a reservoir species that can be removed by deposition and other processes. Its rate had significant uncertainty at the time of the Tonnesen study, and continues to be somewhat uncertain.

In addition to this literature review, several other considerations were taken into account. HRVOCs are thought to be especially important to the highest ozone concentrations in Houston (Cowling and Parrish, 2007), so their oxidation rates could be more important for the study region than in earlier studies. Additionally, N_2O_5 hydrolysis has been a subject of considerable uncertainty, and its rate can significantly influence tropospheric chemistry (Evans and Jacob, 2005). PAN and similar compounds can provide important reservoir species for NO_x.

From the literature review and the other considerations, a list of reactions and sets of reactions was developed to provide a menu of options for further study (Table 3-4). Some of the options were individual reactions found to be important by one or more of the studies in the literature review. Other options capitalize on the flexibility of CAMx-HDDM to consider multiple chemical rate constants in a single sensitivity parameter. For example, this allows consideration of the potential impact if all of the oxidation rates of HRVOCs (i.e., via OH, O_3 and NO_3) were to vary in tandem, causing HRVOCs to be more or less reactive than expected. Options 9 and 10 account for the fact that the equilibria between N_2O_5, PAN, and other peroxyacyl nitrates are better established than the forward and backward reaction rates, so it is more appropriate to consider the forward and backward reactions as systems. Option 12 treats all photolysis rates as a single parameter to mimic the impact of higher or lower actinic flux rates than had been modeled.

Table 3-4. Proposed list of reactions for reaction rate sensitivity analysis for TCEQ.

#	REACTION	CB-05 RXN ID	RATIONALE
1	NO2 + hv	R1	See rationale codes 1,4,5,6,7,8
2	NO + O3	R3	See rationale codes 1,4,5,6,7,8
3	NO2 + OH	R28	See rationale codes 1,2,3,4,5,6,7,8; subject of Tonnesen paper; HNO_3 formation, NO_x and HO_x loss
4	HCHO + hv	R74	See rationale codes 2,3,4,5,6,7,8; interest in HCHO
5	HRVOCs + OH	R120, R124, R128	HRVOCs critical to Houston; examine relative importance of alternate oxidation routes; or, run all as single parameter to check overall importance of HRVOC oxidation
6	HRVOCs + O3	R121, R125, R129	ibid
7	HRVOCs + NO3	R122, R126, R130	ibid
8	N2O5 + H2O (+H2O)	R19,R20	Key uncertainty in N2O5 hydrolysis
9	NO2 + NO3 ↔ N2O5	R18, R21	Equilibrium for N2O5 better established than each rate; NOx reservoir
10	C2O3 + NO2 ↔ PAN CXO3 + NO2 ↔ PANX	R88-90 R103-105	PAN equilibrium better established than each rate; PANX rates set based on PAN
11	C2O3 + NO → products CXO3 + NO → products and other PAN & PANX loss	R87, R91-94, R102, R106-111	Loss processes that break PAN and PANX equilibria; PANX rates set based on PAN
12	All photolysis reactions	R1, R8-9, R14-15, R25, R36, R51-53, R62, R65, R72, R75-76, R87, R91, R97, R102, R106, R138, R143, R152	Sensitivity to actinic flux

Rationale Codes:

1. Top 10 contributor (among chemical reaction rates, emission rates, deposition velocities, and meteorology parameters) to uncertainty in ozone concentrations in 1 or more of the California cities examined by Bergin et al (1999), SAPRC93 mechanism.
2. Top 6 contributor to uncertainty in ozone sensitivity to VOC control in 1 or more of the California cities examined by Bergin et al (1999), SAPRC93 mechanism.
3. Top 6 contributor to uncertainty in ozone sensitivity to NOx control in 1 or more of the California cities examined by Bergin et al (1999), SAPRC93 mechanism.
4. Top 5 reaction rate contributing to uncertainty in urban ozone concentrations for 1 or more of the ROG/NOx ratios considered in Gao et al (1996), RADM-2 mechanism.
5. Top 5 reaction rate contributing to uncertainty in ozone sensitivity to VOC control for 1 or more of the ROG/NOx ratios considered in Gao et al (1996), RADM-2 mechanism.
6. Top 5 reaction rate contributing to uncertainty in ozone sensitivity to NOx control for 1 or more of the ROG/NOx ratios considered in Gao et al (1996), RADM-2 mechanism.
7. Top 9 reactions causing uncertainty in ozone concentrations, Gao et al. (1995), RADM-2.
8. Reaction considered in Paris ozone uncertainty studies, CHIMERE model with MEL-CHIOR mechanism (Beekman and Derognat, 2003; Deguillaume et al., 2008; Deguillaume et al., 2007). These studies did not rank reactions by impact.

From the menu of options in Table 3-4, a set of five sensitivity parameters was selected for modeling in this study. Those five parameters, and their corresponding number from Table 3-4, are:

1. $NO_2 + OH \rightarrow HNO_3$ (#3 from Table 3-4)
2. HRVOC oxidation (#5-7)
3. N_2O_5 hydrolysis (#8)
4. $NO_2 + NO_3 \leftrightarrow N_2O_5$ (#9)
5. All photolysis reactions (#12)

A limited subset was necessary because subsequent analysis requires not only modeling the first-order sensitivities, but also second-order cross sensitivities to examine how uncertainty in these rates generates uncertainty in responsiveness to emissions.

3.2.2. Results

Sensitivities to the five sets of reaction rates and associated cross-sensitivities were computed for the entire June 2005 episode. Figures 3-30 to 3-32 show the first-order sensitivities of 8-hour ozone concentrations to each parameter for June 21, 22, and 23.

As would be expected, ozone concentrations show a strong positive sensitivity to photolysis rates (Figures 3-30 to 3-32, top left). The sensitivity coefficient to photolysis gets as large as 52 ppb on June 23, indicating that a 10% change in all photolysis rates (i.e., a 10% change in actinic flux) would result in a more than 5 ppb change in 8-hour ozone at that location. By comparing these plots to Figures 3-19 to 3-21, it can be noted that sensitivity to photolysis rates tends to be greatest where ozone concentrations are highest, accentuating the importance of these rates.

Ozone concentrations show a significant negative sensitivity to the rate of the reaction $OH+NO_2 \rightarrow HNO_3$ (Figures 3-30 to 3-32, top right). That reflects the fact that this reaction converts HO_x and NO_x into a reservoir species and keeps them from being involved in additional ozone formation. The sensitivity coefficient reaches as low as -20 ppb on June 23, indicating that a 10% increase in this reaction rate would cause 8-hour ozone concentrations to be up to 2 ppb lower.

The first-order sensitivity coefficients of 8-hour ozone concentrations to HRVOC oxidation (Figures 3-30 to 3-32, bottom left) reached only 2 ppb during the three days shown, and reached 3 ppb later in the episode. Thus, moderate changes in these oxidation rates would cause ozone concentrations to change by only a fraction of a ppb. As noted earlier, the amount of ozone formed from HRVOCs was smaller than expected. Larger HRVOC inventories would likely lead to greater importance for the HRVOC oxidation rates than was modeled here.

Eight-hour ozone concentrations were not very sensitive to N_2O_5 hydrolysis rates (Figures 3-30 to 3-32, bottom right) and showed negligible sensitivity to N_2O_5 equilibrirum rates (not shown). Examination of hourly data showed that the impact of N_2O_5 hydrolysis was larger in the morning hours, but even then did not reach more negative than -2 ppb. The negative sign reflects that N_2O_5 hydrolysis causes N_2O_5 to form HNO_3 rather than regenerating NO_x.

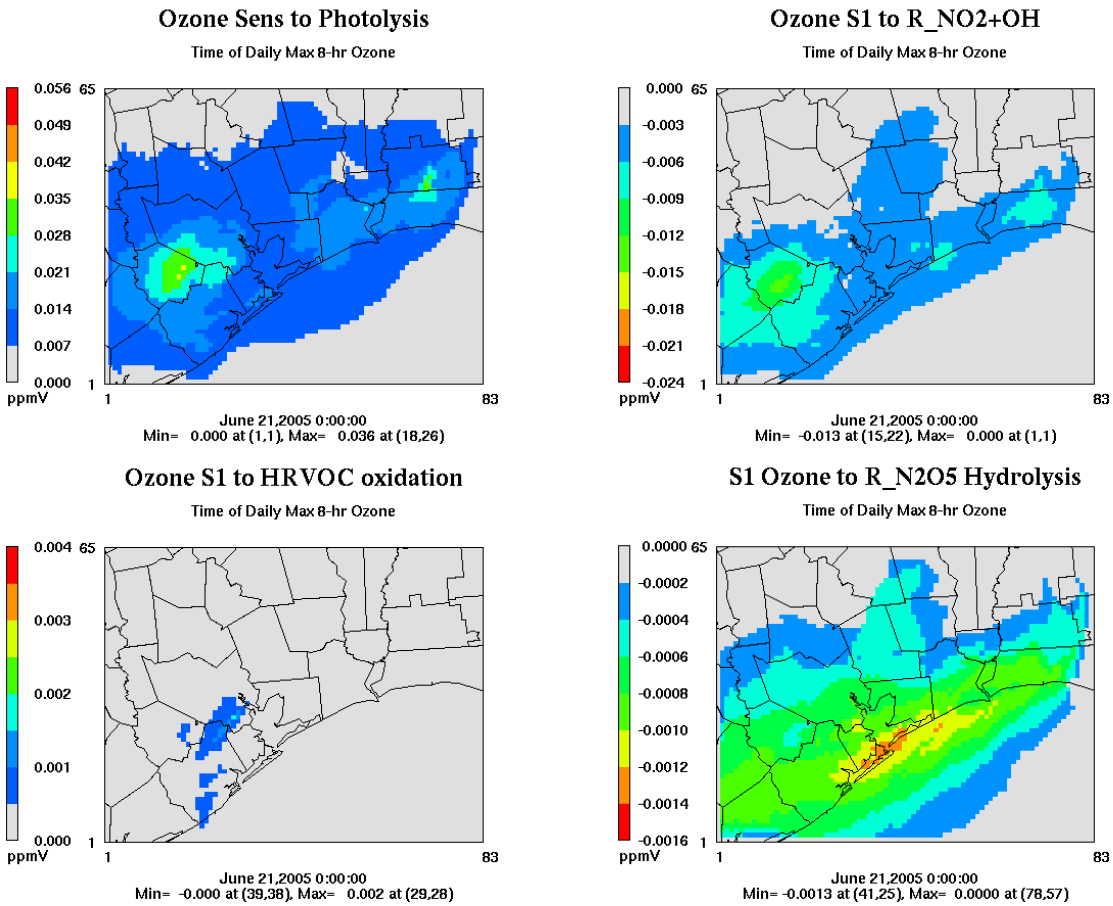

Figure 3-30. First-order sensitivity coefficients of 8-hour ozone on June 21 to rate constants for: all photolysis rates (top left), NO_2+OH (top right), HRVOC oxidation (bottom left), and N_2O_5 hydrolysis (bottom right). Ozone sensitivity to N_2O_5 equilibrium was extremely small (not shown). Note the different scales for each plot.

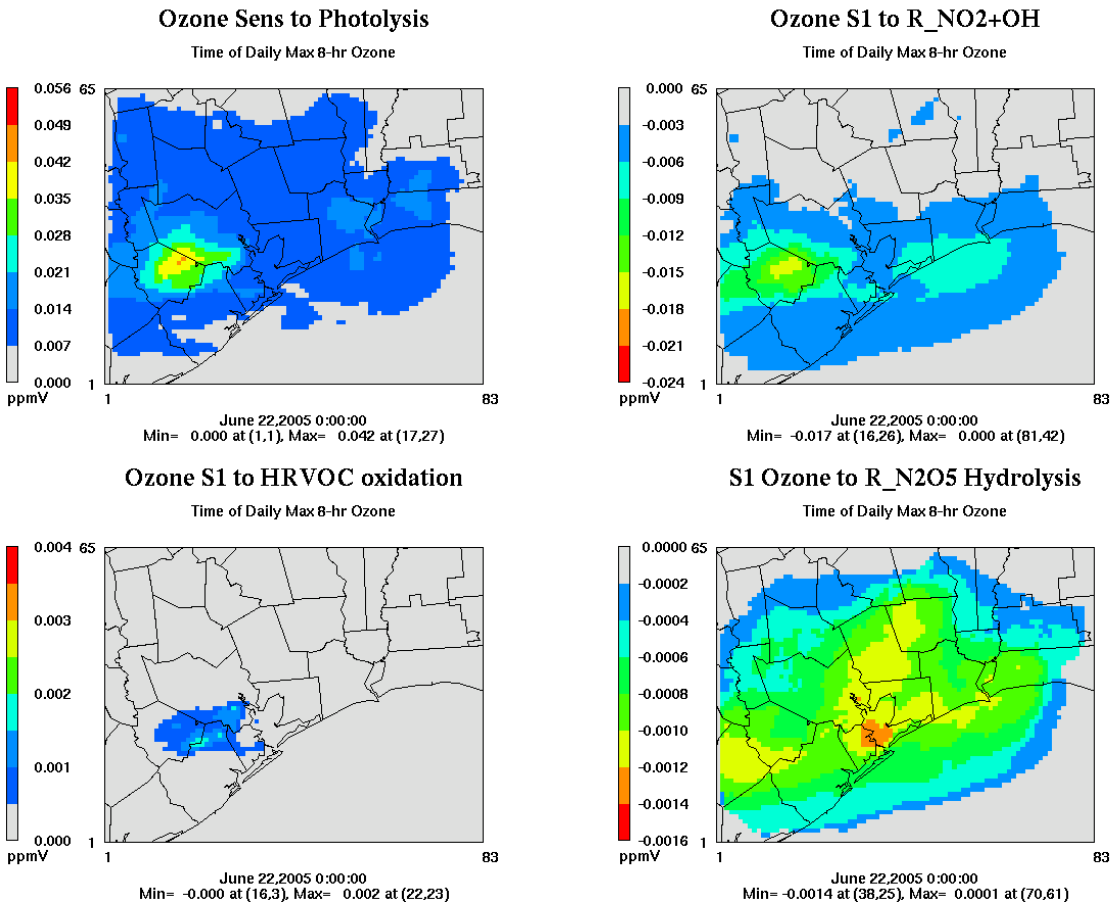

Figure 3-31. As in Figure 3-30, for June 22.

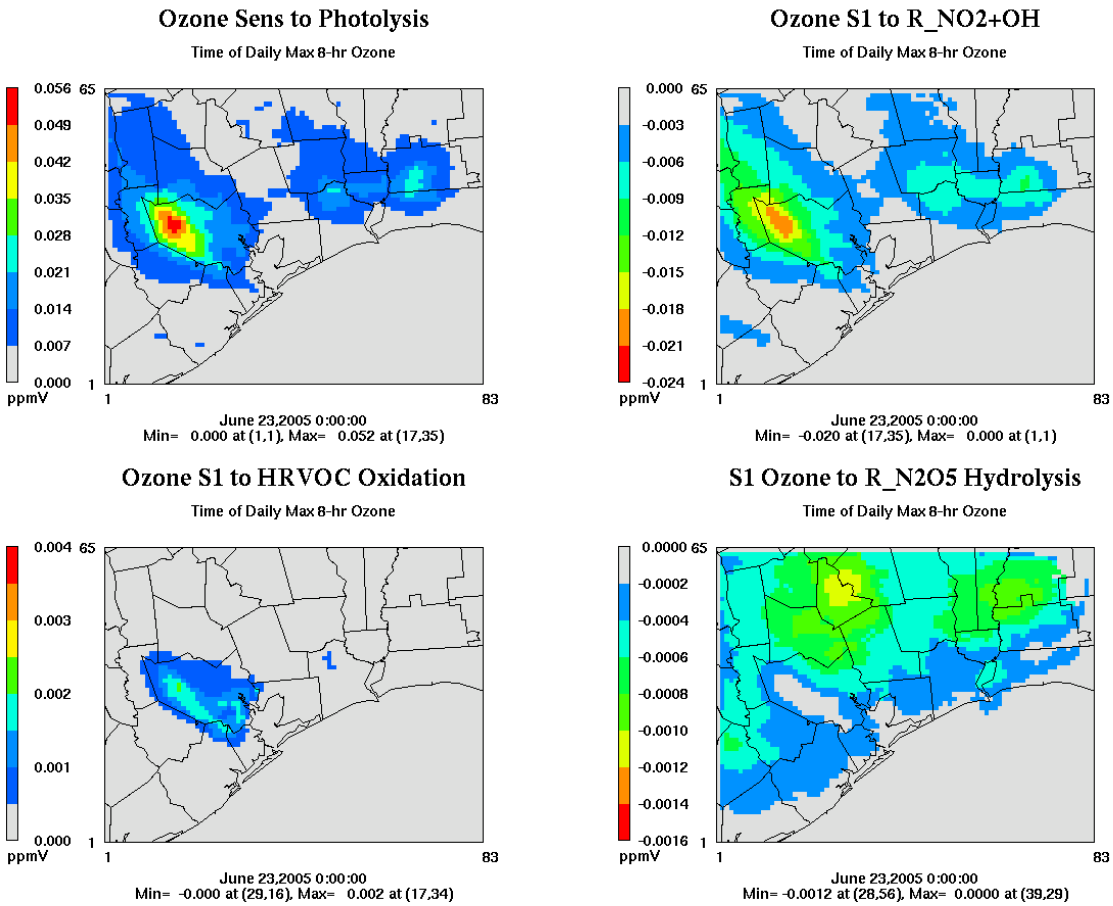

Figure 3-32. As in Figure 3-30, for June 23.

The second-order cross-sensitivities of 8-hour ozone to emissions and reaction rate parameters indicate the extent to which changes in that reaction rate would influence ozone sensitivity to that type of emissions. The left panels of Figures 3-33 to 3-35 show the cross-sensitivity coefficients for ozone to Houston NO_x emissions and reaction rates; the right panels are for Houston VOC emissions and reaction rates.

The cross-sensitivity coefficients between NO_x emissions and photolysis rates (Figures 3-33 to 3-35, top left) are large and positive, reaching as large as 82 ppb on June 23. The 82 ppb value indicates that if photolysis rates were 10% larger, than the first-order sensitivity coefficient of ozone to NO_x would be 8.2 ppb larger (i.e., that the ozone reduction impact of a 10% NO_x reduction would be 0.82 ppb larger than expected). The cross-sensitivity is almost always positive, indicating that the higher the photolysis rates, the larger the sensitivity of ozone to NO_x. A small exception occurs on June 23, when the cross-sensitivity becomes negative over a small portion of Harris County. Comparing Figure 3-21 and Figure 3-35, it can be noted that this occurs where there was an especially strong disbenefit to NO_x, so higher photolysis rates would accentuate the disbenefit there. Comparing Figures 3-33 to 3-35 with Figures 3-19 to 3-21, it can also be noted that the largest positive cross-sensitivity of NO_x and photolysis generally occurs where ozone concentrations are highest.

The cross-sensitivity with NO_x emissions and the $OH+NO_2$ reaction is similar to the pattern for NO_x and photolysis, but with the opposite sign and smaller magnitudes (Figures 3-33 to 3-35, middle left). A distinction is that the cross-sensitivity with $OH+NO_2$ remains uniformly negative, in contrast to the flipped sign noted for photolysis in a small area on June 23.

The cross-sensitivity coefficients of VOC emissions and photolysis rates (Figures 3-33 to 3-35, top right) are small on June 21 and June 22, but show a pronounced divide between positive and negative on June 23. Comparing Figure 3-35 with Figure 3-21, it can be noted that the cross-sensitivity is positive where ozone formation is VOC-limited/NO_x disbenefit, and negative where ozone formation is NO_x-limited. In the NO_x-limited zone, higher photolysis rates would accentuate the NO_x-limited character of the chemical regime and make ozone less sensitive to VOCs. In the VOC-limited area, higher photolysis rates would allow the VOC to form ozone at a greater rate.

For the cross-sensitivity coefficients of VOC emissions and the $OH+NO_2$ reaction, a similar pattern emerges as in the VOC-cross-photolysis case but with the opposite sign. This is especially apparent on June 23 (Figure 3-35, middle right). On that day, a higher rate for the $OH+NO_2$ reaction would limit the sensitivity to VOC in the VOC-limited area by tying up crucial HO_x radicals, but cause a slight increase in sensitivity to VOC in the NO_x-limited area. However, where there is a slight positive cross-sensitivity of this reaction with VOC, it is far smaller in magnitude than the strongly negative cross-sensitivity of this reaction with NO_x.

The cross-sensitivities of both NO_x emissions and VOC emissions with HRVOC oxidation are small and mostly positive (Figures 3-33 to 3-35, bottom). The cross-sensitivity with NO_x tends to peak downwind of the cross-sensitivity with VOC. This is especially apparent on June 23, when the cross-sensitivity of NO_x and HRVOC oxidation resembles the pattern of the ZOC of NO_x emissions (compare Figure 3-21 and Figure 3-35).

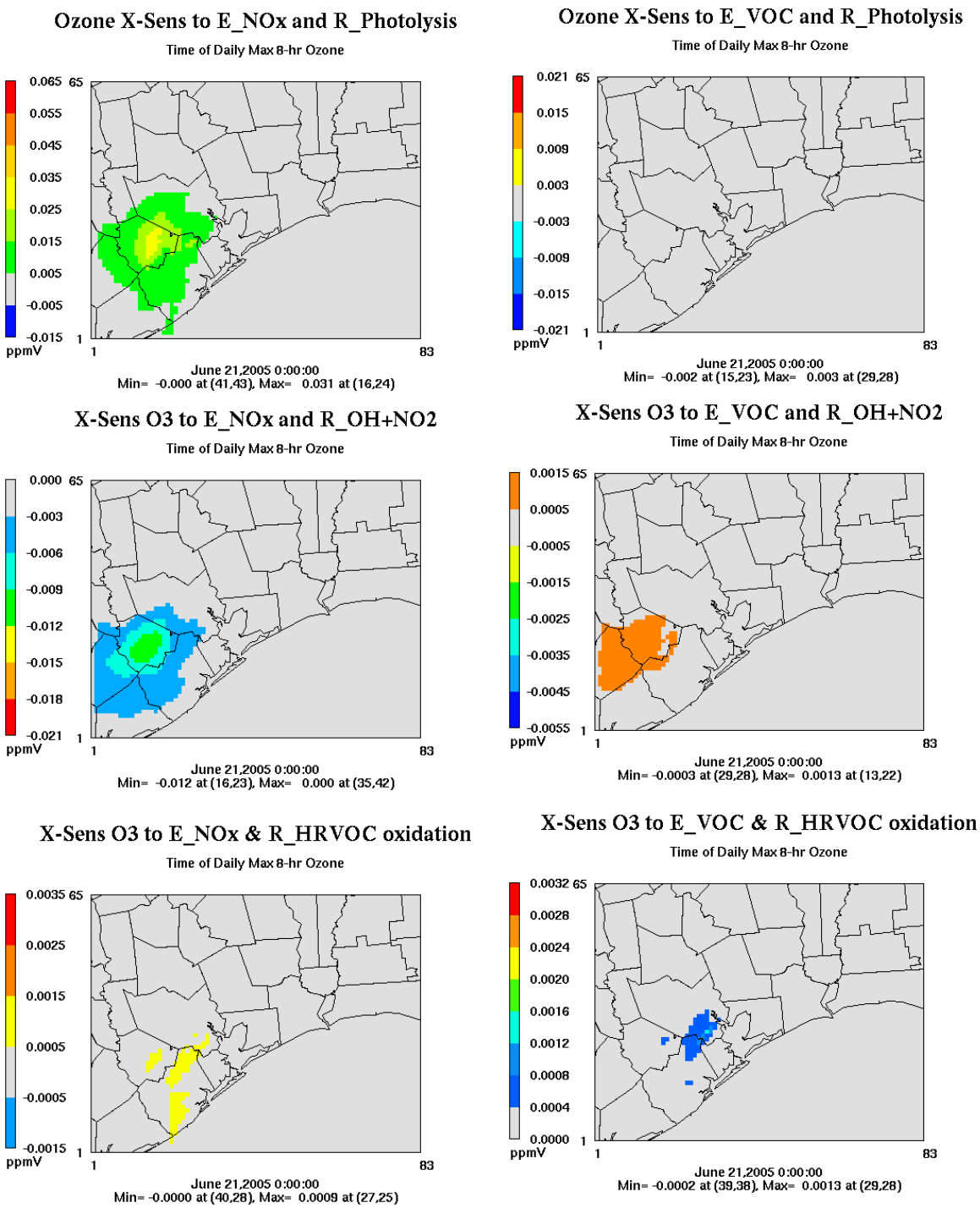

Figure 3-33. Cross-sensitivity coefficients of 8-hour ozone to NO_x emissions (left) and VOC emissions (right) crossed with photolysis rates (top), $OH+NO_2 \rightarrow HNO_3$ (middle), and HRVOC oxidation (bottom), for June 21, 2005. Note the different scales for each plot.

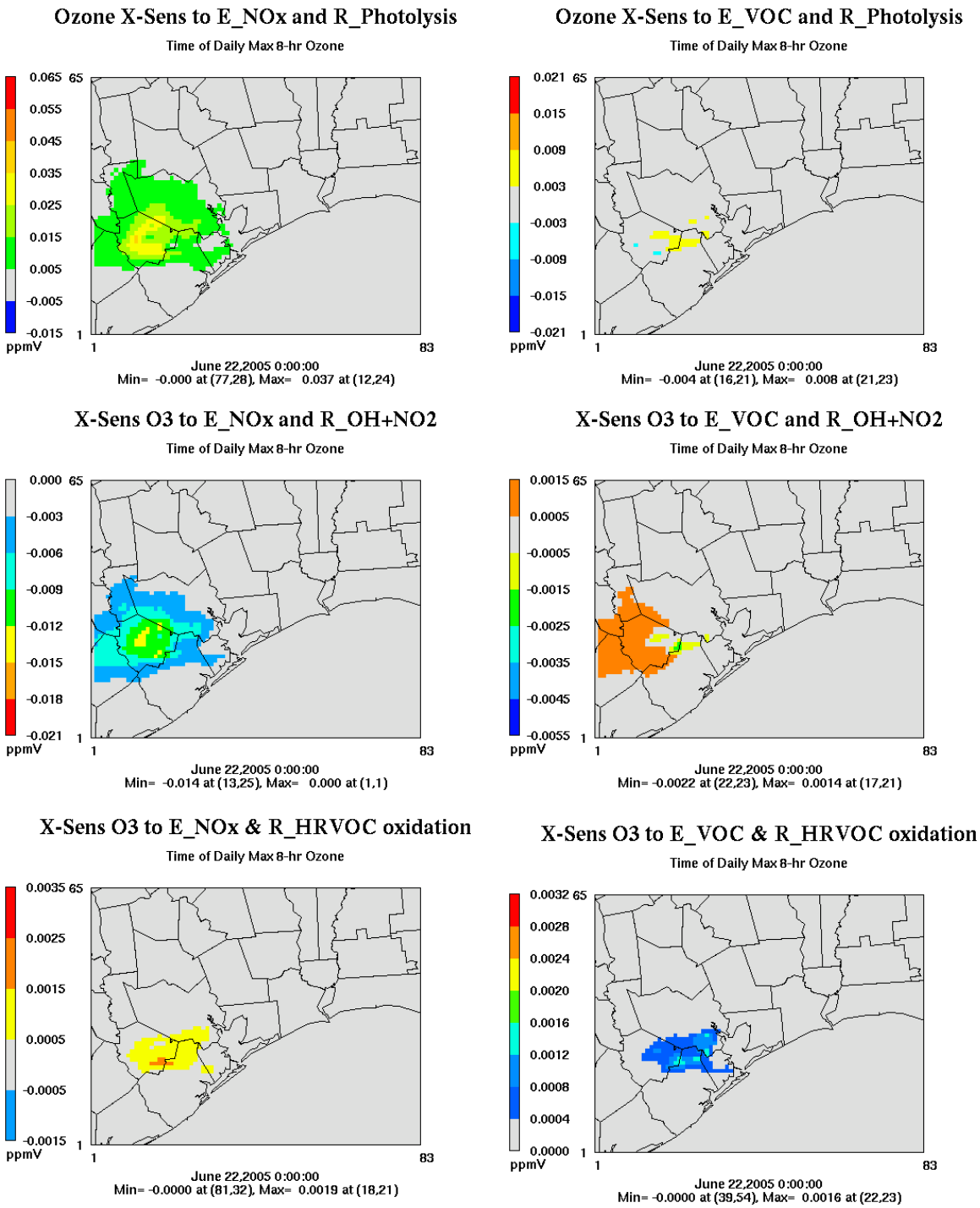

Figure 3-34. As in Figure 3-33, for June 22.

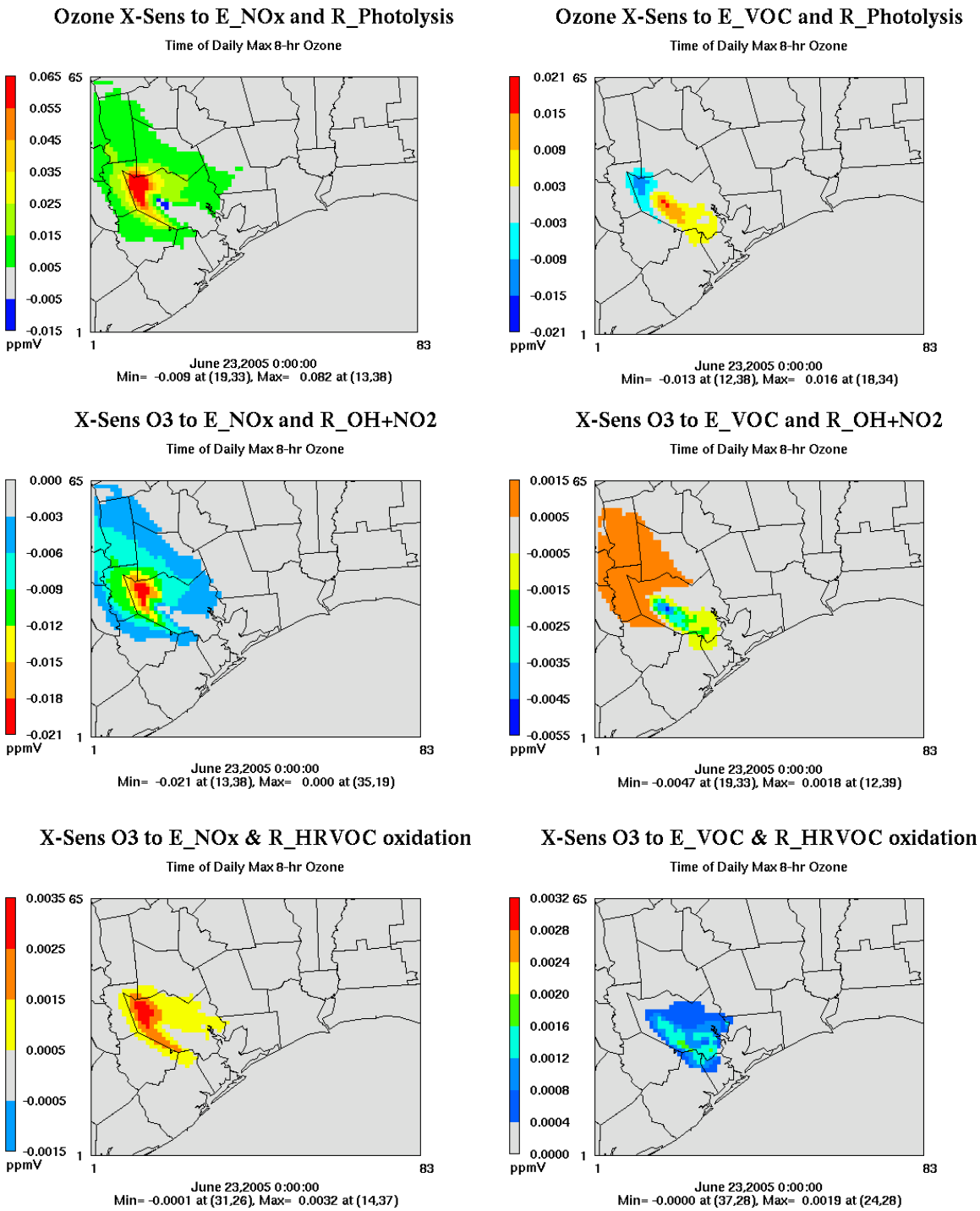

Figure 3-35. As in Figure 3-33, for June 23.

3.3. Uncertainty Analysis

Cohan et al. (2005) introduced a method for using second-order sensitivity coefficients to examine how uncertainty in one model input leads to uncertainty in the ***sensitivities*** of concentrations to that input or to another input parameter. For policy applications, we are typically most interested in how sensitivities of concentrations to emissions would change due to changes in emission rates or other model inputs.

The method can be explained by assuming that some model input, which was set to a value P_j in the model, has an actual value P_j*. Assume that all other inputs, P_k, are correct. We define $\Delta\varepsilon_j$ to be the fractional error in P_j, such that:

$$\begin{aligned} P_j^* &= P_j + \Delta\varepsilon_j P_j \\ P_k^* &= P_k \end{aligned} \qquad (3)$$

The first-order sensitivity coefficients, modeled to be S_j and S_k, can then be adjusted to the values, S_j* and S_k*, that they would have had if the model input had been set to P_j*. This is done using the second-order sensitivity coefficients in the following equation:

$$\begin{aligned} S_j^{(1)*} &= (1+\Delta\varepsilon_j)(S_j^{(1)} + \Delta\varepsilon_j S_{j,j}^{(2)}) \\ S_k^{(1)*} &= S_k^{(1)} + \Delta\varepsilon_j S_{j,k}^{(2)} \end{aligned} \qquad (4)$$

Note that the $(1+\Delta\varepsilon_j)$ term in the equation for S_j* reflects the fact that parameter p_j is now $(1+\Delta\varepsilon_j)$ than had been assumed, so the first-order sensitivity coefficient will be correspondingly larger even before accounting for nonlinearities. If the sensitivity was being expressed on a per-ton basis, that multiplicative term would not appear.

3.3.1. Emissions Uncertainty

Uncertainties in emissions inventories are known to be a leading cause of uncertainty in photochemical modeling (Fine et al., 2003; Russell and Dennis, 2000). Equation 4 was first applied to examine how sensitivities of ozone to Houston emissions of NO_x and VOCs would change if the NO_x or VOC emissions inventories were larger or smaller than expected. For display purposes, we considered how hypothetical cases of +/- 30% changes in Houston NO_x or Houston VOC emissions would affect the ozone sensitivity coefficients to those emissions.

If actual NO_x emissions are smaller than modeled, then ozone formation will be more NO_x-limited and there will be fewer locations with NO_x disbenefits (Figure 3-36). Comparing Figure 3-36 to Figures 3-19 to 3-21, note that the maximal sensitivity coefficient to NO_x is smaller in the -30% case because there is less NO_x to be sensitive to, but that the disbenefit regions are smaller reflecting greater NO_x limitation. Areas of NO_x disbenefit would be much larger if actual NO_x emissions were larger than assumed in the inventory (Figure 3-36, right). Larger NO_x emissions would cause sensitivity to VOC to increase, but only slightly (Figure 3-37).

For changes in the Houston VOC emissions inventory, higher levels of VOCs lead to more ozone sensitivity to NO_x emissions (Figure 3-38). However, the impact of uncertainty in VOC

emissions is much smaller than the impact of uncertainty in NO_x emissions (compare Figure 3-36 and 3-38). The responsiveness of ozone to VOCs is more linear than the responsiveness of ozone to NO_x. Thus, the first-order sensitivity coefficient of ozone to VOC increases almost linearly with changes in VOC emissions (Figure 3-39). In Figure 3-39 it can be noted that the pattern of sensitivity to VOC stays very similar between the -30% and +30% EVOC cases, although the magnitudes change because more EVOC means there will be a larger first-order coefficient. In other words, the *per-ton* impact of VOC on ozone is relatively stable as the VOC emissions inventory changes, though it does decrease somewhat as VOC increases due to the saturating (concave-down) response.

The impacts of uncertainties in biogenic VOC emissions inventories on ozone sensitivities to Houston NO_x and VOC were also examined (not shown). Ozone sensitivity to NO_x was found to increase, and sensitivity to anthropogenic VOC to decrease, with increases in the biogenic emissions inventory. However, the impacts on first-order sensitivity coefficients in most locations were small (~2 ppb or less) for 30% changes in biogenic VOC emissions.

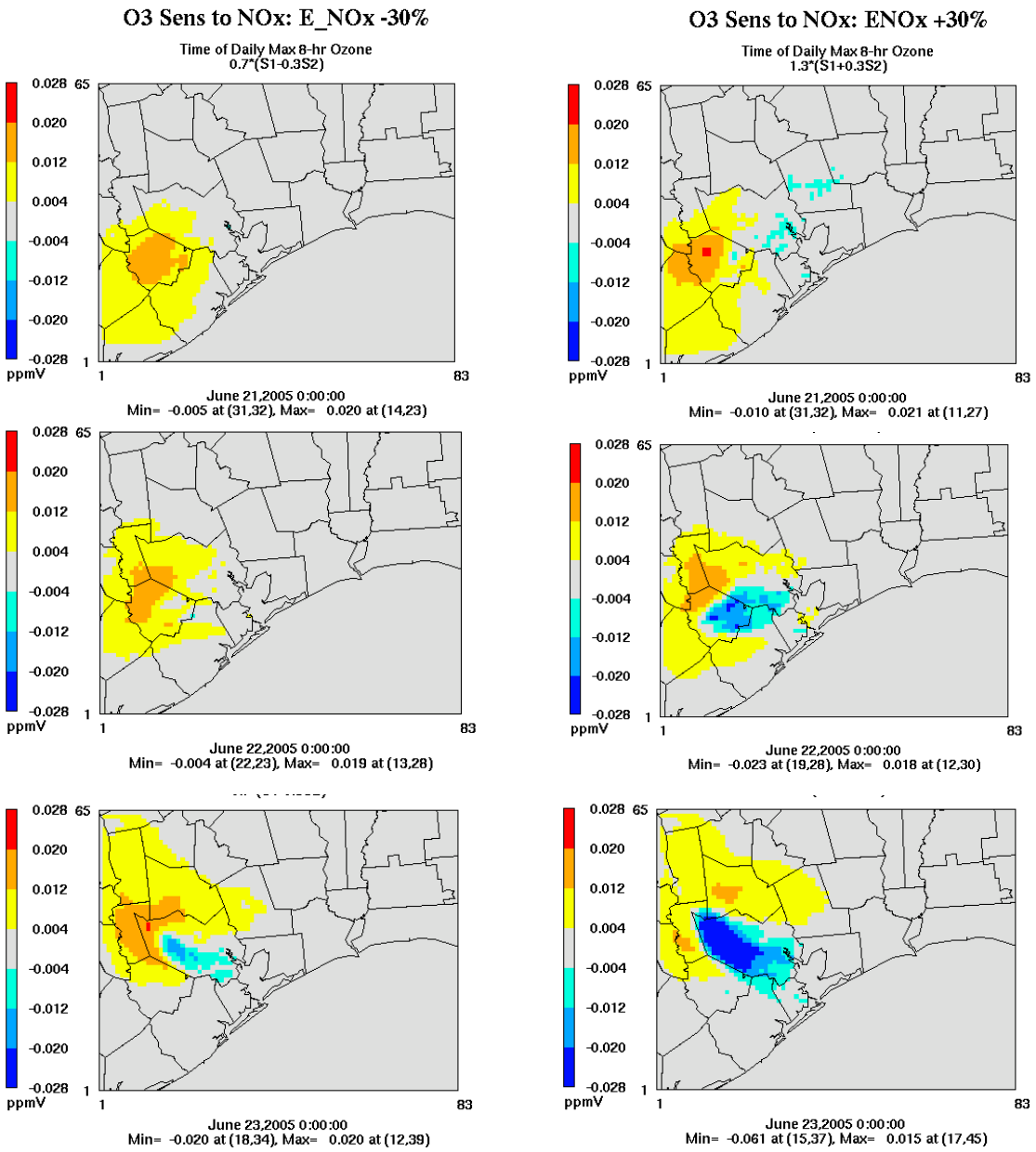

Figure 3-36. First-order sensitivity coefficient of ozone to Houston NO_x emissions if actual NO_x emissions are 30% less than modeled (left) or 30% more than modeled (right), for June 21-23, 2005.

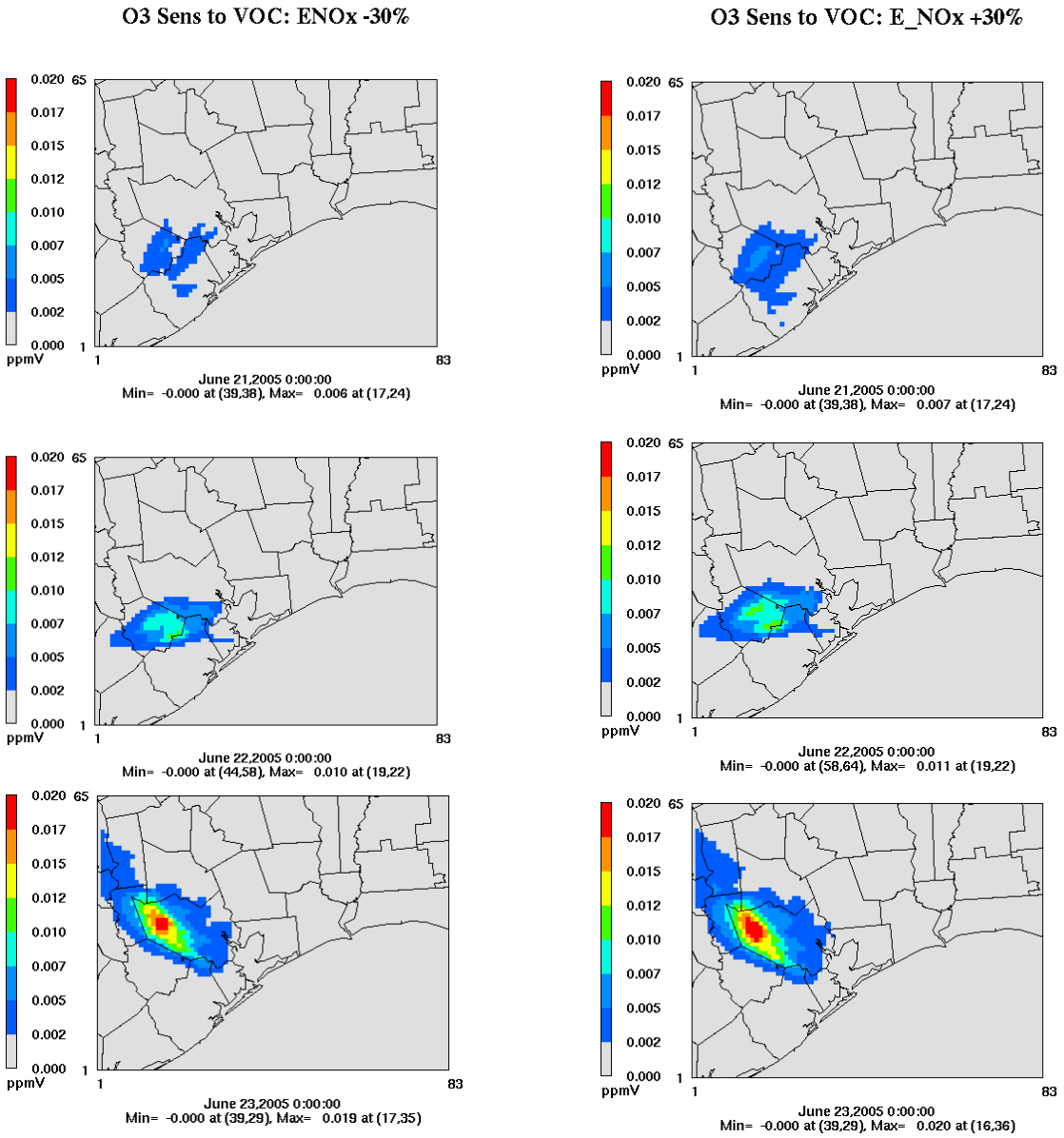

Figure 3-37. First-order sensitivity coefficient of ozone to Houston VOC emissions if actual Houston NO_x emissions are 30% less than modeled (left) or 30% more than modeled (right), for June 21-23, 2005.

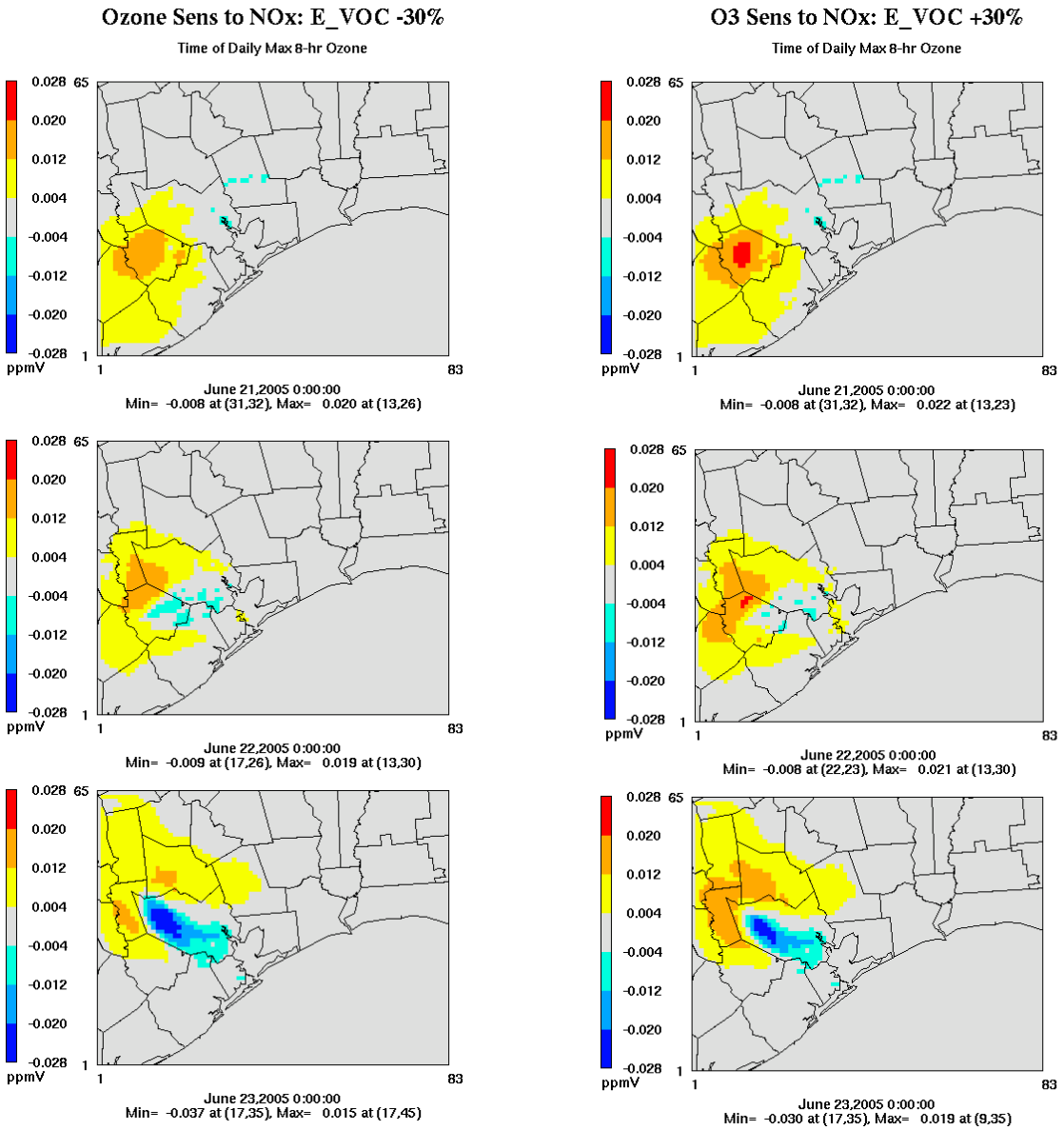

Figure 3-38. First-order sensitivity coefficient of ozone to Houston NO_x emissions if actual Houston VOC emissions are 30% less than modeled (left) or 30% more than modeled (right), for June 21-23, 2005.

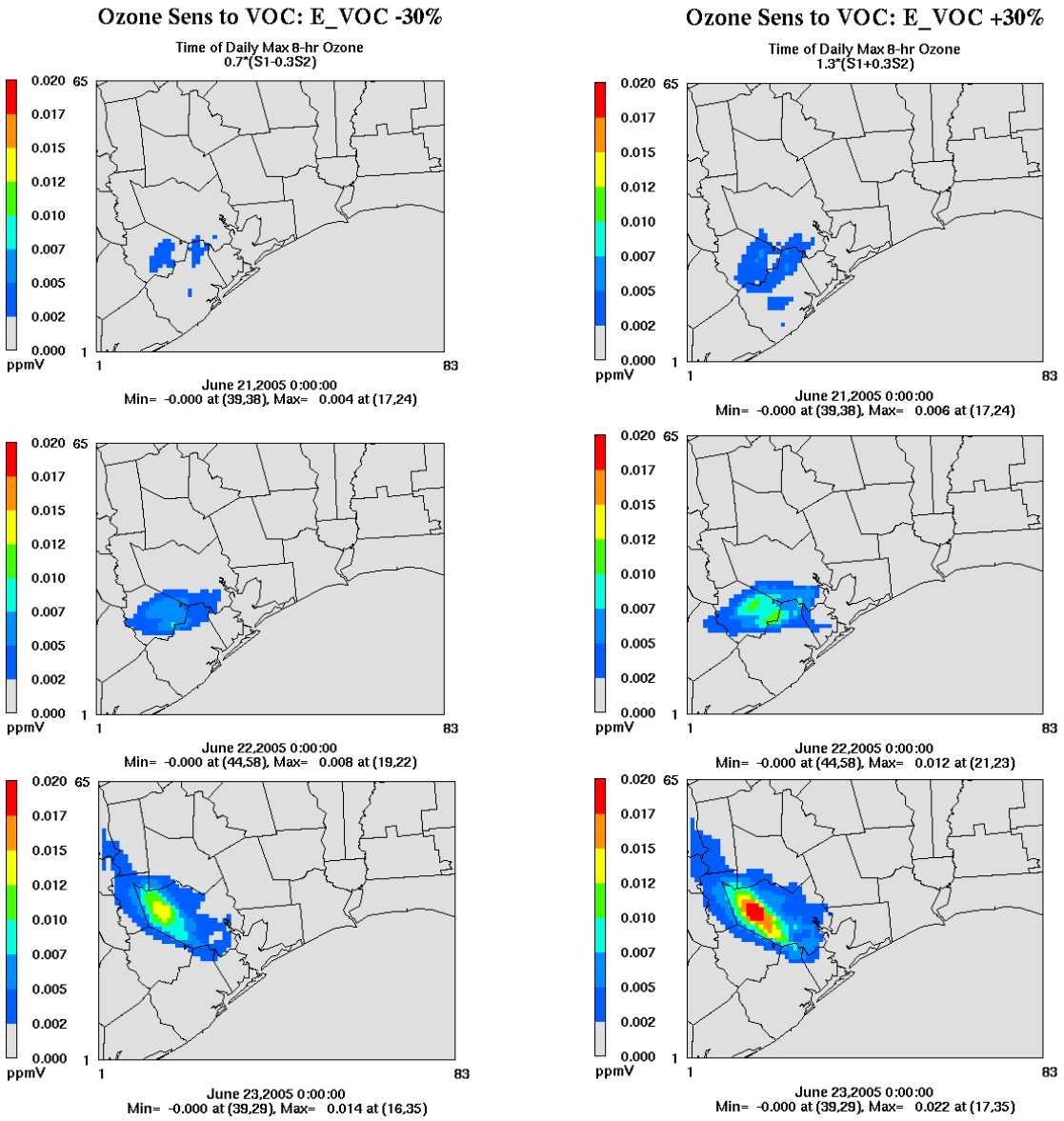

Figure 3-39. First-order sensitivity coefficient of ozone to Houston VOC emissions if actual Houston VOC emissions are 30% less than modeled (left) or 30% more than modeled (right), for June 21-23, 2005.

3.3.2. Reaction Rate Uncertainty

Reaction rate uncertainties are an additional import cause of uncertainty in photochemical modeling. The impacts of these uncertainties on sensitivities to emissions have not been previously examined with HDDM, because HDDM was only recently extended to compute high-order and cross-sensitivities for reaction rates. Here, we apply Equation 4 to consider how changes in reaction rates would impact the sensitivities of ozone to Houston NO_x and VOC emissions.

Of the reaction rate parameters considered (see Section 3.2.1), overall photolysis rates had the greatest impact on sensitivities to NO_x and VOC. If photolysis rates are 30% larger than expected (e.g., because actinic flux is 30% greater than modeled), then sensitivity to NO_x emissions is greatly enhanced (Figure 3-40). Greater photolysis rates also cause somewhat greater sensitivity to VOCs (Figure 3-41). Careful examination of the "plume" of VOC sensitivity Figure 3-41 along with Figure 3-35 reveals that the plume occurs somewhat sooner for higher photolysis rates. This reflects that greater photolysis rates accelerate ozone formation from VOCs, but cause ozone formation to be slightly less VOC-sensitive downwind.

The rate constant for $OH+NO_2 \rightarrow HNO_3$ also causes important impacts on sensitivities to NO_x. The larger the rate constant, the smaller the sensitivity to NO_x and the larger the areas of NO_x disbenefits (Figure 3-42). The impact of this rate constant on sensitivity to VOCs is small (Figure 3-43).

Changes in HRVOC oxidation rates by +/-30% cause only slight changes in sensitivity to VOC emissions (Figure 3-44) and NO_x emissions (not shown). The impacts of +/-30% changes in N_2O_5 hydrolysis and N_2O_5 equilibrium rates on 8-hour ozone sensitivities are even smaller (not shown).

Reviewing these impacts of rate constant uncertainties, the impact of the photolysis rates is especially of note. Meteorological models often due a poor job of simulating the quantities and locations of cloud cover. This could lead to significant discrepancies in actinic flux and hence in photolysis rates. The results suggest that such discrepancies might not only impact simulated ozone concentrations, but also significantly impact predictions of their sensitivities to control measures.

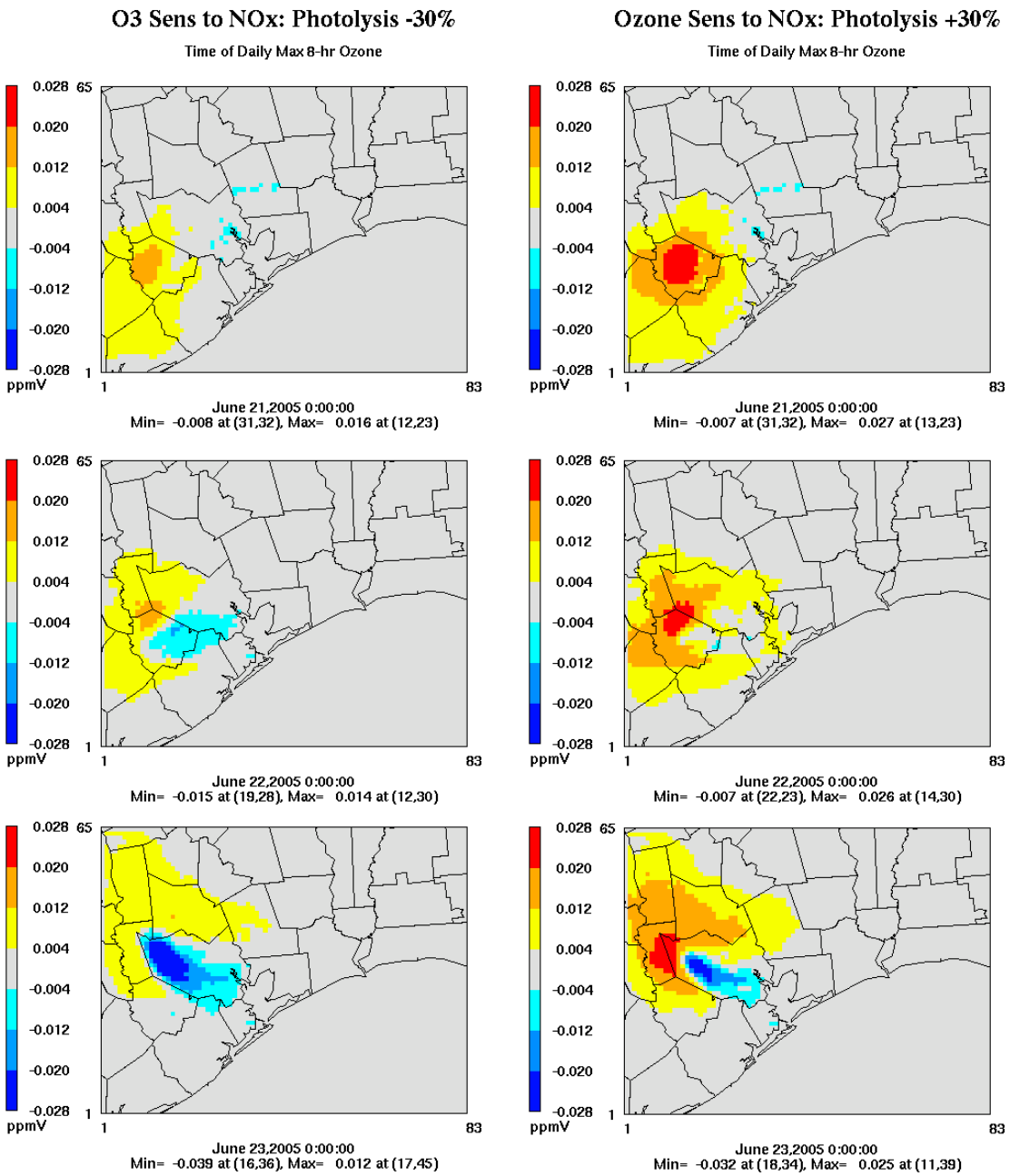

Figure 3-40. First-order sensitivity coefficient of ozone to Houston NO_x emissions if all photolysis rates are 30% smaller (left) or 30% larger (right) than modeled, for June 21-23, 2005.

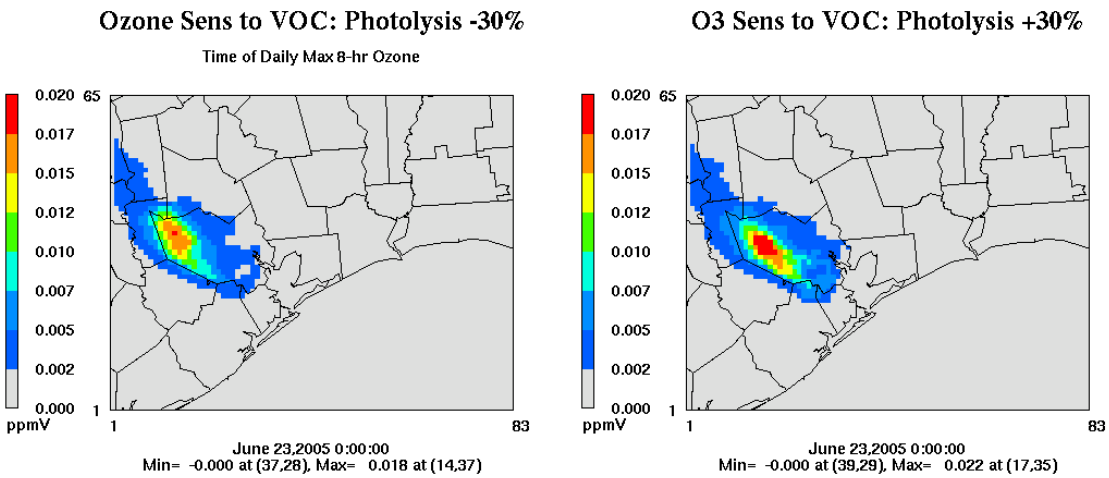

Figure 3-41. First-order sensitivity coefficient of ozone to Houston VOC emissions if all photolysis rates are 30% smaller (left) or 30% larger (right) than modeled, for June 23, 2005.

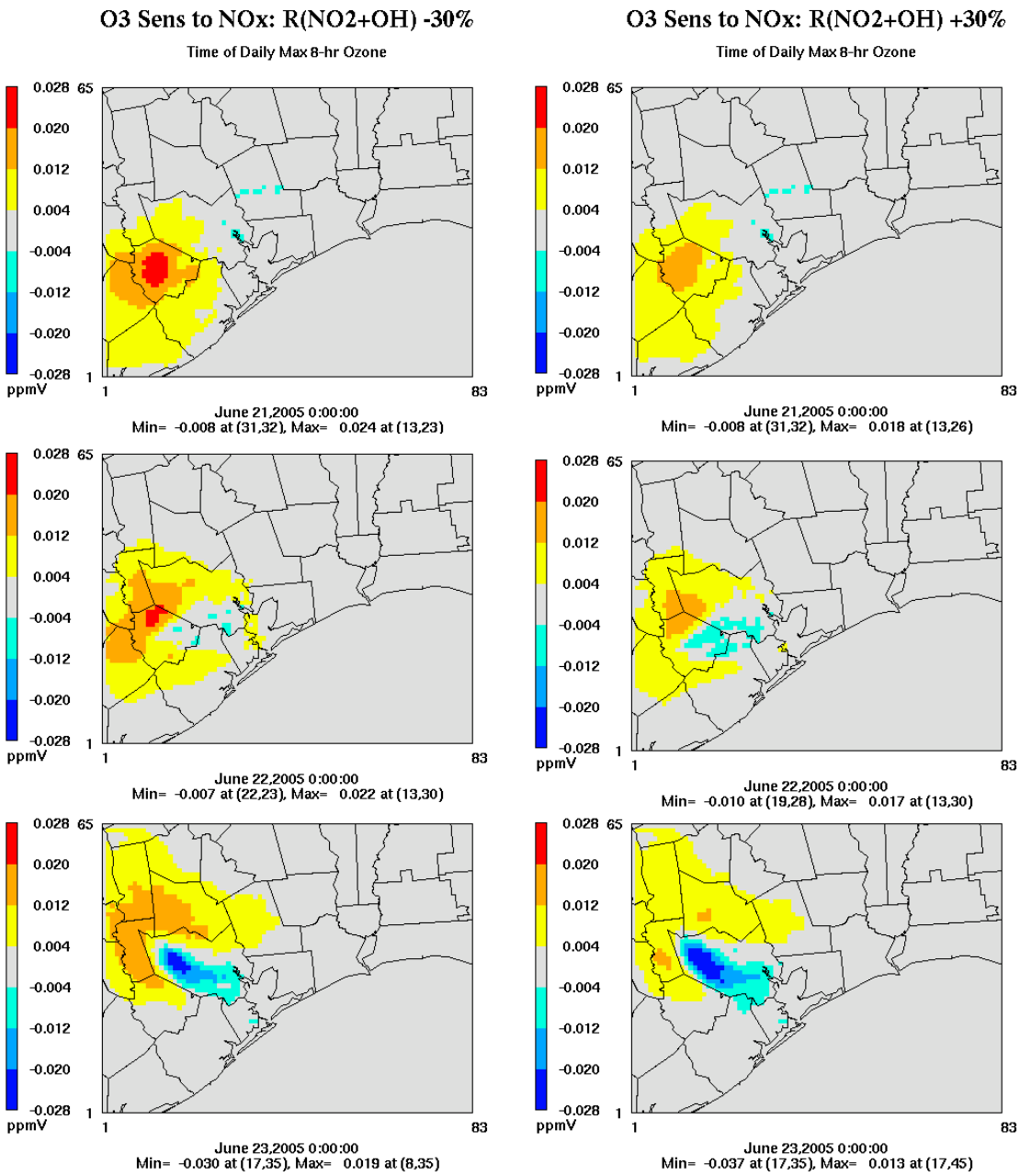

Figure 3-42. First-order sensitivity coefficient of ozone to Houston NO_x emissions if the rate constant for $OH+NO_2 \rightarrow HNO_3$ is 30% smaller (left) or 30% larger (right) than modeled, for June 21-23, 2005.

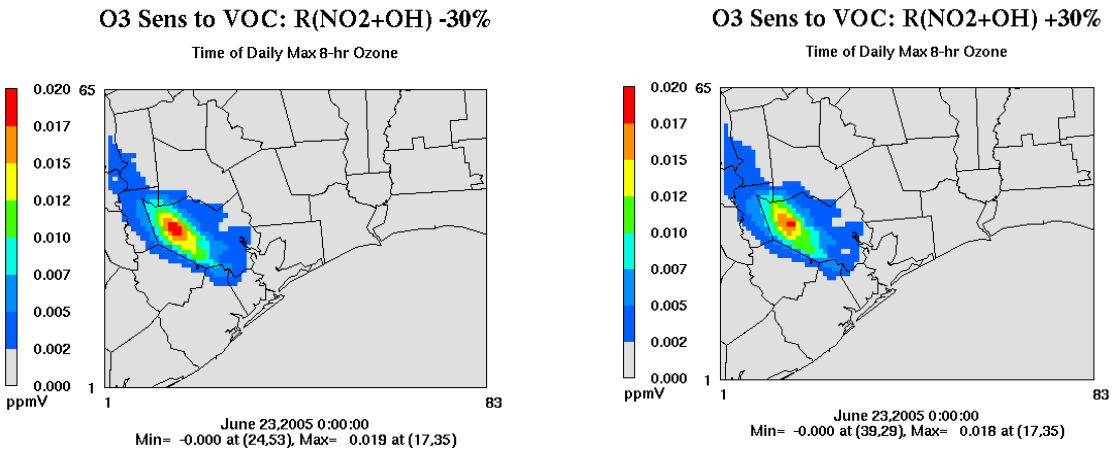

Figure 3-43. First-order sensitivity coefficient of ozone to Houston VOC emissions if the rate of $OH+NO_2 \rightarrow HNO_3$ is 30% smaller (left) or 30% larger (right) than modeled, for June 23, 2005.

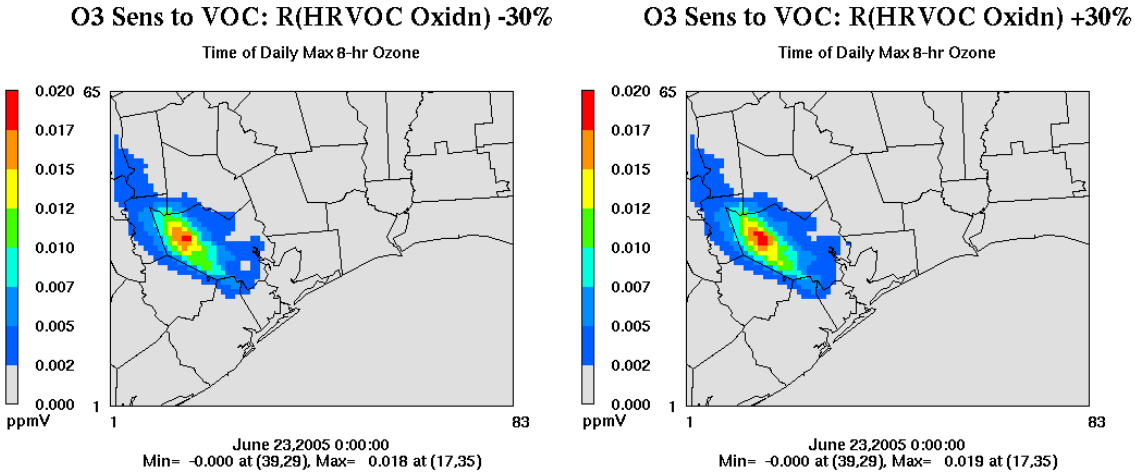

Figure 3-44. First-order sensitivity coefficient of ozone to Houston VOC emissions if the rate of HRVOC oxidation is 30% smaller (left) or 30% larger (right) than modeled, for June 23, 2005.

REFERENCES

Beekman, M. and C. Derognat (2003). Monte Carlo uncertainty analysis of a regional-scale transport chemistry model constrained by measurements from the Atmospheric Pollution Over the Paris Area (ESQUIF) campaign. *Journal of Geophysical Research*. **108**.

Bergin, M.S., G.S. Noblet, K. Petrini, J.R. Dhieux, J.B. Milford, and R.A. Harley (1999). Formal uncertainty analysis of a Lagrangian photochemical air pollution model. *Environmental Science & Technology*. **33**: p. 1116-1126.

Cohan, D.S., A. Hakami, Y.T. Hu, and A.G. Russell (2005). Nonlinear response of ozone to emissions: Source apportionment and sensitivity analysis. *Environmental Science & Technology*. **39**(17): p. 6739-6748.

Cowling, E.B. and D.D. Parrish (2007). *Final Rapid Science Synthesis Report: Findings from the Second Texas Air Quality Study (TexAQS II)*: p. 143.

Deguillaume, L., M. Beekman, and C. Derognat (2008). Uncertainty evaluation of ozone production and its sensitivity to emission changes over the Ile-de-France region during summer periods. *Journal of Geophysical Research*. **113**.

Deguillaume, L., M. Beekman, and L. Menut (2007). Bayesian Monte Carlo analysis applied to regional-scale inverse emission modeling for reactive trace gases. *Journal of Geophysical Research*. **112**.

ENVIRON (2008). User's Guide - Comprehensive Air Quality Model with Extensions Version 4.50. http://www.camx.com.

Evans, M.J. and D.J. Jacob (2005). Impact of new laboratory studies of N2O5 hydrolysis on global model budgets of tropospheric nitrogen oxides, ozone, and OH. *Geophysical Research Letters*. **32**(9): p. 4.

Fine, J., L. Vuilleumier, S. Reynolds, P. Roth, and N. Brown (2003). Evaluating uncertainties in regional photochemical air quality modeling. *Annual Review of Environment and Resources*. **28**: p. 59-106.

Gao, D., W.R. Stockwell, and J.B. Milford (1995). First-order sensitivity and uncertainty analysis for a regional-scale gas-phase chemical mechanism. *Journal of Geophysical Research*. **100**(D11): p. 23153-23166.

Gao, D., W.R. Stockwell, and J.B. Milford (1996). Global uncertainty analysis of a regional-scale gas-phase chemical mechanism. *Journal of Geophysical Research*. **101**(C4): p. 9107-9119.

Hakami, A., M.T. Odman, and A.G. Russell (2003). High-order, direct sensitivity analysis of multidimensional air quality models. *Environmental Science & Technology*. **37**(11): p. 2442-2452.

Hakami, A., M.T. Odman, and A.G. Russell (2004). Nonlinearity in atmospheric response: A direct sensitivity analysis approach. *Journal of Geophysical Research-Atmospheres* **109**(D15). doi: 10.1029/2003JD004502

Hertel, O., R. Berkowicz, J. Christensen, and O. Hov (1993). Test of two numerical schemes for use in atmospheric transport-chemistry models. *Atmos. Environ.*, **27A**, 2591-2611.

Napelenok, S.L., D.S. Cohan, M.T. Odman, and S. Tonse (2008). Extension and evaluation of sensitivity analysis capabilities in a photochemical model. *Environmental Modelling & Software*. **23**: p. 994-999.

NASA-JPL (2006). *Chemical Kinetics and Photochemical Data for use in Atmospheric Studies*. NASA Jet Propulsion Laboratory.

Russell, A. and R. Dennis (2000). NARSTO critical review of photochemical models and modeling. *Atmospheric Environment*. **34**(12-14): p. 2283-2324.

Tonnesen, G.S. (1999). Effects of uncertainty in the reaction of the hydroxyl radical with nitrogen dioxide on model-simulated ozone control strategies. *Atmospheric Environment*. **33**(10): p. 1587-1598.

APPENDIX A

UPDATED DDM SECTION OF CAMx USER'S GUIDE

8. DECOUPLED DIRECT METHOD FOR SENSITIVITY ANALYSIS

Photochemical modelers have traditionally used sensitivity analysis both for model performance evaluation and emission control strategy design. The simplest approach to sensitivity analysis, often referred to as the "brute-force" approach, involves changing a model input parameter, rerunning the model, and then evaluating the change in model output. The change in output is quantified from the difference between the sensitivity case and base case. This approach requires a separate simulation for each parameter investigated. For example, a model performance evaluation may use sensitivity simulations to evaluate the impact of changing the initial conditions (ICs), boundary conditions (BCs), biogenic emissions, anthropogenic emissions, etc. Sensitivity analysis is also used to aid control strategy design. For example, across-the-board VOC and NO_x emission reductions are used to determine whether VOC and/or NO_x reduction strategies are the most effective path to reduce ozone.

The advantages of the "brute force" method for sensitivity analysis are:

- Applicable to any model input parameter;
- Results are conceptually easy to explain and interpret.

The limitations of the "brute force" method are:

- Computationally inefficient;
- Sensitivity depends upon the magnitude of the perturbation if the model response is non-linear;
- Sensitivity derived from small perturbations may contain significant levels of uncertainty (numerical noise).

The last two points bear further explanation. If the model response to an input parameter depends upon non-linear components within the model (e.g., chemistry), then the relative magnitude or even sign of the output response may change for perturbations of different sizes. An example is the response of ozone to NO_x reductions in a VOC-limited environment: smaller reductions in NO_x emissions increase ozone levels whereas larger NO_x reductions decrease ozone.

This situation can be illustrated mathematically. We define a "sensitivity coefficient" (s) which represents the change in concentration (c) with respect to some input parameter (λ), evaluated relative to the base state ($\lambda=\lambda_0$),

$$s = \left.\frac{\partial c}{\partial \lambda}\right|_{\lambda_o}$$

In general, λ can be a vector (denoted as $\underline{\lambda}$), which contains multiple parameters related to processes in the model (e.g., rate constants) or inputs to the model (e.g., emissions). The response of concentration to a change in $\underline{\lambda}$ can be represented by a Taylor series of sensitivity coefficients:

$$c(\underline{x},t;\underline{\lambda}) = c(\underline{x},t;\underline{\lambda}_0) + \sum_{i=1}^{n} \left.\frac{\partial c}{\partial \lambda_i}\right|_{\underline{\lambda}_o} (\lambda_i - \lambda_{i0})$$

$$+ \frac{1}{2}\sum_{i=1}^{n}\sum_{j=1}^{n} \left.\frac{\partial^2 c}{\partial \lambda_i \partial \lambda_j}\right|_{\underline{\lambda}_o} (\lambda_i - \lambda_{i0})(\lambda_j - \lambda_{j0})$$

$$+ \ldots$$

where n is the number of $\underline{\lambda}$ vector elements, $\underline{x}$ is the spatial dimension vector, and t is time. In the example above, the non-linear response of ozone to large NO_x emission reductions indicates that higher-order sensitivity coefficients are significant relative to the first order sensitivity. As the magnitude of the input perturbation tends to zero, the output response will become dominated by the first-order sensitivity. Therefore, very small changes in the input parameter may be required to use the "brute force" method to estimate the first-order (local) sensitivity. The practical limitation to this approach is that since the change in output must be determined from the difference between two simulations, small levels of numerical uncertainty (noise) in two very similar outputs will contaminate the sensitivity calculation.

An alternative methodology for evaluating model sensitivity was developed by Dunker (1980 and 1981) called the decoupled direct method (DDM). The DDM can be used to calculate the same type of sensitivity coefficient as is available from the "brute force" method. The difference is that with DDM, sensitivity coefficients are calculated explicitly by specialized algorithms implemented in the host model. Thus, the DDM offers several advantages over the brute force method:

- Improved computational efficiency;
- Improved accuracy since sensitivities need not be contaminated by numerical noise;
- Multiple sensitivities can be calculated simultaneously

The degree to which these advantages are realized depends upon how the method is implemented, i.e., the algorithms employed and their coding. Fortunately, the performance of the DDM can be evaluated quantitatively by careful comparison of DDM sensitivities against "brute-force" sensitivities.

The first implementation of the DDM into a three-dimensional air quality model used version II of the Urban Airshed Model (Dunker, 1981). This project demonstrated the accuracy and capabilities of the method, but application was restricted by the computing power available to the air quality modeling community at that time. Recently, Yang et al. (1997) described the implementation of the DDM into the California/Carnegie Institute of Technology airshed model, an application termed DDM-3D. The implementation of the DDM into CAMx was performed in a joint project between Dr. Alan Dunker and ENVIRON with sponsorship from the Coordinating Research Council (http://www.crcao.com). A rigorous analysis of the CAMx implementation of the DDM was performed as part of this project, and excellent agreement was demonstrated (Dunker et al., 2002).

The original DDM implementation considered only first-order sensitivity. Recently, High-order DDM (HDDM; Hakami et al., 2003; Cohan et al., 2005) was implemented in CAMx in collaboration with Dr. Daniel Cohan (Rice University) with sponsorship from the Texas Commission on Environmental Quality (TCEQ), enabling CAMx to calculate second-order sensitivities along with first-order ones.

8.1 IMPLEMENTATION

The implementation of DDM into CAMx has focused on the evaluation of first- and second-order sensitivity coefficients that relate predicted concentrations to pollutant sources (i.e., emissions, ICs and BCs). The HDDM implementation in CAMx has recently been extended to calculate first- and second-order sensitivities to chemical rate constants. The DDM has also been applied in the past to the calculation of sensitivities to other model input parameters (e.g., meteorological parameters), but this was not attempted for the CAMx implementation because these sensitivities generally are less useful and because resources were limited. The CAMx implementation could be extended to other sensitivity parameters in the future.

The CAMx DDM permits the evaluation of sensitivity coefficients with respect to parameters related to emissions, BCs, ICs, or rate constants. The sensitivity to be evaluated may bear a simple relationship to the regular model input, such as scaling the ozone boundary concentration by a factor ($BC_{new} = \lambda \times BC_0$), or additively increasing the ozone boundary concentration by a constant amount everywhere ($BC_{new} = \lambda + BC_0$). To allow complete flexibility, the perturbations are specified by providing additional IC, BC, and/or emission input files with the same format as the regular model input files.

In mathematical terms, a regular model input file, for example the BC input file, represents some set of functions of space and time $f_i(\underline{x},t)$, where each chemical species can be defined by a unique function. An additional input file provided for the DDM represents another set of functions of space, time, and chemical species $g_i(\underline{x},t)$ that can be different from the regular input file. The scalar parameter λ_i is then defined by

$$F_i(\underline{x},t) \quad = \quad f_i(\underline{x},t) + \lambda_i \times g_i(\underline{x},t).$$

Here, $\lambda_i \times g_i(\underline{x},t)$ is the perturbation, and the user desires information on how the model would respond if the input $f_i(\underline{x},t)$ is replaced by the input $F_i(\underline{x},t)$. The HDDM calculates the first-order sensitivity $s_i^{(1)}(\underline{x},t)$ and second-order sensitivity $s_i^{(2)}(\underline{x},t)$ with respect to the scalar parameter λ_i. The Taylor series to second order then gives the estimate:

$$c_l(\underline{x},t;\lambda_i) \quad = \quad c_l(\underline{x},t;\lambda_i=0) + \lambda_i \times s_i^{(1)}(\underline{x},t) + \frac{1}{2}\lambda_i^2 \times s_i^{(2)}(\underline{x},t)$$

where $c_l(\underline{x};t;\lambda_i)$ is the estimated model result for species l when $F_i(\underline{x},t)$ is used as input, and $c_l(\underline{x},t;\lambda_i=0)$ is the base case model result when $f_i(\underline{x},t)$ is used as input.

For example, to calculate the sensitivity of the predicted ozone concentration to scaling boundary ozone by a factor, CAMx would be provided with a DDM BC file that has the same ozone values as the regular model BC file. The sensitivity coefficient fields output by CAMx could then be used to estimate the resulting ozone concentration if the ozone BCs were increased by 20%, as follows:

$$c_{\lambda=0.2} \quad = \quad c_{\lambda=0} + 0.2 \times s^{(1)} + 0.5 \times 0.2^2 \times s^{(2)}$$

(For simplicity hereafter, the dependence on space, time, and chemical species will be omitted).

To calculate the sensitivity of the predicted ozone concentration to increasing boundary ozone by 10 ppb, CAMx would be provided with a DDM BC file that has a constant ozone value of 10 ppb. The sensitivity coefficient fields could be used to estimate the ozone concentration if the ozone BCs were increased by 10 ppb as follows:

$$c_{\lambda=1.0} \quad = \quad c_{\lambda=0} + 1.0 \times s^{(1)} + 0.5 \times s^{(2)}$$

An alternative approach here would be to provide CAMx with a DDM BC file that has a constant ozone value of 1 ppb. This perturbation would be associated with a new parameter λ' and a new sensitivity coefficient s'. To estimate the ozone concentration if the ozone BC were increased by 10 ppb, one would use

$$c_{\lambda'=1.0} \quad = \quad c_{\lambda'=0} + 10.0 \times s'^{(1)} + 0.5 \times 10.0^2 \times s'^{(2)}$$

This would give exactly the same estimate as the preceding approach in which CAMx is supplied with a DDM BC file that has an ozone value of 10 ppb everywhere because the two sensitivities are related by $s' = s \times 0.1$ (from the first to second approach, there has been only a change of the scalar variable from λ to λ').

These are examples of relatively simple sensitivities. A more complex example would be to calculate the sensitivity to morning (6-9 AM) NO_x emissions in specific group of grid cells. In this case you would provide CAMx with a DDM emissions file where all values are zero except for the NO_x emissions in the selected grid cells between 6 AM and 9 AM, which would have the same value as the regular emissions file. In this case the sensitivity coefficient for ozone might be interpreted as the increase (or decrease) in ozone concentration due to the selected emissions (however, caution is warranted because sensitivity coefficients are not directly equivalent to a source apportionment). More accurately, the sensitivity coefficient could be used to predict the concentration after a scalar change (λ) in the morning NOx emissions using the equation:

$$c_{\lambda} \quad = \quad c_{\lambda=0} + \lambda \times s^{(1)} + 0.5\lambda^2 \times s^{(2)}$$

Any type of sensitivity perturbation can be described via an input file. However, the CAMx user interface also provides easy ways to define some sensitivities that are likely to be used frequently. For example, in the first example above the DDM BC file was described as having the "same ozone values as the regular model BC file." To make such a file you could copy the BC file and then remove (or zero out) all species but ozone. To avoid the effort of preparing an input file that is trivially different from the regular model file, the user interface allows you to select specific species from an input file to track - in this case ozone. It is possible to separately track the sensitivity to more than one species from the same file (e.g. ozone, and NO). It is also possible to track the combined sensitivity to a group of species, such as NO_x, VOC, HRVOC, or ALL. The user interface also provides a simple way to track sensitivities to emissions from specific grid cells or groups of cells (sub-regions).

Tracking Sensitivity Coefficients Within CAMx

The conceptual approach in tracking DDM sensitivity coefficients is directly parallel to the way

in which CAMx calculates three-dimensional concentration fields. The concentration fields are calculated by a series of code modules that operate sequentially to represent the impact of different physical processes (emissions, advection, diffusion, chemistry, deposition, etc.) on the gridded concentrations. Sensitivity coefficients are calculated by a parallel set of modules which operate in step with the CAMx modules to calculate gridded sensitivity coefficients. For some processes (e.g., chemistry and horizontal advection), the sensitivity coefficient modules make use of information saved from the corresponding CAMx modules. The need to employ this approach arises in cases where the CAMx algorithm depends non-linearly upon species concentrations. In other cases, the sensitivity algorithm turns out to be identical to the CAMx algorithm (e.g., horizontal diffusion) and both concentrations and sensitivity coefficients can be processed by the single module. Finally, there are cases where the sensitivity algorithm turns out to be identical to the CAMx algorithm, but a specialized module has been written for the sensitivity coefficients to improve the computational efficiency (e.g., vertical advection).

Priorities in the DDM coding implementation were:

- Ensuring accuracy by using consistent numerical methods for the concentrations and sensitivities;
- Ensuring accuracy by calculating the concentrations and sensitivities using the same time steps (for original DDM);
- Optimizing the efficiency of the sensitivity coefficient calculations without compromising accuracy;
- Providing a flexible User Interface that allows calculation of sensitivities to all sources and precursors;
- Ensuring that the DDM algorithms have minimal impact on computer resource requirements (memory and CPU time) when the DDM is not being used.

Further details of the implementation of the DDM in CAMx will be published in the near future.

Horizontal Advection and Chemistry

Specialized modules were developed to calculate the effects of chemistry and horizontal advection upon DDM sensitivity coefficients. These DDM modules are exactly matched to the numerical methods employed in the corresponding CAMx modules. CAMx has two separate options for the horizontal advection solver (Bott and PPM) and three options for the gas phase chemistry solver (the EBI solver, IEH solver, and LSODE – Gear – solver). With the resources available, it was only possible to develop DDM implementations for one advection solver (Bott) and one chemistry solver (EBI). The DDM option in CAMx cannot be used with other solver options at the present time. However, HDDM can be used any advection solver and chemistry solver.

The implementation of DDM algorithms for the EBI chemistry solver was integrated with the chemical mechanism compiler (CMC). Therefore, the DDM option is available for the CB4, SAPRC, and CB05 chemical mechanisms, and will be available for additional mechanisms implemented in CAMx in the future. The HDDM is also available for all the chemistry mechanisms.

Plume-in-Grid and Aerosol Processes

Resource constraints did not permit implementation of DDM algorithms for the Plume-in-Grid (PiG) and aerosol chemistry options currently available in CAMx.

Source Code

The coding of DDM algorithms involved the creation of several new subroutines for CAMx. These subroutines are all grouped in a separate directory (called DDM) under the main CAMx source code directory. It was necessary to add additional code for DDM in several existing CAMx subroutines, and the new code is clearly marked by comments.

Flexi-DDM

Although DDM is computationally much more efficient than the BFM, it does require additional CPU time and memory space which can be significant especially when multiple grids are used in two-way nesting. The increased computational cost may not always be worthwhile if only part of the modeling domain is of interest. One way to enhance computational efficiency in such cases is to use one-way nesting where boundary conditions (BCs) for a nested grid are extracted from the full grid modeling. Subsequent runs with sensitivities are performed without outer grids. However, differences between the two nesting schemes (i.e. 1-way vs. 2-way) sometimes cause discrepancies in the model results. An alternative approach is running the full 2-way nested model while "turning off" sensitivity calculations outside nested grids of interest.

CAMx provides a feature called “Flexi-DDM” which allows user to turn off sensitivity calculations for selected grids (normally grids far outside the area of interest) to improve computational efficiency of DDM runs. This will reduce CPU-times but not reduce memory requirements. Also, note that turning off sensitivity calculations for outer grids is only appropriate for certain types of sensitivity calculations: e.g., sensitivity to BCs cannot be calculated with Flexi-DDM.

8.2 RUNNING CAMx WITH DDM and HDDM

This section describes how to specify the sensitivity coefficients to be calculated and the additional input files that must be supplied. Since CAMx already contained a methodology for probing source-receptor relationships called OSAT (ozone source apportionment technology, see Section 6), the DDM user interface was designed along similar lines to the existing OSAT user interface. This makes it easier to learn how to use both options and promotes consistency in analyses performed using OSAT and DDM.

Inputs in the CAMx Control File

DDM is invoked similarly to the other Probing Tools within the CAMx control file. In the `&CAMx_Control` namelist module, the variable `Probing_Tool` must be set to either

"DDM" or "HDDM". An additional namelist module called `&DDM_Control` must then be provided in the control file to configure the DDM portion of the model. The additional namelist module is described below. The order of the variables follow the template available with the source code. An example of the DDM portion of the CAMx run control file is shown in Figure 8-1.

Description of DDM Control in the CAMx Run Control File

`&DDM_Control`	Label for the Probing Tool namelist module that configures the DDM option; it must begin in column 2
`&`	Flag ending a namelist; it must be in column 2
`DDM_File_Root`	Character root output path/filename
`DDM_Master_Sfc_Output`	Logical flag for master grid surface output (TRUE=DDM file will be output for all sensitivities, FALSE=DDM file will not be output)
`DDM_Nested_Sfc_Output`	Logical flag for nested grid surface output (TRUE=DDM file will be output for all sensitivities, FALSE=DDM file will not be output)
`DDM_Stratify_Boundary`	Logical flag to stratify boundary types (TRUE=separate sensitivity types will be used for the N, S, E, W, and Top boundaries, FALSE=a single sensitivity type will be used for all 5 boundaries)
`DDM_Number_of_Source_Regions`	Integer number of source regions to be tracked. This must be the same as the number of source areas defined in the DDM_`Source_Area_Map` file. This value may be zero.
`DDM_Number_of_Source_Groups`	Integer number of emission groups to be tracked. This determines the number of emission files that must be supplied (additional details below). This value may be zero.
`Number_of_IC_Species_Groups`	Integer number of species or species groups in the initial conditions to be tracked. This number may be between zero and the number of species being simulated plus four (allowing for the four species groups VOC, HRVOC, NOX, ALL).
`IC_Species_Groups`	Character array (by IC group) names of the species or species groups in the initial conditions to be tracked. Allowed names are any species being simulated by the mechanism in use (e.g., O3, PAR, NO, etc.) plus the species groups NOX, VOC, HRVOC, and ALL. It is permissible to specify both a species and a group containing that species, e.g., both NO and NOX. Each name may have up to 10 characters. Note that if you select a species that is not present on the IC file provided, the initial sensitivities for that species will be set to zero. This variable may be left blank if the number of initial condition species

groups is zero.

`Number_of_BC_Species_Groups` Integer number of species or species groups in the boundary conditions to be tracked. This number may be between zero and the number of species being simulated plus four (allowing for the four species groups VOC, HRVOC, NOX, ALL).

`BC_species_Groups` Character array (by BC group) names of the species or species groups in the boundary conditions to be tracked. See description for `IC_Species_Group` above.

`Number_of_EM_Species_Groups` Integer number of species or species groups in the emissions to be tracked. This number may be between zero and the number of species being simulated plus four (allowing for the four species groups VOC, HRVOC, NOX, ALL).

`Emis_Species_Groups` Character array (by emissions group) names of the species or species groups in the emissions to be tracked. See description for `IC_Species_Group` above.

`Number_of_Rate_Const_Groups` Integer number of reaction rate sensitivity groups to be tracked. This number may be zero.

`Rate_Const_Groups` Character string containing each reaction rate sensitivity group name and reaction numbers that belong to the group. Group name and reaction numbers are separated by colon (:) and each reaction number is separated by comma (,).

`Number_of_HDDM_Sens_Groups` Integer number of HDDM sensitivity groups to be tracked. This number may be zero.

`HDDM_parameters` Character array names of the first-order sensitivity parameters to which second-order sensitivity is computed. The naming of the first-order parameters is the same as the long name of sensitivities with the first 4 characters omitted. For each of HDDM sensitivity group, two first-order parameters are required (the same can be used twice). All the first-order parameters must be included in the modeling.

`DDM_Receptor_Definitions` Character input DDM receptor definition path/filename

`DDM_Source_Area_Map` Character array (by CAMx grid) input DDM source area definition path/filename (required for master grid, optional for nested grids). Source regions are defined using a map in the same format as an OSAT source area map (Section 6); however, DDM does not require that all parts of the modeling domain be tracked, therefore it is permissible to define an area numbered zero in the source area map (emissions from those areas will not be tracked). The non-zero source region numbers must be between 1 and the number of regions.

`DDM_Calc_Grid` Logical array containing Flexi-DDM flag for each grid. .TRUE.

	if calculating sensitivities in the grid; otherwise, .FALSE..
`DDM_Initial_Conditions`	The name of the sensitivity initial condition file. Leave the file name blank for restart days or if sensitivity to initial conditions is not being calculated.
`DDM_Boundary_Conditions`	The name of the sensitivity lateral boundary condition file. Leave the file name blank if sensitivity to boundary conditions is not being calculated.
`DDM_Top_Concentrations`	The name of the sensitivity top boundary condition file. Leave the file name blank if sensitivity to boundary conditions is not being calculated.
`DDM_Master_Restart`	Character input master grid DDM restart path/filename (ignored if `Restart=FALSE`)
`DDM_Nested_Restart`	Character input nested grid DDM restart path/filename (ignored if `Restart=FALSE` or `Number_of_Grids=1`)
`DDM_Points_Group`	Character array (by source group) input DDM elevated point source emissions path/filename (optional, ignored if `Point_Emissions=FALSE`)
`DDM_Emiss_Group_Grid`	Character array (by source group, by CAMx grid) input DDM gridded emissions path/filename (optional, ignored if `Gridded_Emissions=FALSE`)

```
&DDM_Control

 DDM_File_Root                 = '$DDM_OUT/CAMx.08jul95.runA',
 DDM_Master_Sfc_Output         = .true.,
 DDM_Nested_Sfc_Output         = .true.,
 DDM_Stratify_Boundary         = .false.,
 DDM_Number_of_Source_Regions = 4,
 DDM_Number_of_Source_Groups  = 2,

 Number_of_IC_Species_Groups = 1,
 IC_Species_Groups(1)        = 'ALL',
 Number_of_BC_Species_Groups = 1,
 BC_species_Groups(1)        = 'ALL',
 Number_of_EM_Species_Groups = 2,
 Emis_Species_Groups(1)      = 'NOX',
 Emis_Species_Groups(2)      = 'VOC',
 Number_of_Rate_Const_Groups = 1,
 Rate_Const_Groups(1)        = 'RXN1: 120,121,122',
 Number_of_HDDM_Sens_Groups  = 1,
 HDDM_parameters(1,1)        = 'EM0101NOX_',
 HDDM_parameters(1,2)        = 'EM0101VOC_',

 DDM_Receptor_Definitions  = '$DDM_IN/receptor.cities',
 DDM_Source_Area_Map(1)    = '$DDM_IN/source_map.DDM.4areas',
 DDM_Source_Area_Map(2)    = ' ',

 DDM_Calc_Grid(1)          = .true.,
 DDM_Calc_Grid(2)          = .true.,

 DDM_Initial_Conditions    = ' ',
 DDM_Boundary_Conditions   = '$DDM_IN/BC.08jul95',
 DDM_Top_Concentrations    = '$DDM_IN/TC.08jul95',
 DDM_Master_Restart        = '$DDM_OUT/CAMx.07jul95.runA.sa.inst',
 DDM_Nested_Restart        = '$DDM_OUT/CAMx.07jul95.runA.sa.finst',

 DDM_Points_Group(1)       = ' ',
 DDM_Points_Group(2)       = '$DDM_PT/ptsr.ng.08jul95',

 DDM_Emiss_Group_Grid(1,1) = '$DDM_EMIS/bio.cc.08jul95',
 DDM_Emiss_Group_Grid(1,2) = '$DDM_EMIS/bio.ff.08jul95',
 DDM_Emiss_Group_Grid(2,1) = '$DDM_EMIS/anthro.cc.08jul95',
 DDM_Emiss_Group_Grid(2,2) = '$DDM_EMIS/anthro.ff.08jul95',

 &
```

Figure 8-1. Example input of DDM options and filenames via the CAMx control file. In this case, CAMx is run with two grids, and DDM is configure to track emissions from four source regions and two source groups (biogenic and anthropogenic). Initial and boundary conditions are tracked as a single sensitivity called “ALL”, while emissions are tracked with three sensitivities called “NOx”, “VOC”, and “ALL”. Additionally, second-order sensitivities to biogenic VOC emissions from the first source region will be computed. No source region map is provided for the nested grid (the region assignments on the nest are defined by the master grid). Initial condition sensitivity is not being tracked (no file provided), and only the group 2 point sources are tracked (no biogenic point sources are available).

8.3 APPROACHES TO DEFINE IC, BC AND EMISSIONS SENSITIVITIES

The description above shows how to specify the IC, BC and emissions files for DDM sensitivity calculations. The formats for each of these files are identical to the CAMx input files of these types. In many cases, users may choose to specify exactly the same file for a CAMx input file and a DDM input file. (Be aware that some computer systems do not allow a file to be opened twice by the same application. A work around for this problem is to copy or link the file "filename" to another file of different name, such as "filename.copy").

The user can perform many different sensitivity calculations in a single run according to the content of the DDM input files. Take initial conditions (ICs) as an example. If the same IC file is specified for both CAMx and DDM, the output sensitivity fields represent the sensitivity of the predicted concentrations to the ICs. Therefore, simply scaling the output sensitivity coefficients fields provides the incremental concentrations resulting from scaling the ICs.

As another example, if a DDM emissions file is supplied to CAMx that has a constant VOC emission rate everywhere, the sensitivity will correspond to a uniform absolute increase in the VOC emission rate rather than a percentage increase as described above. Another possibility would be a DDM emission file with a different spatial pattern than the CAMx input file. The sensitivity coefficient would then correspond to changing both the geographic distribution and magnitude of emissions. Still another possibility would be a DDM file that has zero emissions for all hours except midnight to 5 AM on the third simulated day. The program would then calculate the sensitivity to early morning emissions on the third day. In this case, just the concentrations could be simulated for the first two days and the DDM calculation begun on the third day, because sensitivities on the first two days are identically zero.

In short, the DDM input file can be arbitrary – different from the CAMx input file in the overall magnitude of concentrations or emissions, different in the geographic and temporal distribution, and different in the relative proportions of the chemical species. However, the user must understand what perturbations are being considered in order to properly interpret the resulting output sensitivity coefficient fields. Also, the user should recognize that as the size of perturbations increase, the second- and higher-order terms eventually become important, usually when the emissions are altered by more than 20-30%.

8.4 DDM OUTPUT FILES

The output file types for a DDM simulation are described in Table 8-1. These files have the same format as corresponding concentration output files, described in Section 5.

Table 8-1. DDM output file suffix names.

File Name Suffix	DDM File Type
.ddm.inst	Binary master grid instantaneous sensitivity file at end of simulation (used for restart), 3-D, all sensitivities, µmol m^{-3} $parameter^{-1}$ units.
.ddm.finst	Binary nested grid instantaneous sensitivity file at end of simulation (used for restart), 3-D, all sensitivities, µmol m^{-3} $parameter^{-1}$ units.
.ddm.grd*nn*	Binary average sensitivity file for grid *nn*, 2-D, surface layer sensitivities only for affected species requested in the CAMx average file, ppm $parameter^{-1}$ units.
.ddm.receptor	Text hourly average sensitivities at user specific receptor locations. This file is in comma delimited ASCII format suitable for importing into a spreadsheet.

8.5 DDM SENSITIVITY COEFFICIENT NAMES

Each DDM sensitivity coefficient tracks the influence of a species from a specific source (the *influencing species*) on a predicted concentration (the *affected species*). The sensitivity coefficient names are constructed to show this relationship, as follows:

{Affected Species} {Pollutant Source} {Influencing Species}

This is a lot of information to encode in a name that must conform to the ten character limit imposed by the binary I/O file formats. Because of this, two naming systems are used in CAMx:

- Long Names - these names are easy to read, but since they are more than ten characters in length they cannot be used in sensitivity coefficient binary output files. If an alternate I/O format is implemented in the future it may be possible to use the long names on sensitivity output files.

- Short Names - these convey the same information as the long names but require more practice to learn. They are used in the sensitivity coefficient binary output files.

At the start of each CAMx run a concordance of Long and Short sensitivity coefficient names is written to the diagnostic output file (.diag file). An example concordance is shown in Figure 8-2, and a detailed explanation of the naming convention follows.

Affected Species	Influencing Species	Source Type	Group	Region	Long Name	Short Name
NO	NO	EM	1	2	NO__EM0102NO__	01E0102001
NO2	NO	EM	1	2	NO2_EM0102NO__	02E0102001
O3	NO	EM	1	2	O3__EM0102NO__	03E0102001
PAN	NO	EM	1	2	PAN_EM0102NO__	04E0102001
NXOY	NO	EM	1	2	NXOYEM0102NO__	05E0102001
OLE	NO	EM	1	2	OLE_EM0102NO__	06E0102001
PAR	NO	EM	1	2	PAR_EM0102NO__	07E0102001
TOL	NO	EM	1	2	TOL_EM0102NO__	08E0102001
XYL	NO	EM	1	2	XYL_EM0102NO__	09E0102001
FORM	NO	EM	1	2	FORMEM0102NO__	10E0102001
ALD2	NO	EM	1	2	ALD2EM0102NO__	11E0102001
ETH	NO	EM	1	2	ETH_EM0102NO__	12E0102001
CRES	NO	EM	1	2	CRESEM0102NO__	13E0102001
MGLY	NO	EM	1	2	MGLYEM0102NO__	14E0102001
OPEN	NO	EM	1	2	OPENEM0102NO__	15E0102001
PNA	NO	EM	1	2	PNA_EM0102NO__	16E0102001
CO	NO	EM	1	2	CO__EM0102NO__	17E0102001
HONO	NO	EM	1	2	HONOEM0102NO__	18E0102001
H2O2	NO	EM	1	2	H2O2EM0102NO__	19E0102001
HNO3	NO	EM	1	2	HNO3EM0102NO__	20E0102001
ISOP	NO	EM	1	2	ISOPEM0102NO__	21E0102001
MEOH	NO	EM	1	2	MEOHEM0102NO__	22E0102001
ETOH	NO	EM	1	2	ETOHEM0102NO__	23E0102001
ISPD	NO	EM	1	2	ISPDEM0102NO__	24E0102001
NTR	NO	EM	1	2	NTR_EM0102NO__	25E0102001

Figure 8-2. Example concordance of long and short sensitivity coefficient names from the CAMx diagnostic output file.

Initial Condition Sensitivity Names

Long Name **NNNNIC____MMMM**

where:

- **NNNN** Affected species name with trailing underscore to pad blanks
- **IC** Indicates the sensitivity coefficient is for initial conditions
- **____** Four underscores to pad the name to 14 characters
- **MMMM** Influencing species name with trailing underscore to pad blanks

Examples:

```
FORMIC____VOC_
O3  IC    O3
```

Short Name **nnI____mmm**

where:

- **nn** Affected species number
- **I** Indicates the sensitivity coefficient is for initial conditions
- **_____** Four underscores to pad the name to 10 characters
- **mmm** Influencing species number or name of a species group (NOX, VOC, HRVOC or ALL).

Examples:

`10I  VOC` (where FORM is species number 10)
`03I____003` (where O3 is species number 3)

Boundary Condition Sensitivity Names

Long Name **NNNNBCRRR MMMM**

where:

NNNN	Affected species name with trailing underscore to pad blanks
BC	Indicates the sensitivity coefficient is for boundary conditions
RRR	NTH, STH, EST, WST or TOP if stratified by boundary; ALL if not stratified by boundary
_	Underscore to pad the name to 14 characters
MMMM	Influencing species name with trailing underscore to pad blanks

Examples: `FORMBCALL_VOC_`
`O3  BCTOP O3`

Short Name **nnBRRR_mmm**

where:

nn	Affected species number
B	Indicates the sensitivity coefficient is for initial conditions
RRR	NTH, STH, EST, WST or TOP if stratified by boundary; ALL if not stratified by boundary
_	Underscore to pad the name to 10 characters
mmm	Influencing species number or name of a species group (NOX, VOC, HRVOC or ALL)

Examples: `10BALL_VOC` (where FORM is species number 10)
`03BTOP_003` (where O3 is species number 3)

Emissions Sensitivity Names

Long Name **NNNNEMGGRRMMMM**

where:

NNNN	Affected species name with trailing underscore to pad blanks
EM	Indicates the sensitivity coefficient is for emissions
GG	Emissions group number
RR	Emissions region number
MMMM	Influencing species name with trailing underscore to pad blanks

Examples: `FORMEM0103VOC_`
`O3  EM0201O3`

Short Name **nnEGGRRmmm**

where:

nn	Affected species number

E	Indicates the sensitivity coefficient is for emissions
GG	Emissions group number
RR	Emissions region number
mmm	Influencing species number or name of a species group (NOX, VOC, HRVOC or ALL)

Examples: `10E0103VOC` (where FORM is species number 10)
`03E0201003` (where O3 is species number 3)

Reaction Rate Sensitivity Names

Long Name **NNNNRATE__MMMM**

where:

NNNN	Affected species name with trailing underscore to pad blanks
RATE	Indicates the sensitivity coefficient is for rate constants Two underscores to pad the name to 14 characters
MMMM	Reaction rate sensitivity group name with trailing underscore to pad blanks

Examples: `NO__RATE__RXN1`
`O3  RATE  R28`

Short Name **nnRATE_mmm**

where:

nn	Affected species number
RATE	Indicates the sensitivity coefficient is for rate constants Underscore to pad the name to 10 characters
mmm	Reaction rate sensitivity group number

Examples: `01RATE_001` (where NO is species number 1)
`03RATE_002` (where O3 is species number 3)

HDDM Sensitivity Names

Long Name **NNNNHDDMLLLMMM**

where:

NNNN	Affected species name with trailing underscore to pad blanks
HDDM	Indicates the sensitivity coefficient is second-order
LLL	The index of the first 1st-order sensitivity parameter in the internal list of the 1st-order parameters
MMM	The index of the second 1st-order sensitivity parameter in the internal list of the 1st-order parameters

Examples: `NO__HDDM001001`

`O3  HDDM001002`

Short Name **`nnEGGRRmmm`**

where:

`nn`	Affected species number
`HDDM`	Indicates the sensitivity coefficient is second-order
`ll`	The index of the first 1st-order sensitivity parameter in the internal list of the 1st-order parameters
`mm`	The index of the second 1st-order sensitivity parameter in the internal list of the 1st-order parameters

Examples: `01HDDM0101` (where NO is species number 1)
`03HDDM0102` (where O3 is species number 3)